# Detector Physics

Lichtenberg figure: captured lightning

Gauß Weber: first telegraph

1905: new physics building

Debye Scherrer Method: Si powder

G. Eigen, University of Bergen

HASCO July 22-27, 2018 Göttingen

# Introduction

- In particle physics, we build so-called multi-purpose detectors
- These are dedicated instruments that measure particular observables: vertex, track positions, particle IDs, momentum, energy, time, …
- In colliding-beam experiments, subdetectors are placed in layers around the interaction region in cylindrical geometry, like onion shells
- In the endcaps they are stacked behind each other to close the cylinder
- Though physics processes can be manifold and complex, we only encounter a few stable particles in the final state: $e^{\pm}$, $\mu^{\pm}$, $\pi^{\pm}$, $K^{\pm}$, $p^{\pm}$, $\gamma$, (n)
- In matter, these particles interact electromagnetically
- With modern vertex detectors, we are able to reconstruct decay vertices

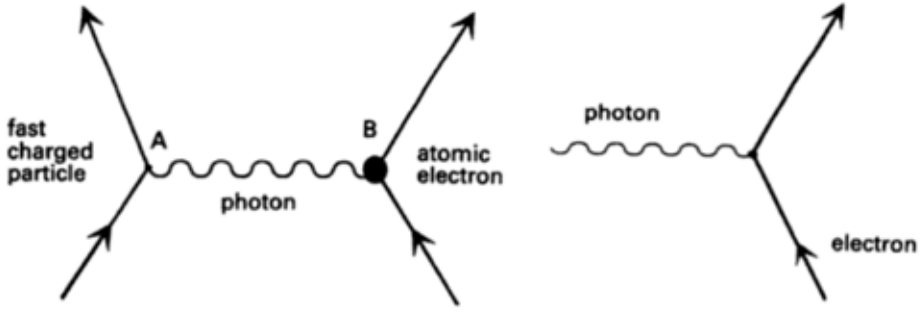

# Multipurpose Detectors at LHC

- Each LHC experiment has about 100 million sensors
- Think that your 6MP digital camera takes 40 million pictures/s

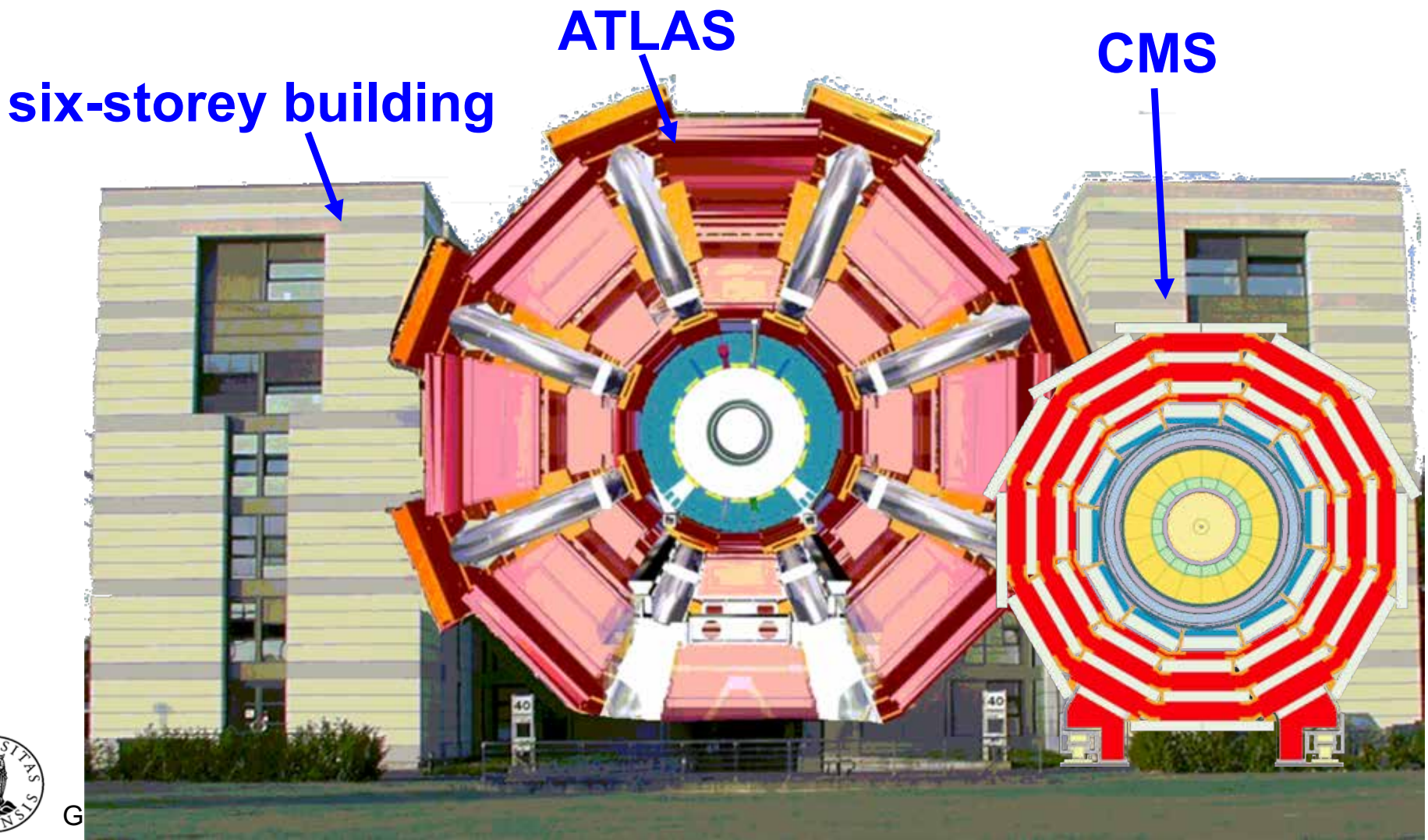

# Outline

- Ionization, Excitation & Electrons in Gases
- Gaseous Tracking Detectors
- Solid State Detectors
- Momentum Measurements
- Electrons and Photons in Matter
- Electromagnetic Calorimeters
- Hadronic Calorimeters
- Particle Flow Calorimeters
- Transition Radiation Detectors
- Trigger and Data Acquisition

---

- LHC Detectors

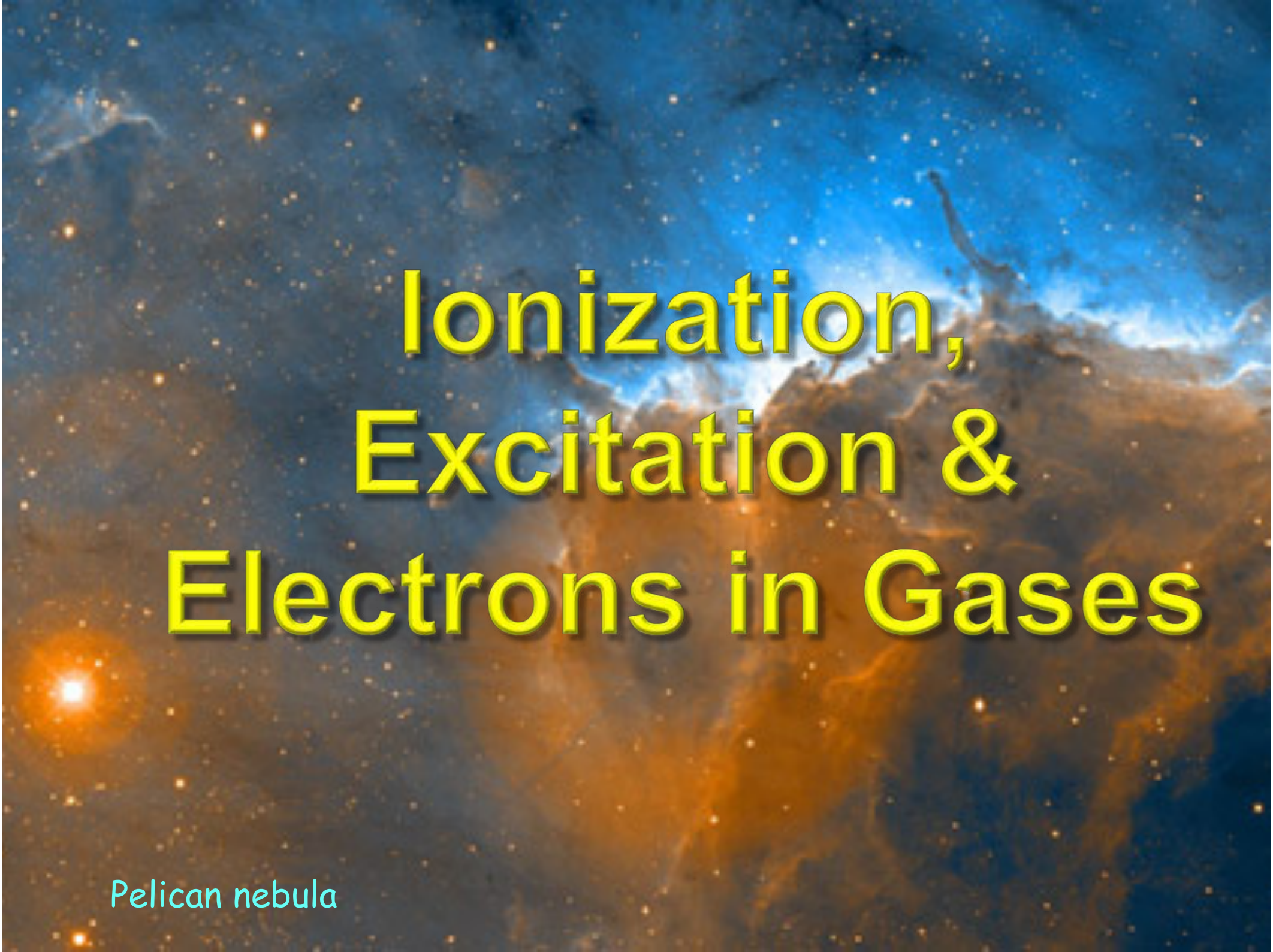
Ionization,
Excitation &
Electrons in Gases
Pelican nebula

# Heavy Charged Particle in Medium

- A heavy charged particle traversing a medium loses in a single collision the energy W in thickness $\Delta x$

mass: $m>m_e$, velocity: $\vec{\beta}=\vec{p}/E$, $\gamma=\vec{p}/m$,
momentum: $\vec{p}$, energy $E$, $\gamma=E/m$

dielectric constant: $\varepsilon=(\varepsilon_1+i\varepsilon_2)$,
atomic number $Z$ thickness $\Delta x$

- The probability for an interaction is given by the total collision cross section $N\int (d\sigma(W, \beta\gamma)/dW)\, dW$ per unit length

*N:* atomic density

- Photoabsorption ionization cross section by Allison & Cobb (neglecting $\delta$-rays & Cherenkov radiations)

$$\frac{d\sigma(W,\beta\gamma)}{dW} = \frac{\alpha}{\beta^2\pi}\frac{\sigma_\gamma(W)}{WZ}\ln\left[\frac{1}{\left(1-\beta^2\varepsilon_1\right)^2+\varepsilon_2^2}\right] + \frac{\alpha}{\beta^2\pi}\frac{\sigma_\gamma(W)}{WZ}\ln\left[\frac{2mc^2\beta^2}{W}\right]$$

- The zeroth and first moments, $M_0$ & $M_1$, yield the average number of collisions and the average energy loss $<\Delta E>$ in $\Delta x$

$$M_0 = N\Delta x\int_I^{W_{max}}\frac{d\sigma(W,\beta\gamma)}{dW}dW \qquad M_1 = N\Delta x\int_I^{W_{max}} W\frac{d\sigma(W,\beta\gamma)}{dW}dW$$

- The details of the photoabsorption cross section $\sigma_\gamma(W)$ determine how well $<\Delta E>$ is calculated

$\sigma_\gamma(W) \sim \varepsilon_2(\hbar\omega)$

$d\sigma(W, \beta\gamma)$ in Si

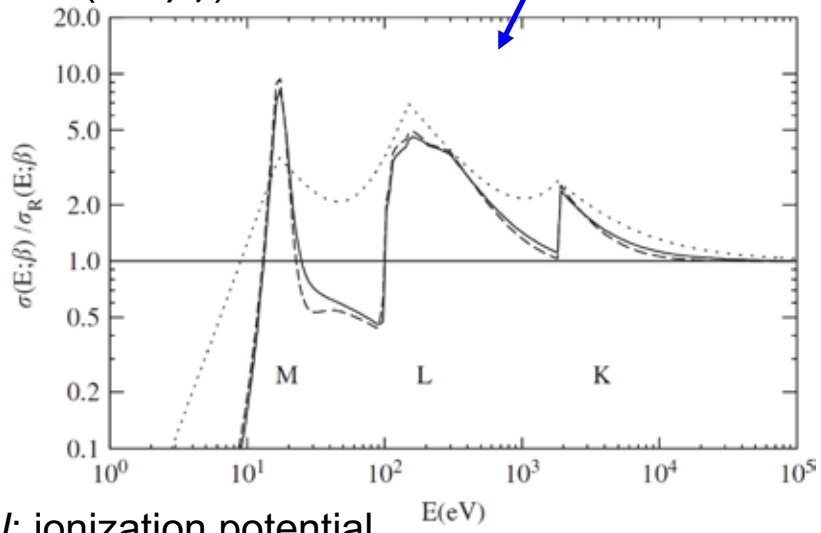


*I*: ionization potential

# Ionization and Excitation

- The **average** energy loss for a heavy particle is given by Bethe-Bloch

$$-\left\langle \frac{dE}{dx} \right\rangle = Kz^2\rho\frac{Z}{A}\frac{1}{\beta^2}\left[\frac{1}{2}ln\left(2m_e c^2\beta^2\gamma^2\frac{T_{max}}{I^2}\right)-\beta^2-\frac{\delta(\beta\gamma)}{2}-\frac{C}{Z}\right] \qquad (m>>m_e)$$

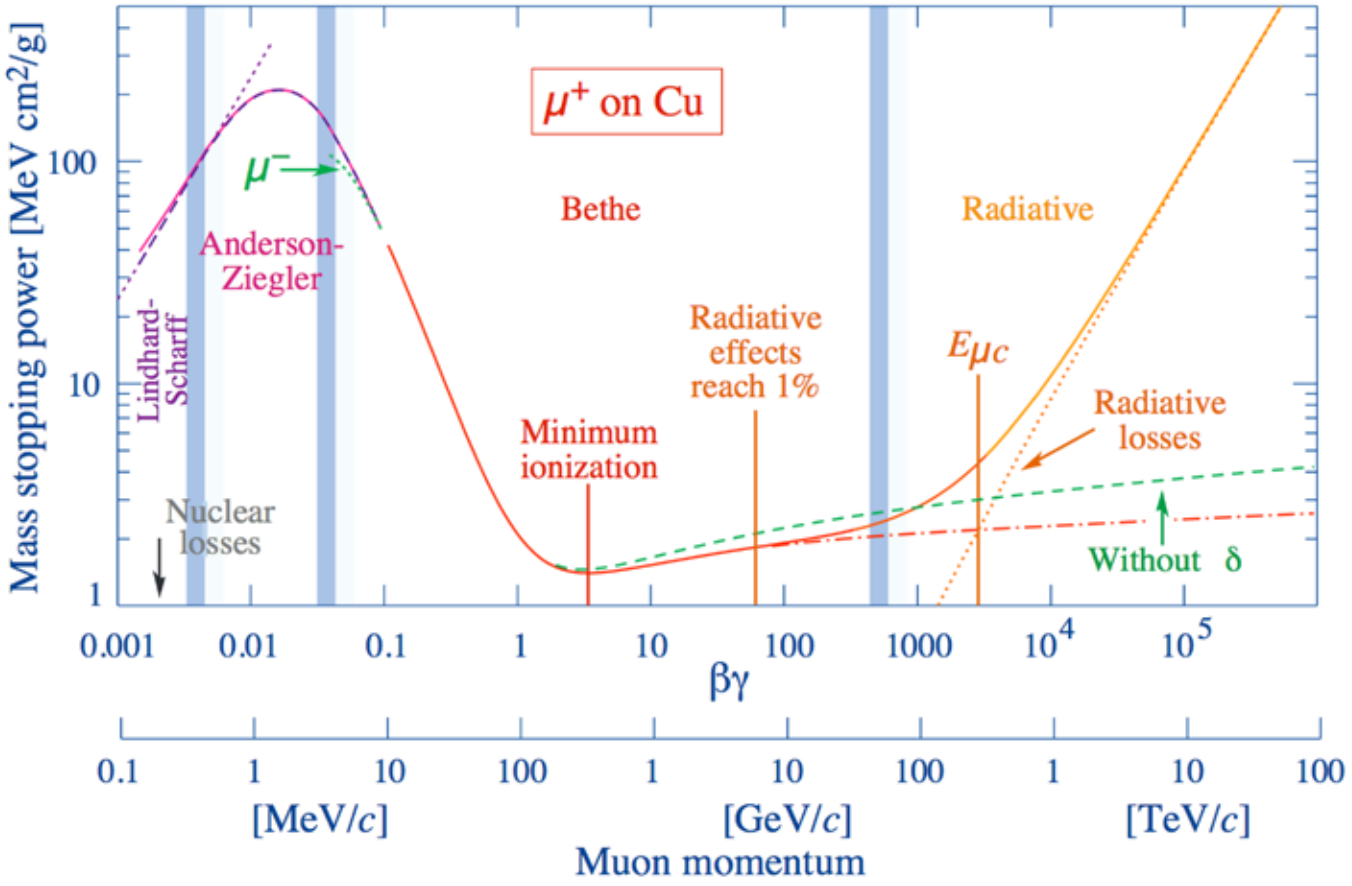


$$T_{max} \cong W_{max}$$

$$T_{max} = \frac{2m_e c^2\beta^2\gamma^2}{1+2\frac{m_e}{m}\sqrt{1+\beta^2\gamma^2}+\frac{m_e^2}{m^2}}$$

Medium

- $A$: atomic weight
- $Z$: atomic number
- $\rho$: density
- $I$: ionization potential
- $\alpha$=1/137
- $m_e$: electron mass
- $C$: shell correction
- $\delta(\beta\gamma)$: density effect
- K=0.307 MeV cm²/g

Particle

- $T_{max}$: maximum kinetic energy
- $z$: particle charge
- $\beta$=|p|/E
- $\gamma$=E/m

# *dE/dx* for Particle Identification

- Since the measured energy loss allows us to determine the particle velocity, we use it to identify particle types at low momenta
- Instantaneous energy loss in thin layers is given by a Landau distribution

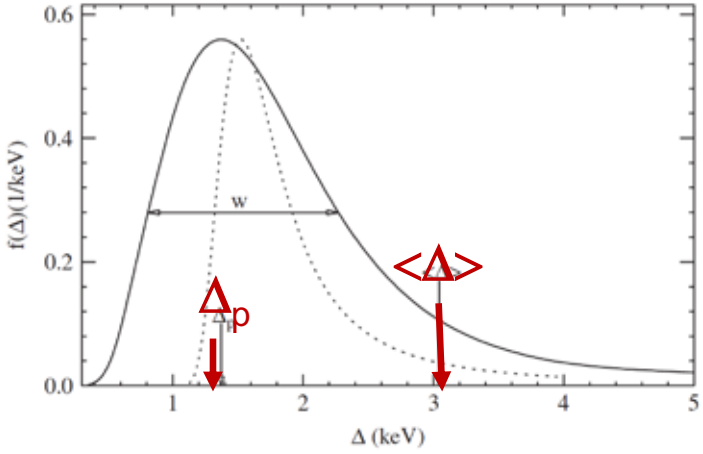


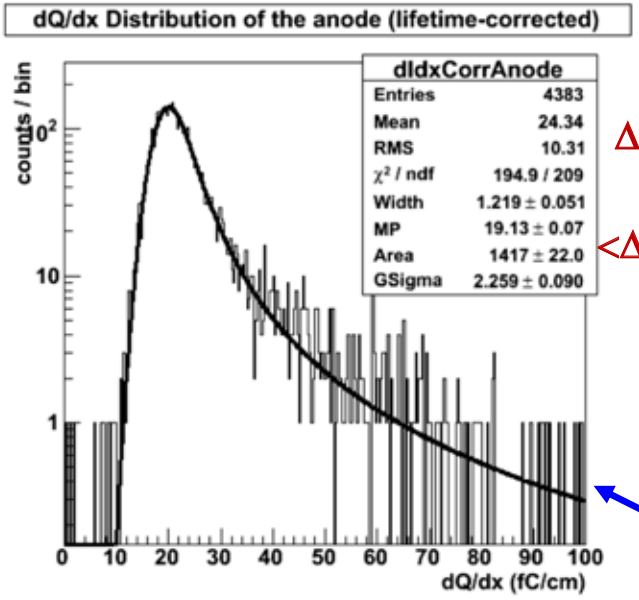


$\Delta_p$: most probable energy loss

$\langle\Delta\rangle$: average energy loss

Measured energy loss in the ALICE TPC

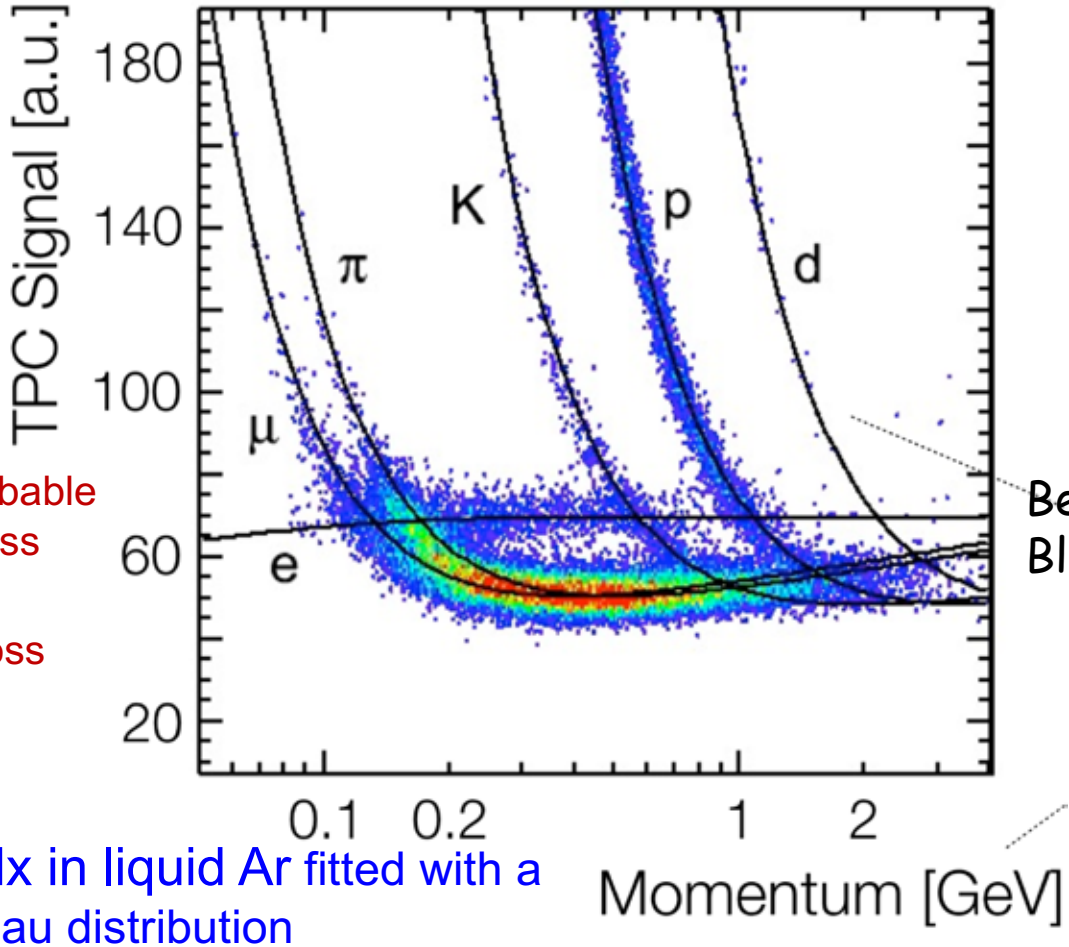


Bethe-Bloch

dE/dx in liquid Ar fitted with a Landau distribution

# Average Energy Loss in Different Materials

- For low $\beta\gamma$ values ➔ <dE/dx> decreases as $1/\beta^2$
- For $\beta\gamma$ of ~ 3-4 ➔ average energy loss is minimum
- For $\beta\gamma$ > 4 ➔ relativistic rise
- For $\beta\gamma$> 2000 ➔ dominant energy loss occurs via radiation
- Minimum energy loss can be parameterized by: **$\langle dE/dX \rangle_{min} = 2.35 - 0.28\ \ln(Z)$**

Energy loss at minimum

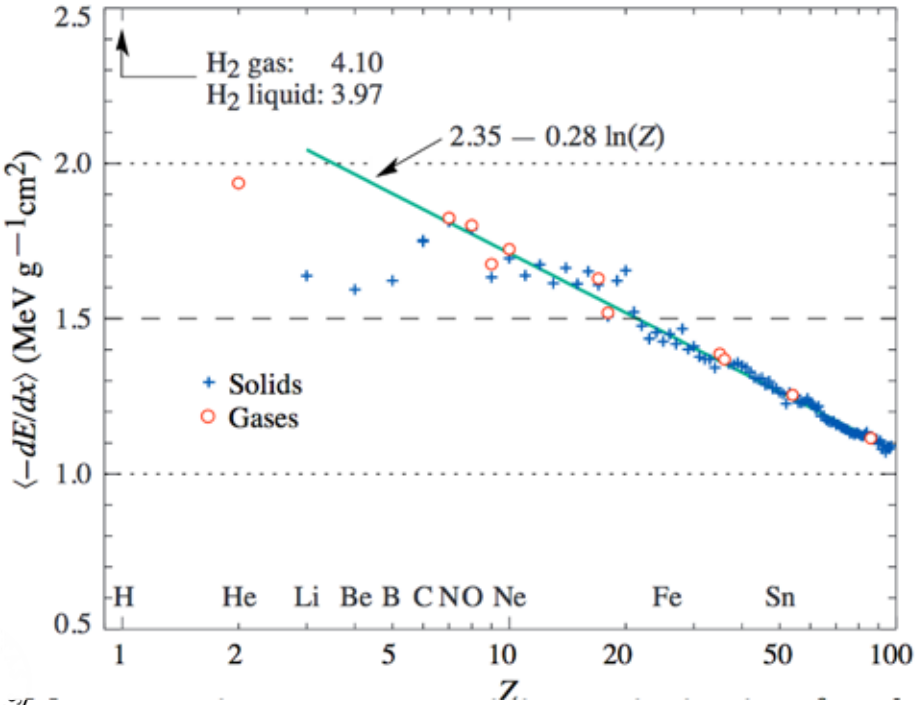


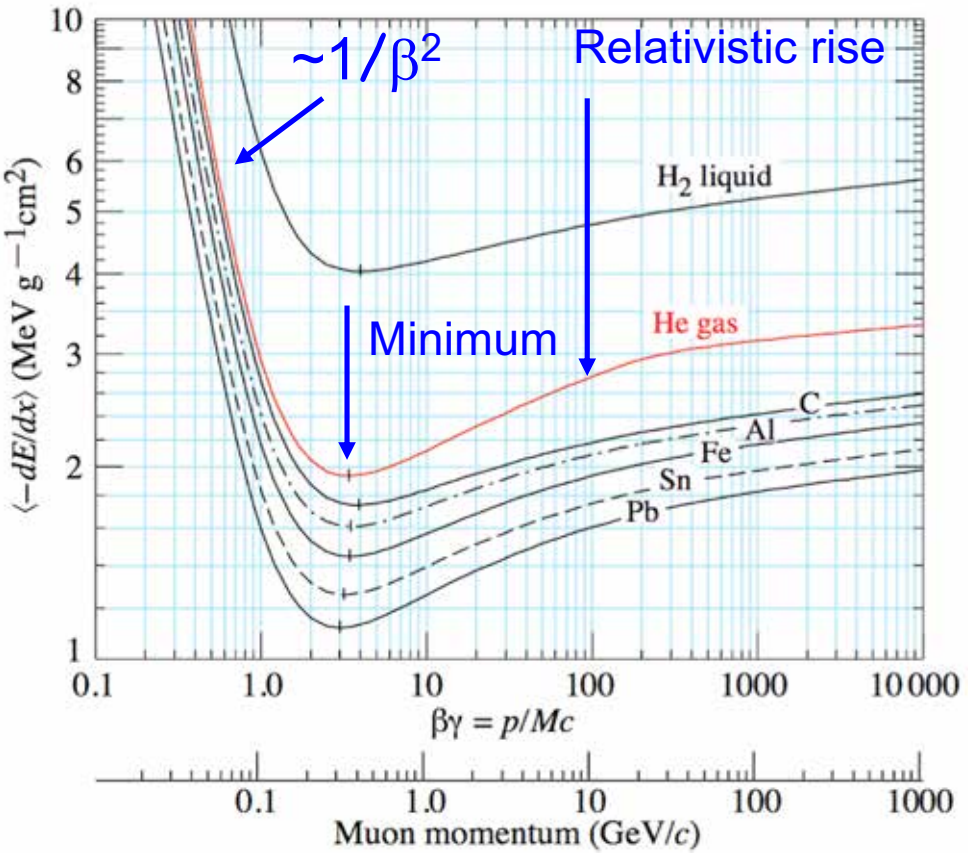

# Drift Velocity

- A cloud of electrons ($e^-$) or ions ($i^+$) placed in an electric field of strength $\vec{E}$, is accelerated by the $\vec{E}$ field and decelerated by collisions in the gas
  ➔ the motion can be described by a constant drift velocity $\vec{v}_D$

- The drift velocity can be expressed in terms of the mean free path $\lambda_e$, thermal velocity **u**, electric field $\vec{E}$, charge *q* and particle mass *m*

$$\vec{v}_D = \frac{q\vec{E}}{m}\left\{\frac{2}{3}\left\langle\frac{\lambda_e(u)}{u}\right\rangle + \frac{1}{3}\left\langle\frac{d\lambda_e(u)}{du}\right\rangle\right\}$$

$\lambda_e$ : average distance between 2 collisions

- If $\lambda_e$ is independent of the thermal velocity, the second term vanishes

- For some gases, $\vec{v}_D$ is independent of $\vec{E}$ in some range (Ar-$CH_4$ 90:10) or is only slightly dependent on $\vec{E}$

- Electron drift velocities of are ~1-10cm/μs and $e^-$ mean free paths are considerably larger:
  $\lambda_e = \lambda_{ion} \cdot 5.66$

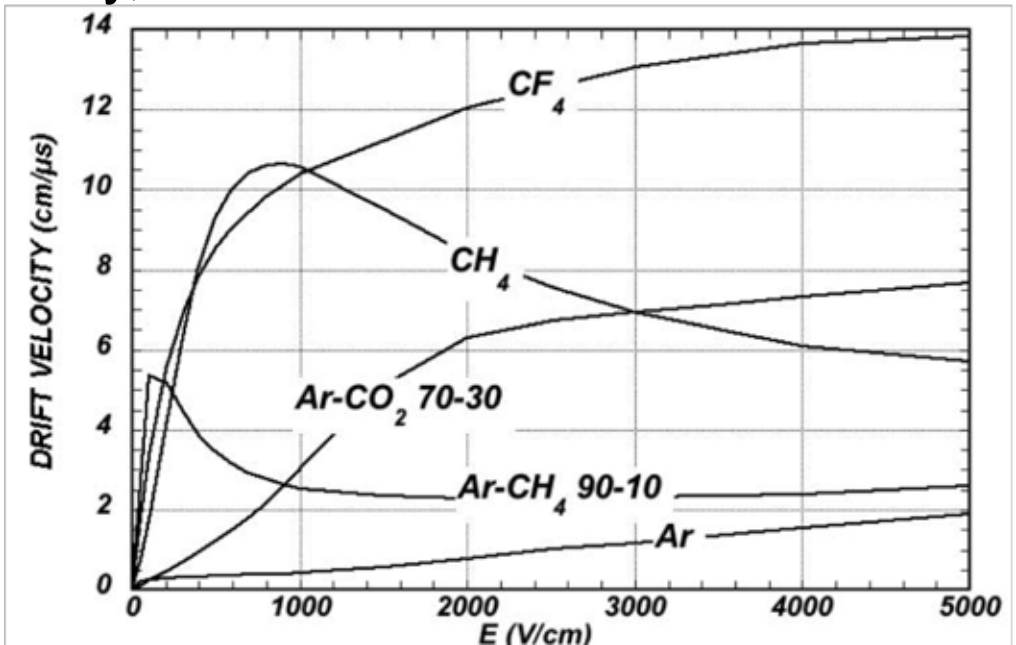

# Drift of Electrons in $\vec{E}$ & $\vec{B}$ Fields

- A charge in an electromagnetic field moving through a gas-filled volume is subject to the force

$$m\dot{\vec{v}} = q\left(\vec{E} + \vec{v}\times\vec{B} + mA(t)\right)$$

Langevin

Coulomb

Lorentz

- Stochastic acceleration averaged over time compensates translational acceleration where $\tau$ is average time between 2 collisions

$$\left\langle \vec{A}(t) \right\rangle = -\frac{\vec{v}_D}{\tau}$$

- In a constant $\vec{E}$ field we have

$$\vec{v}_D = \frac{\mu}{1+\omega^2\tau^2}\left[\vec{E} + \frac{\vec{E}\times\vec{B}}{|\vec{B}|}\omega\tau + \frac{\left(\vec{E}\cdot\vec{B}\right)\cdot\vec{B}}{|\vec{B}|^2}\omega^2\tau^2\right]$$

- In the presence of $\vec{E}$ & $\vec{B}$ fields the drift velocity has 3 terms

  i) one parallel to $\vec{E}$

  ii) one parallel to $\vec{B}$

  iii) one perpendicular to plane spanned by $\vec{E}$ & $\vec{B}$

$$\vec{\omega} = -\frac{q}{m}\vec{B}$$

Cyclotron frequency

$$\left|\frac{\vec{\omega}}{\vec{B}}\right| = 17.6\ MHz/G$$

- If $\vec{E}$ and $\vec{B}$ are not parallel, there is angle between $\vec{v}_D$ and $\vec{E}$ called Lorentz angle $\alpha$

$$\tan\alpha = \omega\tau$$

# Diffusion of Ions in a Field-free Gas

- A charge distribution $Q(t)$ localized at (0,0,0) at $t$=0 is diffused by multiple scattering

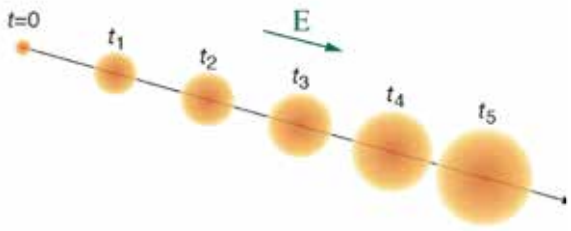


- At time $t$, $Q(t)$ is Gaussian with center at origin

Charge density distribution for 5 equidistant time intervalls:

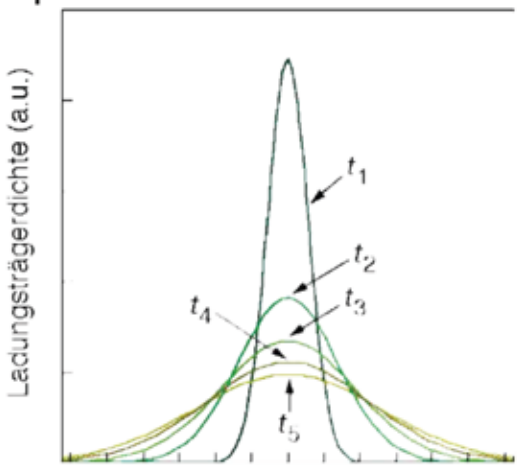


ε : kinetic energy

- The rms spread is proportional to the diffusion coefficient $D = \frac{1}{3}\int u\lambda_e(\varepsilon)F(\varepsilon)d\varepsilon$

  where F(ε) is the Maxwell-Boltzmann distribution

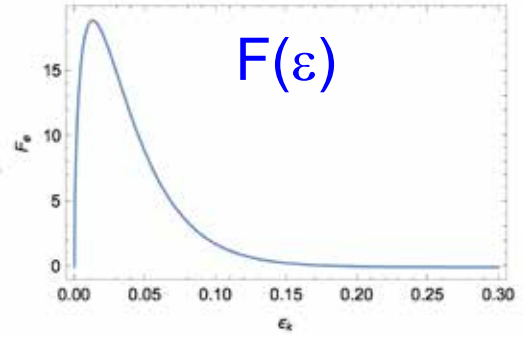


- For energy-independent $\lambda_e$ we obtain $D = \frac{1}{3}u\lambda_e$

- For a classical ideal gas we have $\lambda_e(\varepsilon) = \frac{1}{N\sigma(\varepsilon)}$

where $\sigma(\varepsilon)$ is the collision cross section and N is number of molecules per unit volume

$$N = 2.69\times10^{19}\,\frac{P}{760}\,\frac{273}{T}\left[\frac{moles}{cm^3}\right]$$

# Diffusion of Electrons in $\vec{E}$ & $\vec{B}$ Fields

- Diffusion parallel (L) and perpendicular (T) to the drift direction depends on the nature of the gas
- Typically faster gases yield smaller diffusion than slower gases
- The spatial resolution is depends on time and the diffusion coefficient

$$\sigma = \sqrt{2Dt}$$

- Since $t = L/|\vec{v}_D|$ & $D = u\lambda/3$, we get in absence of a magnetic field

$$\sigma = \sqrt{\frac{2L}{3|\vec{v}_D|}}\sqrt{u\lambda}$$

- In the presence of a magnetic field spatial resolution improves by

$$\left(1+\omega^2\tau^2\right)^{-1}$$

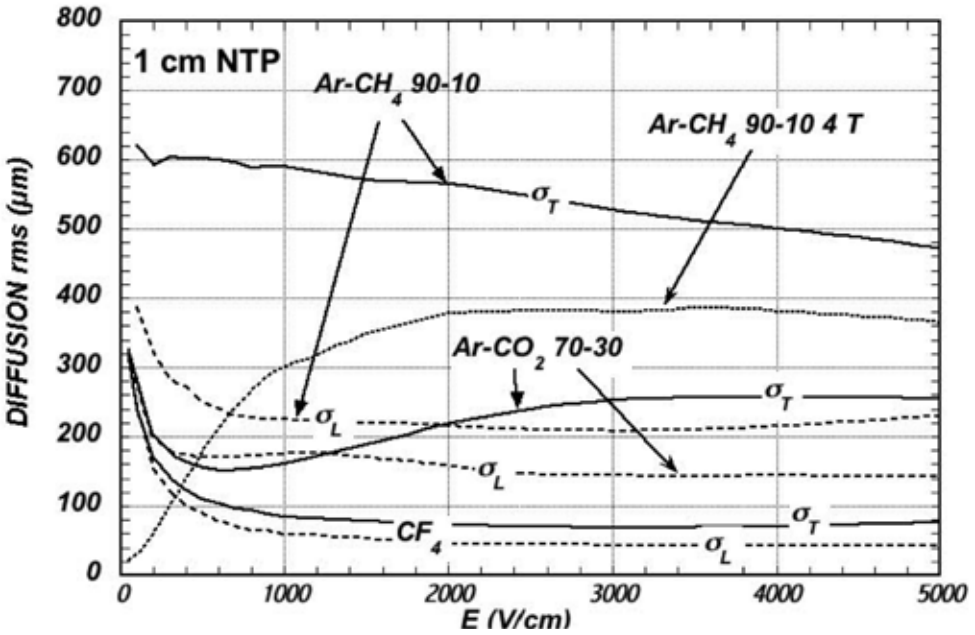


**Figure 28.5:** Electron longitudinal diffusion ($\sigma_L$) (dashed lines) and transverse diffusion ($\sigma_T$) (full lines) for 1 cm of drift. The dotted line shows $\sigma_T$ for the P10 mixture at 4T [67].

$\tau$: time between 2 collisions


# Gaseous Tracking Detectors

ALICE TPC

# Proportional Counter

- Consider a tube with a wire placed at its center filled with a gas
- Apply a high electric field between anode wire and cathode $10^4$-$10^5$ V/cm
  ➔ electrons from primary ionization gain enough energy between 2 collisions to cause further ionizations

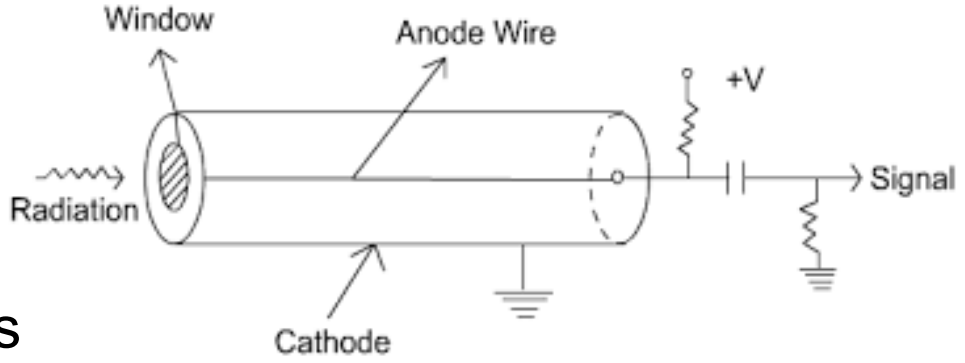


- For certain $\vec{E}$ fields & gas pressures, gain ***A*** is independent of amount of primary ionization ➔ observed signal is proportional to primary ionization
- This range of field strengths is called proportional region ➔ here $A \approx 10^4$-$10^6$
- Achieve high field strengths with thin anode wires (20 μm-100 μm)
- Amplification will start in close vicinity to anode
- In addition, ionization processes due to UV photons contribute to gas gain
- These UV photons originate from de-excitations of atoms excited in collisions that produce $e^-$s via photo-effect in gas atoms or the cathode

# First Townsend Coefficient

- The number of $e^-$-$i^+$ pairs formed by $e^-$ along a 1cm path is called the first Townsend coefficient $\alpha=\sigma_i N$ where $\sigma_i$ is ionization cross section and $N=2.69\times10^{19}$ atoms/cm$^3$

- If $N_0$ is number of primary $e^-$ at x=0 and N(x) is number of $e^-$ at path x

➔ $$N(x) = N_0 \exp\left( \int_x \alpha(x')\,dx' \right)$$

$A(x)$

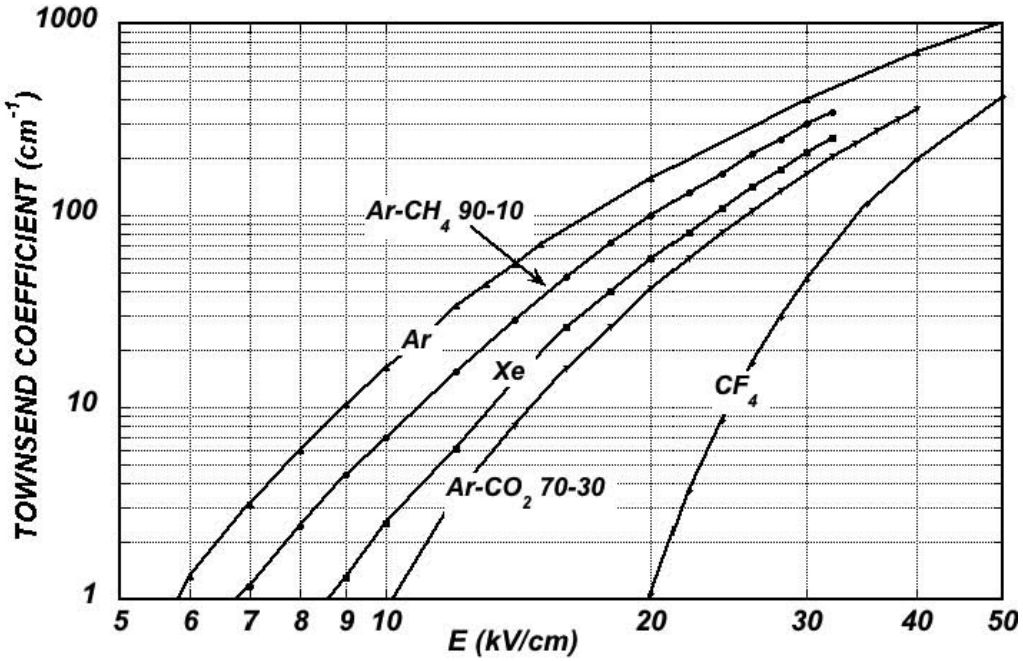


- Note that $\alpha(x)=1/\lambda_e(x)$

- Townsend coefficients for fast gases are considerably smaller than those for slow gases

- Including the contributions from UV photons, the gas amplification becomes

$$A_\gamma = \frac{A}{1 - A\cdot\gamma}$$

$\gamma$ « 1 fraction of UV photons

- For $A\cdot\gamma\rightarrow1$, $A_\gamma$ diverges & signal no longer depends on primary ionization
  ➔ This is called Geiger-Müller region ($A_\gamma$ ~$10^8$-$10^{10}$)

# Multi-Wire Proportional Chamber

- In a multi-wire proportional chamber (**MWPC**) a plane of anode wires is sandwiched between cathode planes

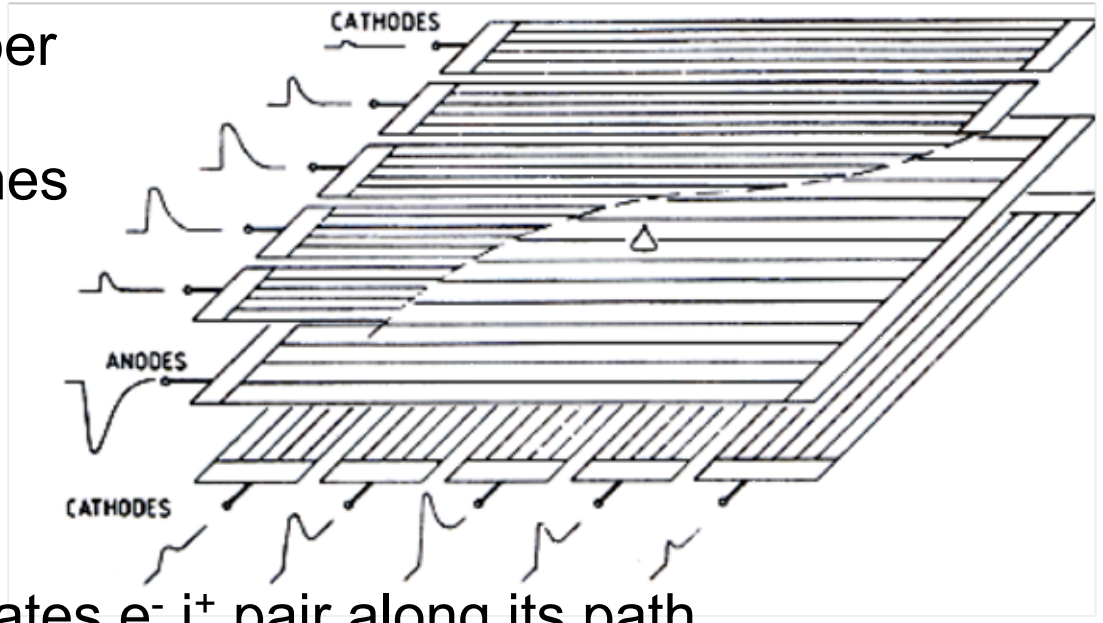


- Cathode planes are segmented into strips; strips in one (other) plane run parallel (perpendicular) to the anode wires
- A traversing charged particle liberates $e^-$ $i^+$ pair along its path
- $e^-$ are accelerated towards the anode wire & $i^+$ towards cathode plane
- The $\vec{E}$ field is chosen sufficiently high so that secondary ionization sets in and an avalanche is formed near the anode wire and signals are induced on the cathode strips
- Anode wires: 20 μm thick Au-plated W, Al; 2 mm spacing
  Counting gas: Ar, Kr, or Xe with admixture of $CO_2$, $CH_4$, isobutane, …
  Amplification: $10^5$; efficiency: ~100%
  with cathode readout measure x and y positions

# Position Determination

- Position is usually obtained by center-of-gravity method

$$y = \frac{\sum_i (Q_i - b) y_i}{\sum_i (Q_i - b)}$$

$y_i$: y-position of wire i

$Q_i$: Charge of wire i

$b$: Small bias voltage to correct for noise

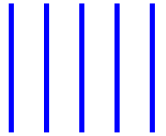

$y_i$

- Achieve resolutions of 110-170 μm, 35 μm in small chamber

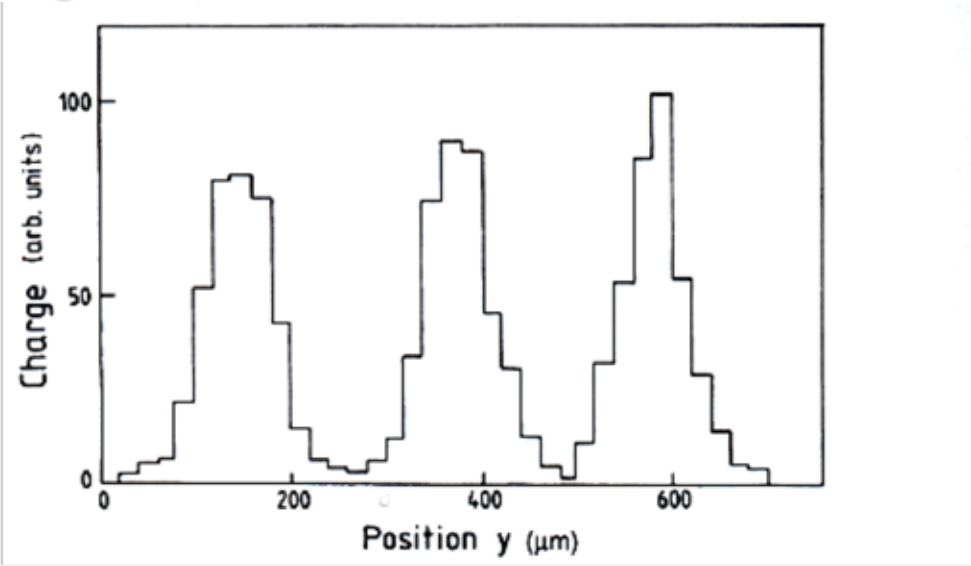


- Position along the wire is obtained via charge division
  - ➔ Need to read out both wire ends

- For charge measurements $Q_A$ & $Q_B$ obtain position along the wire

$$x = L \frac{Q_A - b}{Q_A + Q_B - 2b}$$

- Accuracies are ~0.4% of wire length

# Principle of Drift Chambers

- We can obtain spatial information by measuring the drift time of electrons produced in ionization processes
- The drift time $\Delta t$ between primary ionization $t_0$ & the time $t_1$ when $e^-$ enters the high $\vec{E}$ field generating an avalanche is correlated with the rising edge of the anode pulse

⇨ For constant drift velocity $\vec{v}_D(t)$ drift distance for this $\Delta t$ interval is

$$z = \left|\vec{v}_D\right|\left(t_1 - t_0\right) = \left|\vec{v}_D\right| \Delta t$$

- Constant $\vec{v}_D$ results from constant $\vec{E}$, which is not achieved in MWPCs

➔ Need to introduce a field wire at potential -HV1 between anode wires

- Choice of gas Ar-$C_4H_{10}$ (purity)
  Use slower $\vec{v}_D$ to optimize spatial resolution ⇨ large DC: 55-200 μm, small DC: 30-70 μm

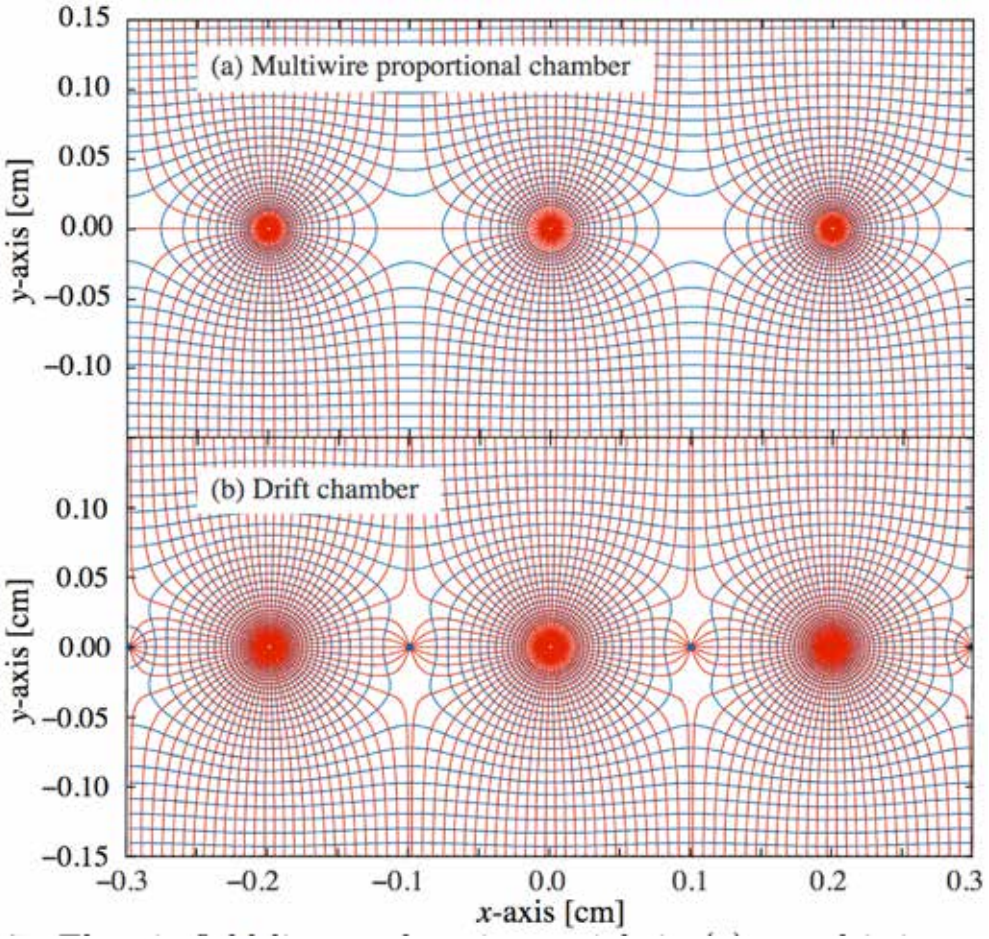

# Position Measurements in Cylindrical DCs

- $\vec{E}$ field lines lie in the r-φ plane, perpendicular to axial $\vec{B}$ field
- The $\vec{E}$ field is generated by a suitable arrangement of potential wires, which are parallel to each other surrounding a single signal wire

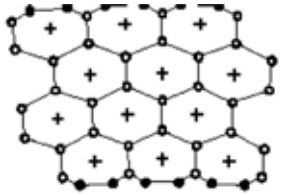

- A large fraction of layers (typically ≥ 50%) have wires running parallel to $\vec{B}$ field (axial layers) & rest have wires running skew under stereo angle γ=±few $^0$ wrt $\vec{B}$ field axis (stereo layer)
- Axial wires only give r-φ position, stereo wires allow to get z position
- One determines r-φ position from all axial wires, then the stereo wires are added by moving along z-position till the r-φ fits with that of axial layers
- For each signal wire $t_0$ and the time-to-distance relation need to be measured
- BABAR drift chamber: 40 layers, $\sigma_{r\varphi}$≈125 μm

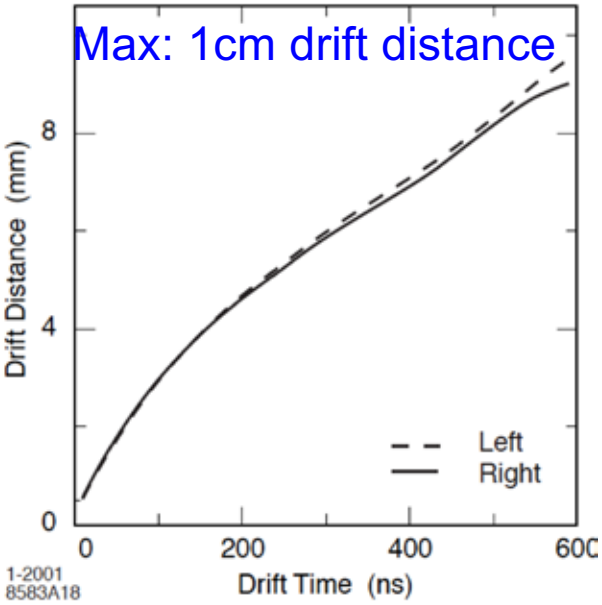

# Principle of Time Projection Chambers

- The Time Projection Chamber combines principles of a drift chamber & proportional chambers to measure 3-dimensional space points

- A high $\vec{E}$ field is placed parallel to a high $\vec{B}$ field (1.5 T)
  ➔ no Lorentz force on drifting $e^-$

## ALICE TPC

- 845 < r < 2466 mm
- drift length 2 x 2.5 m
- drift gas Ne:$CO_2$:$N_2$ (85.7:9.5:4.8)
- gas volume 95 $m^3$
- 557568 readout pads

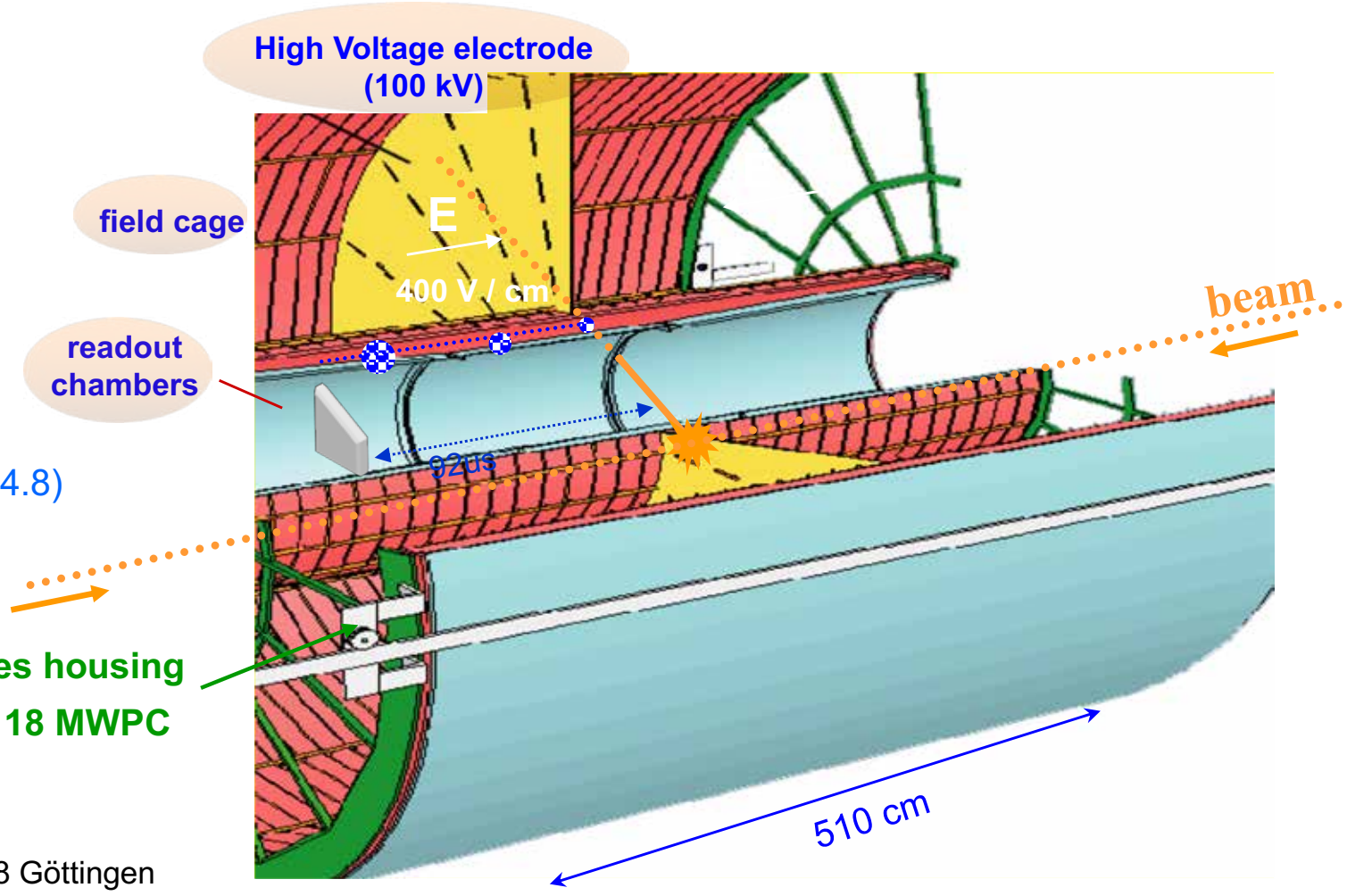

# Position Measurements in TPCs

- $e^-$ produced by ionization of a charged track passing the **TPC** drift towards the endcaps, which are instrumented with MWPCs
- The image is broadened by diffusion during the drift process
  ➔ broadening can be considerably reduced by strong $\vec{B}$ field
- $e^-$ are forced to perform helical movement around $\vec{B}$ field lines
- Transverse diffusion coefficient is reduced by $1/(1+\omega^2\tau^2)$, with $\omega=(e/m)|\vec{B}|$ & $\tau$ is mean free time between 2 collisions
- **TPC** measures 3-dimensional space points, r-$\phi$ in **MWPC** and z from drift time
- Spatial resolution:
  $\sigma_{r\phi}$=180 μm, $\sigma_z$=200 μm

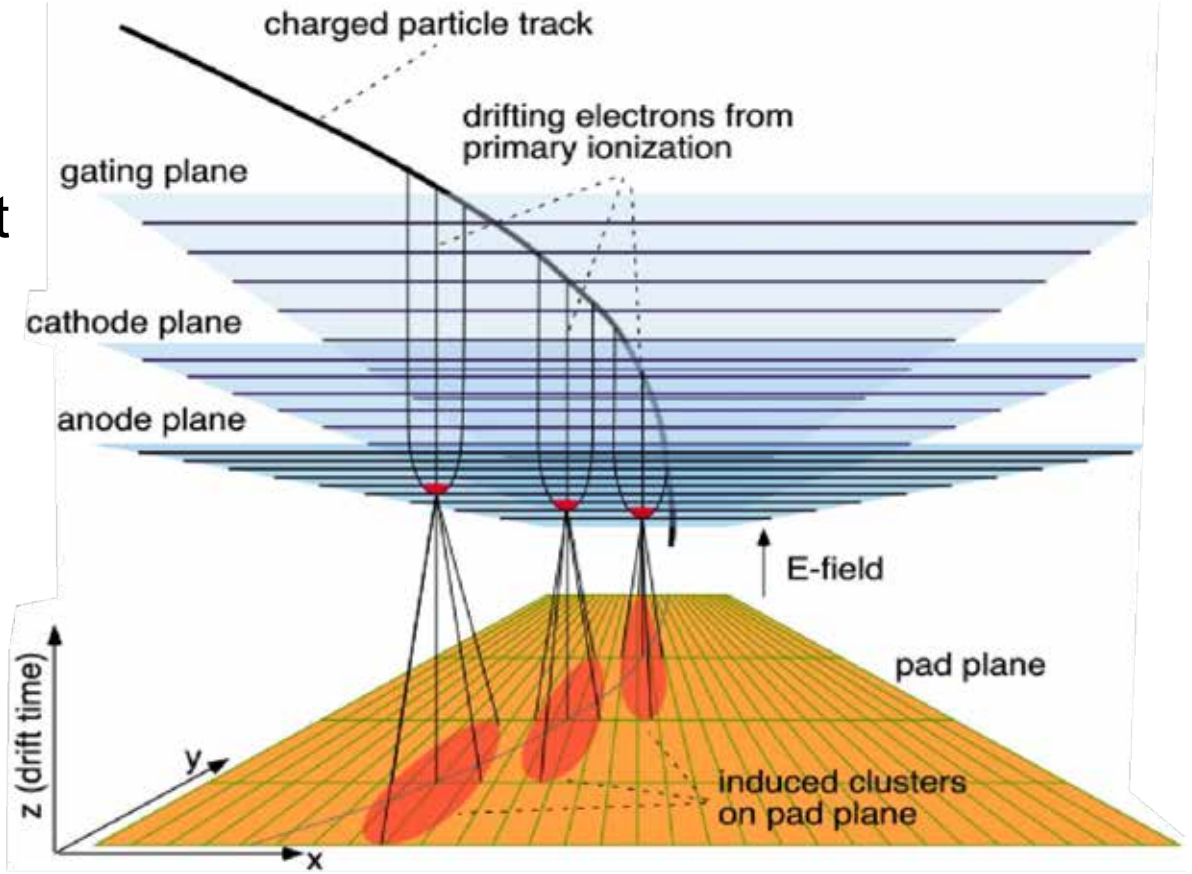

# Gas Electron Multiplier

- Position-sensitive gas detectors based on wire structure are limited by diffusion processes and space charge effects to accuracies of 50-100 μm
- A **GEM** detector consist of a thin Cu-Kapton-Cu sandwich into which a high density of holes is chemically processed: 25-150 μm ⌀, 50-200 μm pitch
- A high E field 50-70 kV/cm is applied across holes
  ➔ broadening electron produces avalanche in hole
- Coupled with a drift electrode above and a readout electrode below it acts as a highly performing micro amplifying detector
- Amplification and detection are decoupled
  ➔ broadening operate readout at zero potential
- With several layers gain of $10^4$ is achievable
- GEMs have higher rate capability than MWPCs

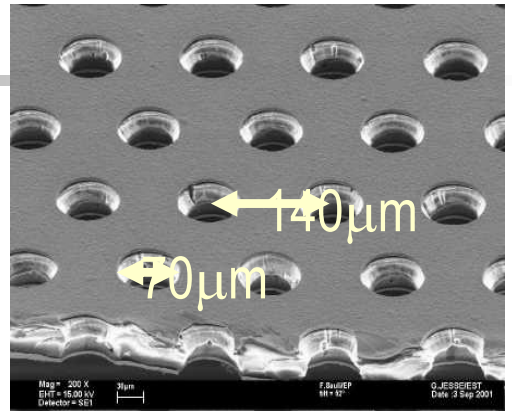


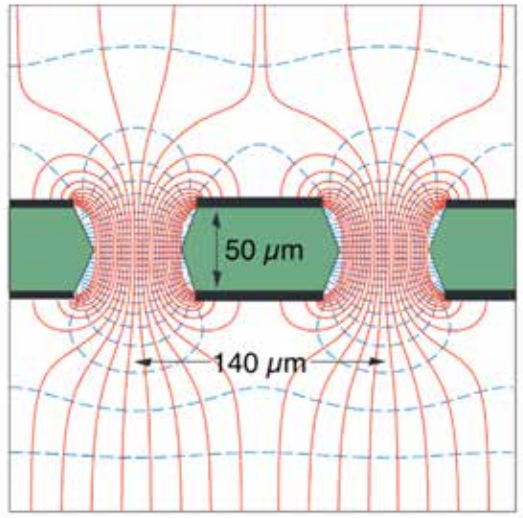


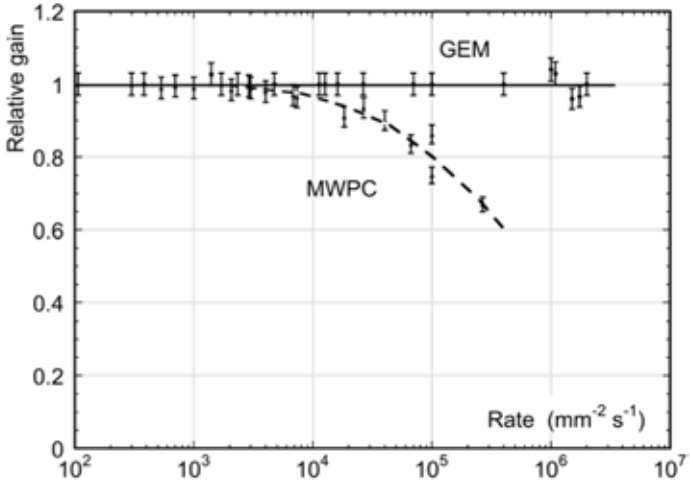

# Micro-MEsh GAseous Structure

- The micro-mesh gaseous structure is a thin parallel-plate avalanche counter
- It has a drift region & a narrow amplification gap (25-150 μm) between a thin micro mesh & the readout electrode (conductive strips or pads printed on insulator board)
- Primary $e^-$ drift through the mesh holes into the amplification gap where they are amplified
- Homogeneous E fields, 1 kV/cm in drift region & 50-70 kV/cm in amplification gap

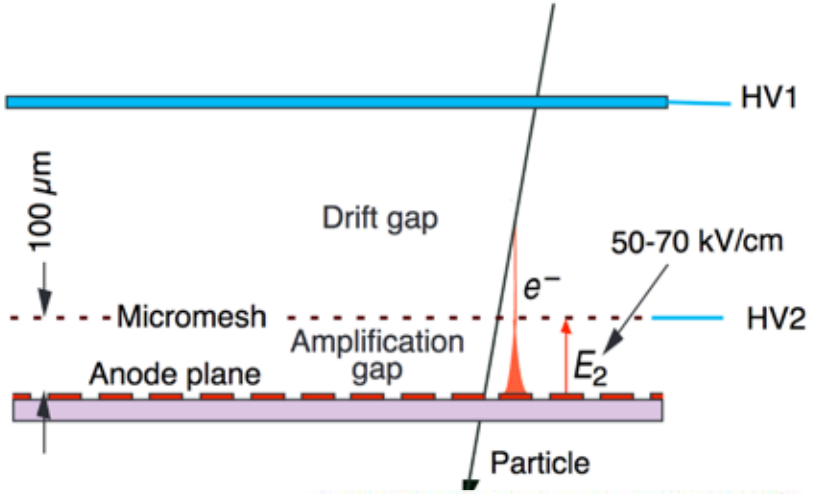


- Excellent spatial resolution of 12 μm, good time resolution and good energy resolution for 6 keV X-rays of 12% at FWHM
- New developments of **MicroMEGA**s with pixel readout will integrate amplification grid with the CMOS readout, use 1 μm Al grid above 50 μm ➔ broadening expect excellent spatial and time

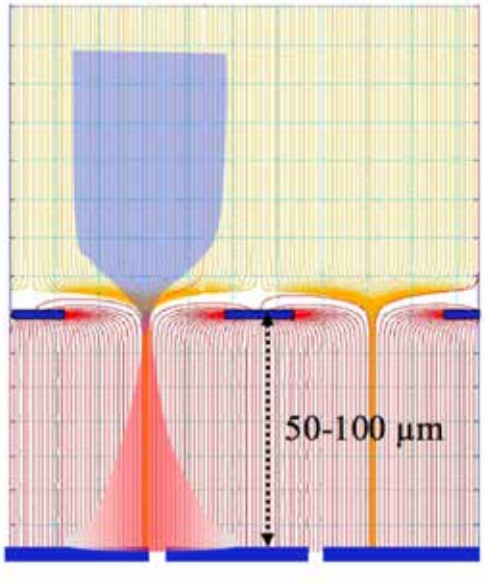

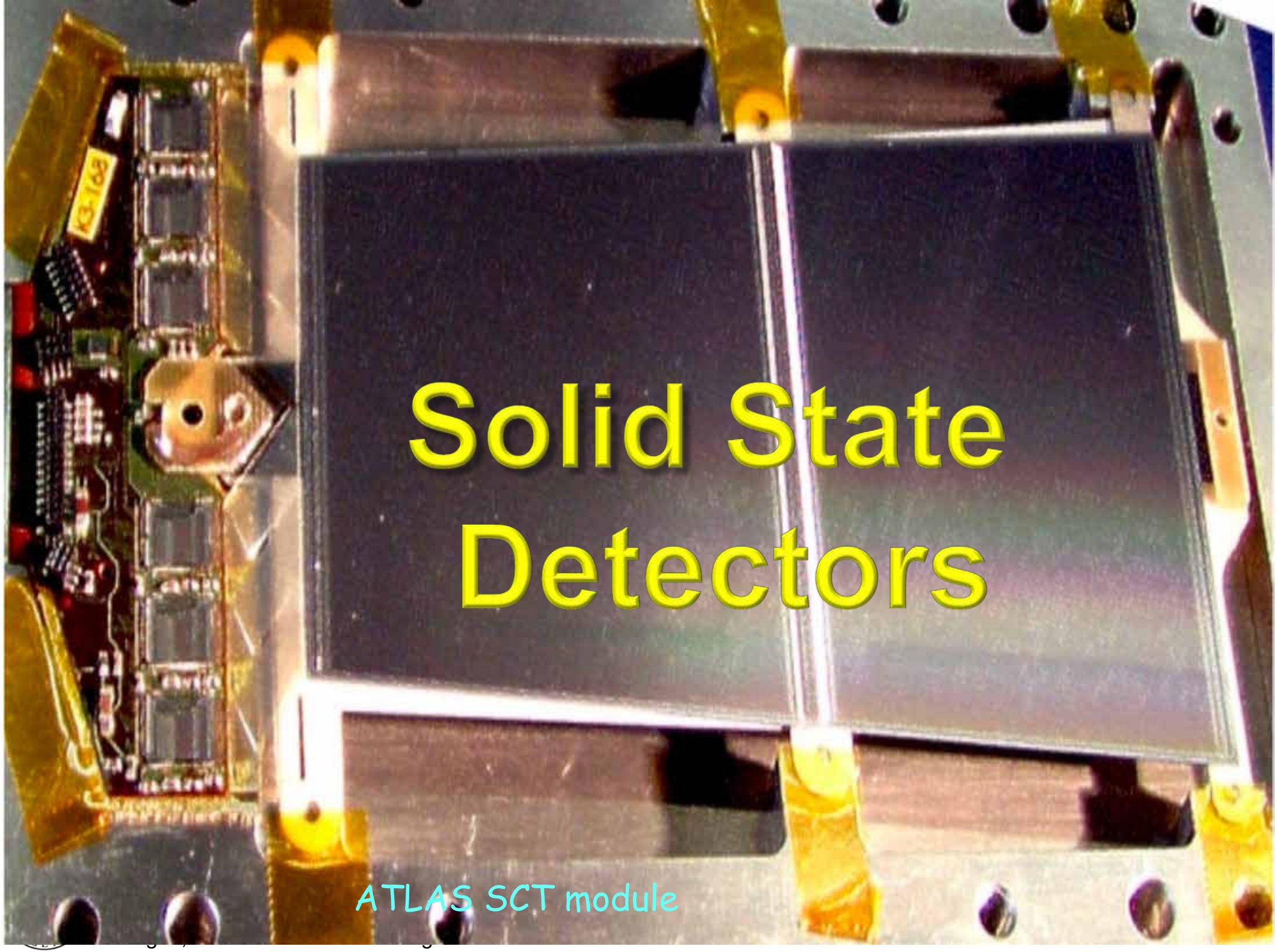
Solid State
Detectors
ATLAS SCT module

# Properties of Silicon

- Si has 4 valence $e^-$
  - ➔ Each valence $e^-$ is coupled to $e^-$ of neighboring atom via covalent bound
- At T=0, all $e^-$ are bound & cannot conduct any current
  - ➔ full valence band, empty conduction band, separation: 1.1 eV
- At room temperature thermal energy is sufficient to liberate $e^-$ into conduction band ($10^{11}/cm^3$)
- However, usually we add controlled level of impurities

  i) Elements with 3 valence $e^-$ (p-type)
  *B, Ga, In* ⇒ hole carriers, acceptor impurity

  ii) Elements with 5 valence $e^-$ (n-type)
  *Sb, P, As* ⇒ $e^-$ carriers, donor impurity

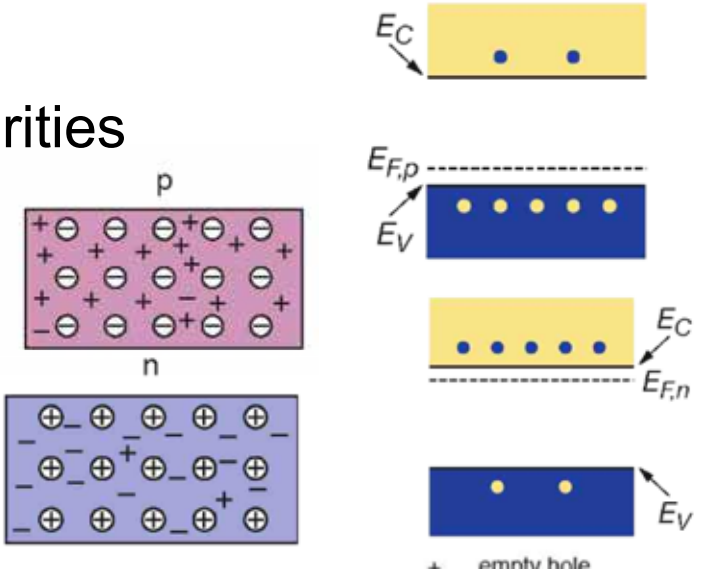


- Concentration of electrons (n) and holes (p) satisfies

$$n \cdot p = N_c N_v \exp\left(\frac{E_g}{kT}\right) = cons$$

$N_v$: # of allowed levels in valence band

$N_c$: # of allowed levels in conduction band

$E_g$: energy gap

# p-n Junction

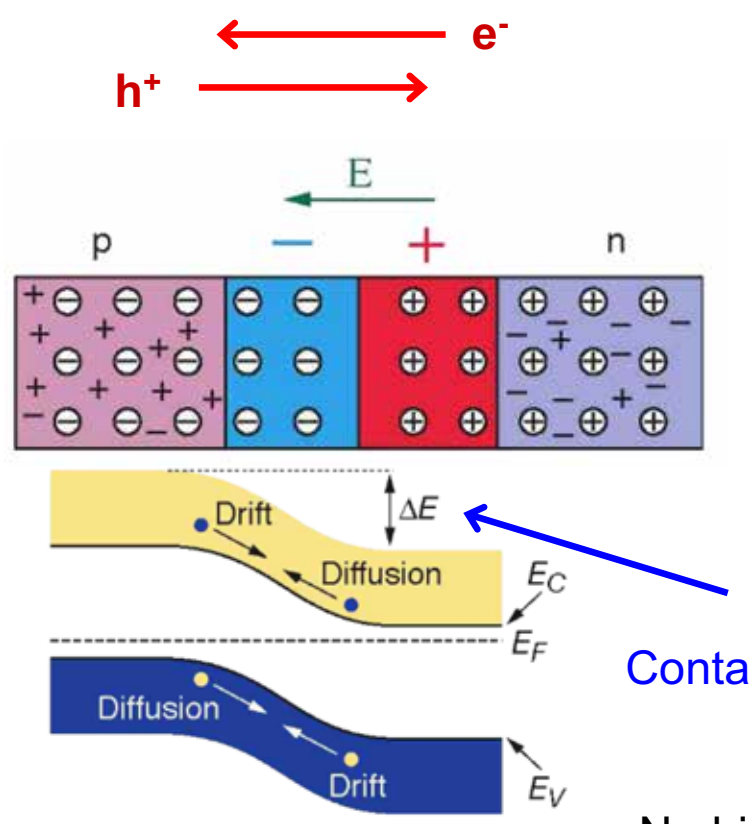


Contact potential $V_0$

No bias voltage

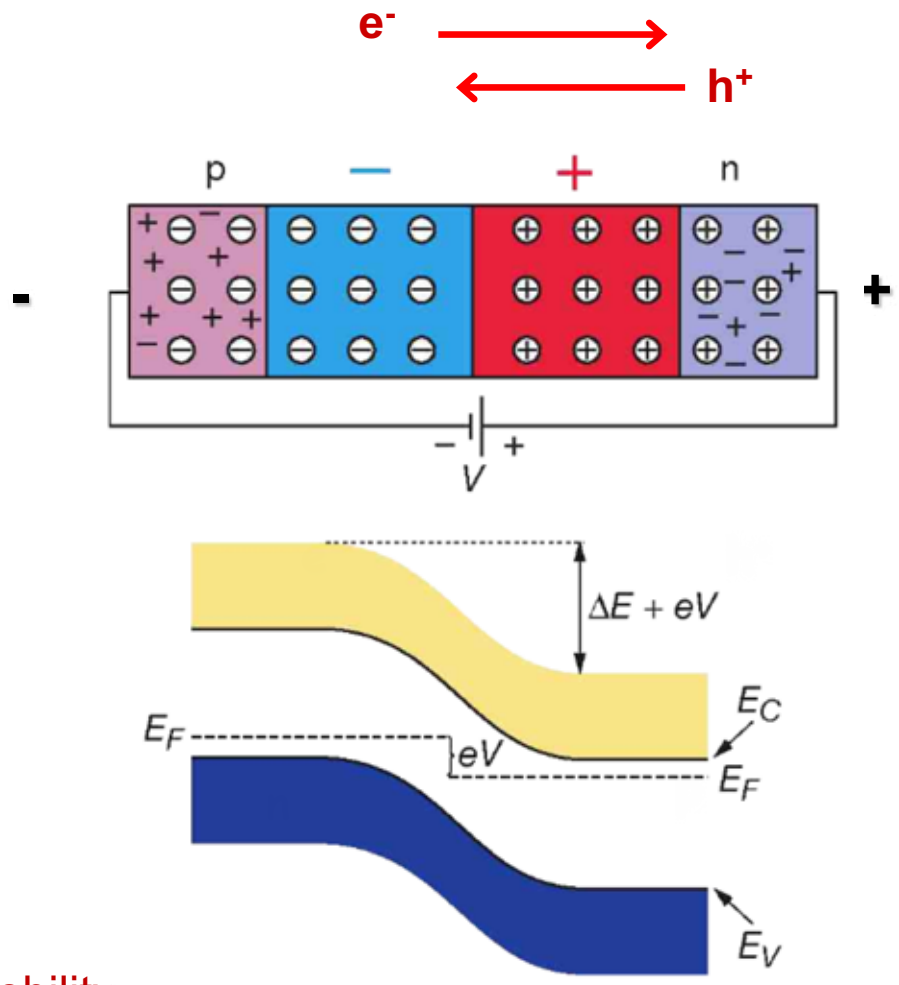


With reverse bias voltage $V_b$

❒ Depletion layer

$$d = x_n = \left(2\varepsilon\varepsilon_0\rho_n\mu_e\left(V_0 + V_b\right)\right)^{1/2}$$

$m_e$: electron mobility
$r_n$: n-region resistivity
e: dielectric constant

❒ When ionization liberates charge in depletion layer, $e^-$ & $h^+$ drift apart due to strong internal field & produce a current

# Si Microstrip Detectors

- A typical n-type Si microstrip detector has
  - $p^+n$ junction: $N_p \approx 10^{15}$ cm$^{-3}$, $N_n \approx 1\text{-}5 \times 10^{15}$ cm$^{-3}$
  - N-type bulk: $\rho$>2 k$\Omega$cm, thickness 300 $\mu$m
  - Operating voltage < 200 V
  - $n^+$ layer at the backplane to improve ohmic contact
  - Aluminum metalization
- About 30000 $e^-h^+$ pairs are liberated by a traversing charged particle via dE/dx by ionization
- Charges drift towards electrodes where they produce a signal on that strip
- Each strip is coupled to a preamplifier
- Use AC-coupling block leakage currents from amplifier

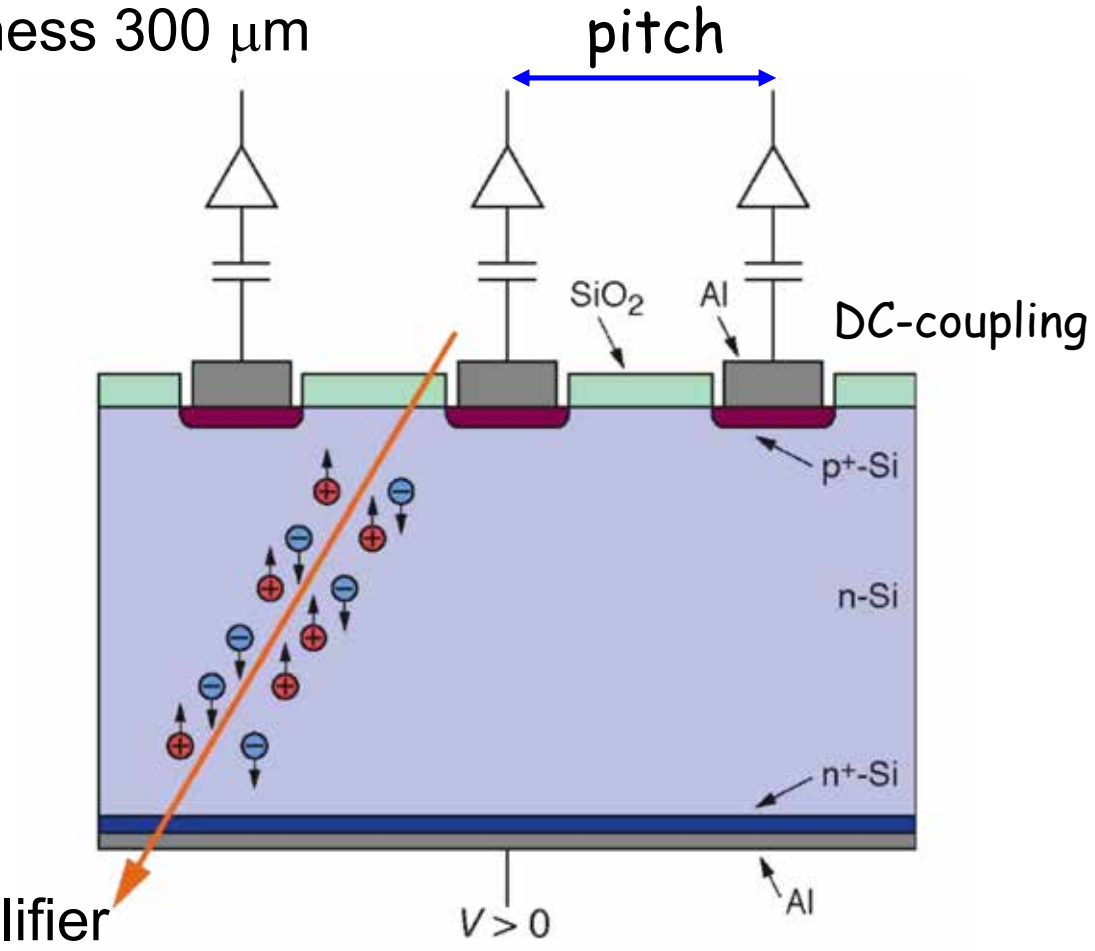

# Noise

- The main source of noise is due to statistical fluctuations in the number of carriers, leading to changes in conductivity
- The most important noise contributions are (Equivalent Noise Charge)
  - leakage current ($\overline{ENC_I}$)
  - detector capacity ($\overline{ENC_C}$)
  - detector parallel resistor ($\overline{ENC_{Rp}}$)
  - detector serial resistor ($\overline{ENC_{Rs}}$)

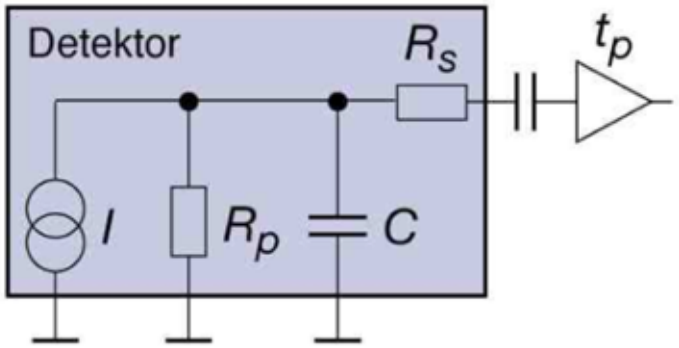

Alternate circuit diagram of a silicon detector.

- The overall noise is the quadratic sum of all contributions
- The detector capacity is typically the dominant noise source

$$\overline{ENC_C}^2 = 8kTC_d / f_T \tau_f$$

$\tau_f$: time constant of filter

$f_T$: frequency for unity gain of amplifier

kT=25.85 T/300K [meV]

- For typical values of $f_T$=1GHz and $\tau_f$=100 ns we estimate $\overline{ENC_C}$=1.13×10$^2$ $C_d^{1/2}$ [rms e$^-$] with $C_d$ in pF

Signal: 30,000e$^-$

  - for $C_d$=1pF ➔ $\overline{ENC_C}$≈113 e$^-$, for $C_d$=100pF ➔ $\overline{ENC_C}$≈1130 e$^-$

# Position Resolution

- The dE/dx energy loss produces a Landau-like distribution that is different for pions and protons of the same momentum

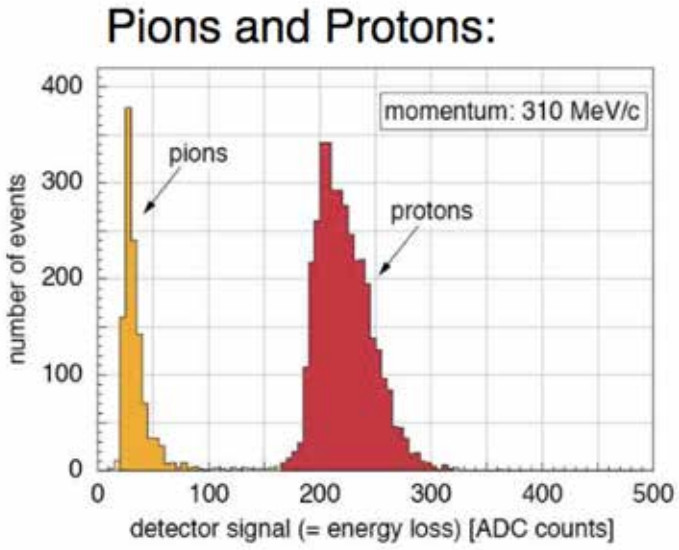


- For a single strip the position resolution is

$$\sigma_x = \frac{p}{\sqrt{12}}$$

$p$: pitch

- For two or more strip hits we use the center-of-gravity method

- Here, a large signal-to-noise (S/N) ratio improves the spatial resolution

$$\sigma_x \propto \frac{p}{S/N}$$

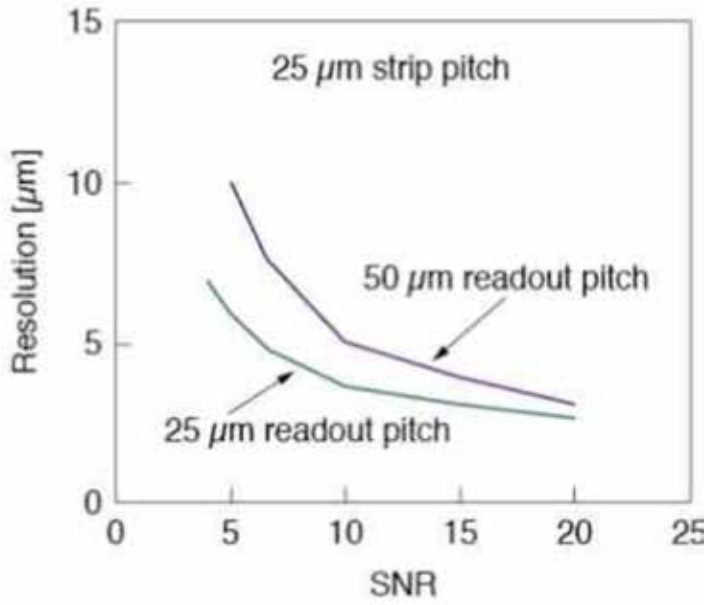


- Diffusion broadens the spatial resolution
  ➔ broadening depends on the drift length

# ATLAS Semi-Conductor Tracker

- 4 layers with 2 planes each, r-φ strips and r- φ strips slightly tilted by 40 mrad

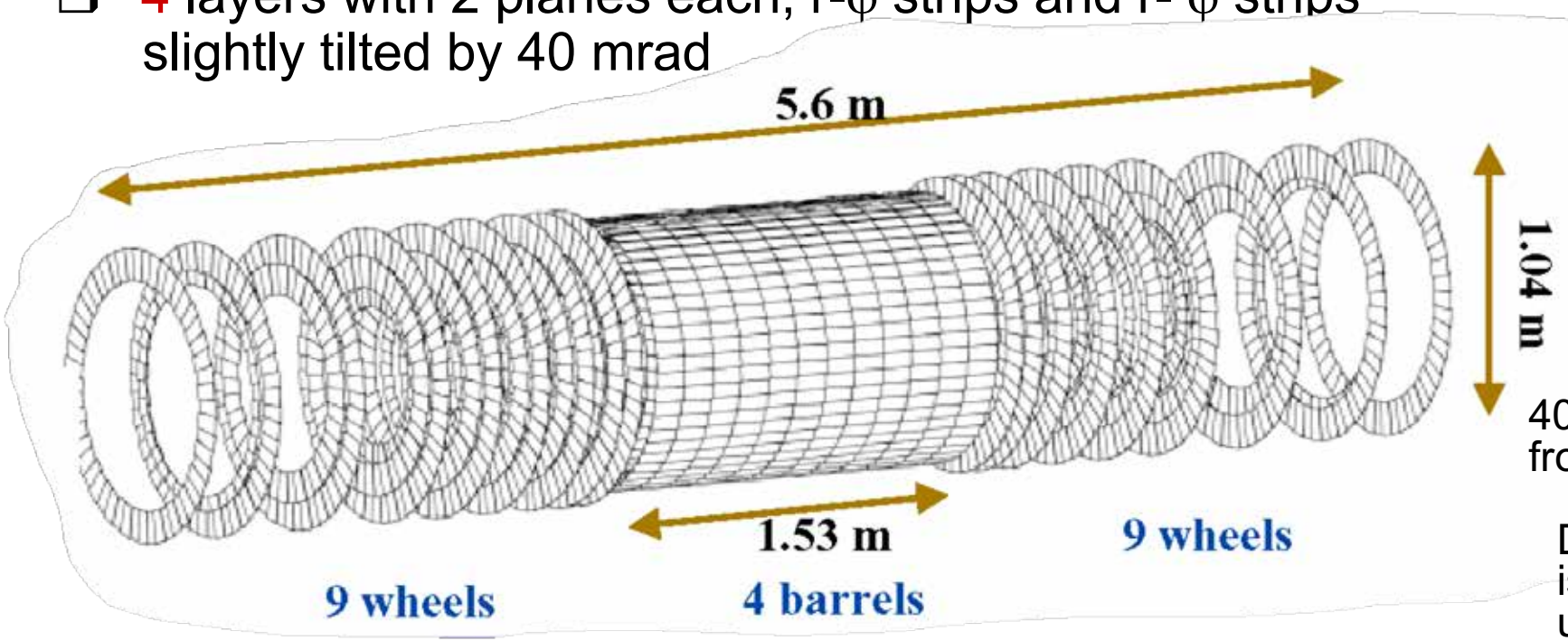


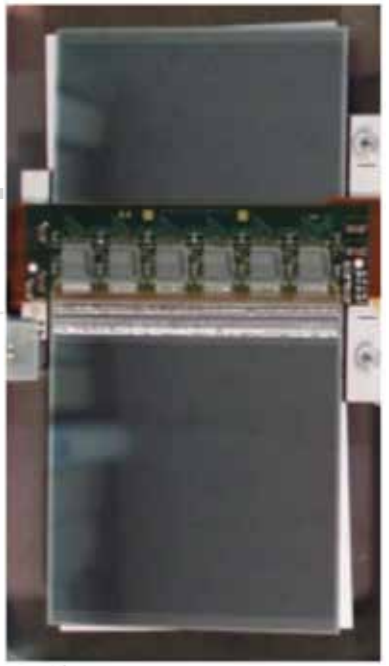

**SCT** module
40 mrad between
front & back sensor

Due to radiation issues ATLAS uses p-in-n Si

- In $\phi$, modules are tilted wrt to surface of support structure by ($11^0$, $11^0$, $11.25^0$ & $11.5^0$)
- ~ 61 $m^2$ of Si, ~$6.3\times10^6$ readout channels
- Sensor thickness: 285 μm, 80 μm pitch
- Position resolution in barrel from $Z\rightarrow\mu^+\mu^-$: $\sigma_{x,y}$=24.0 μm

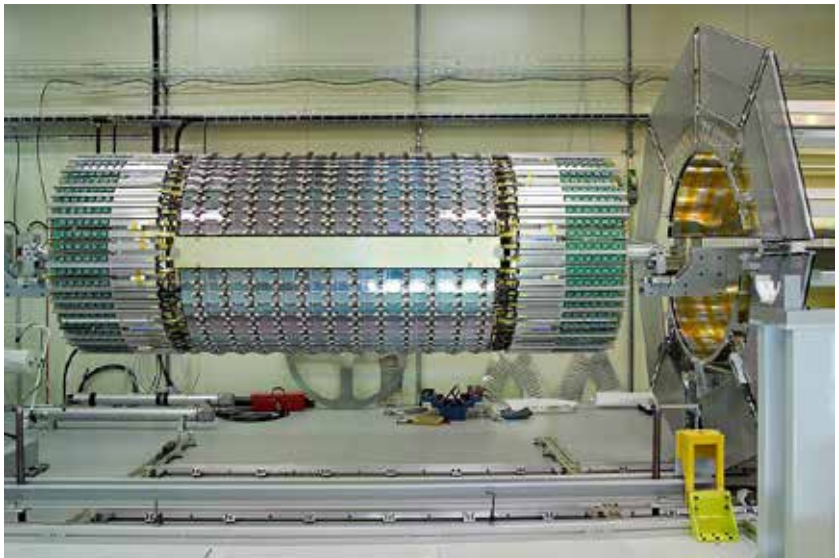

# Power of Microstrip Detectors

- The power of Si vertex detector measurements (ALEPH)

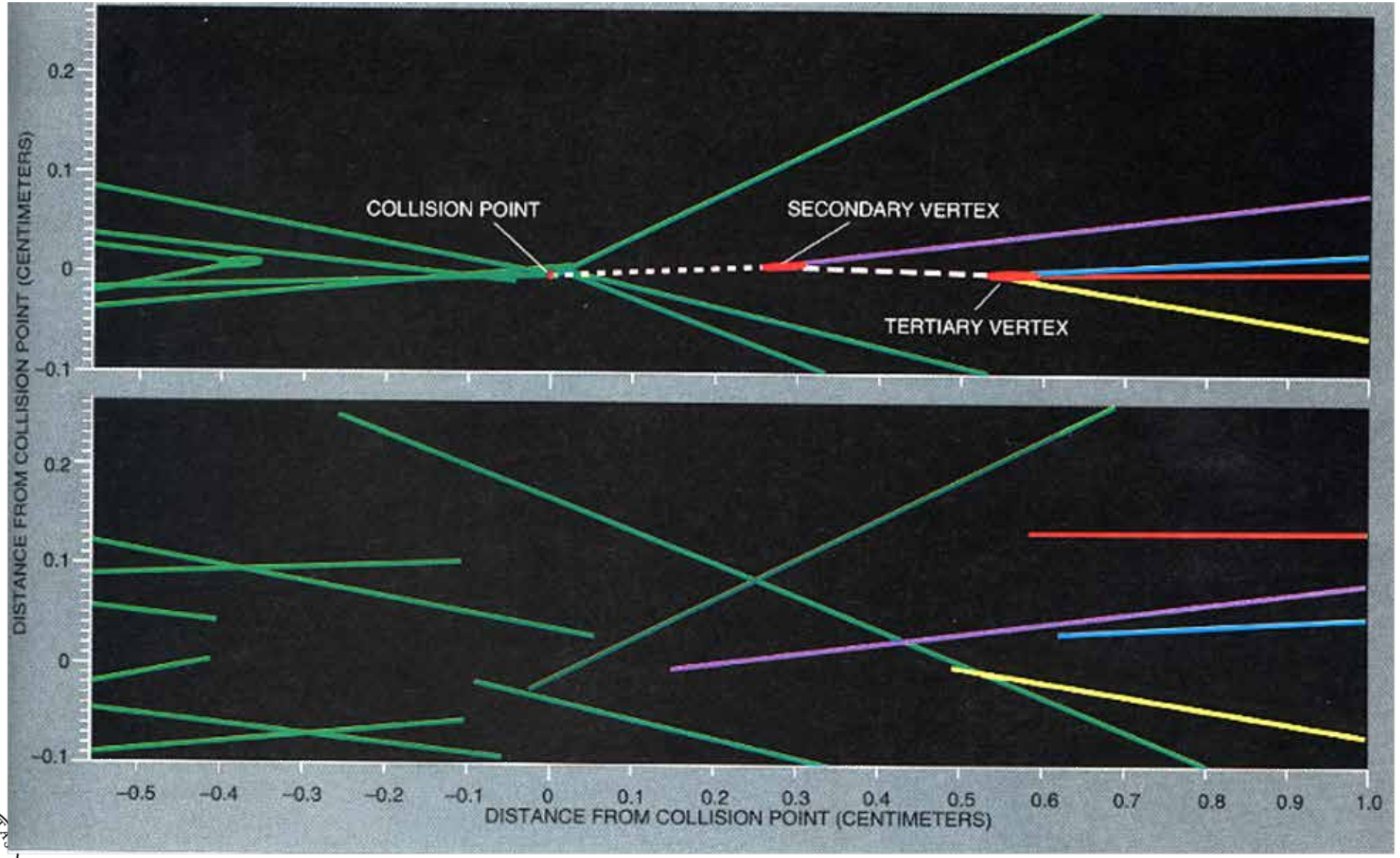

# Pixel Detectors

- Pixel detectors are made of an array of small Si pixels, i.e. physically isolated pads, providing both r-φ & z measurements
- Pixels are bump-bonded to a pixelated readout chip
- Advantage: excellent 2-track resolution, take high occupancies
  ➔ important for high rates close to beam pipe
- Typical pixel dimensions:
  ATLAS: $50\times300\ \mu m^2 \Rightarrow 8.\times10^7$ pixels
  CMS: $150\times150\ \mu m^2 \Rightarrow 3.9\times10^7$ pixels

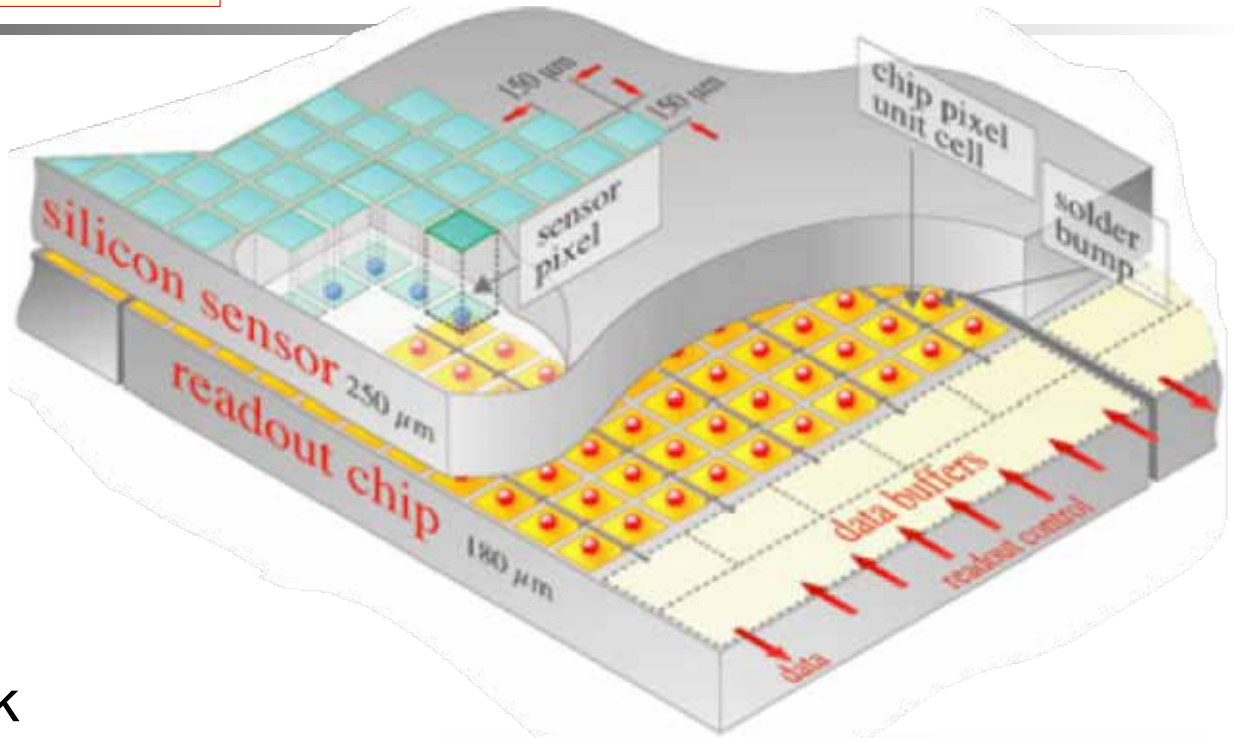


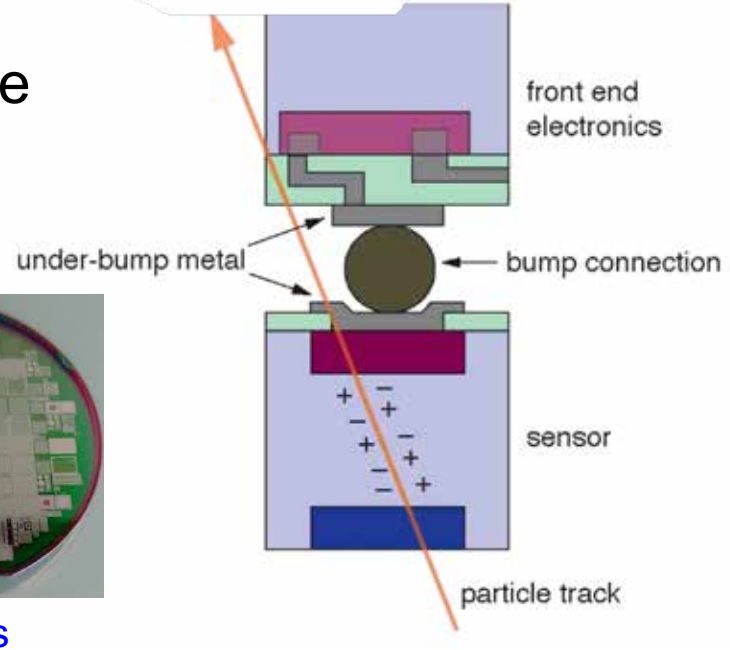


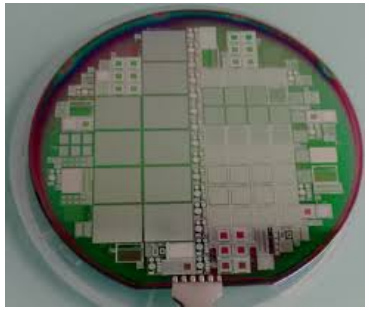

ATLAS pixels

# ATLAS Pixel Detector

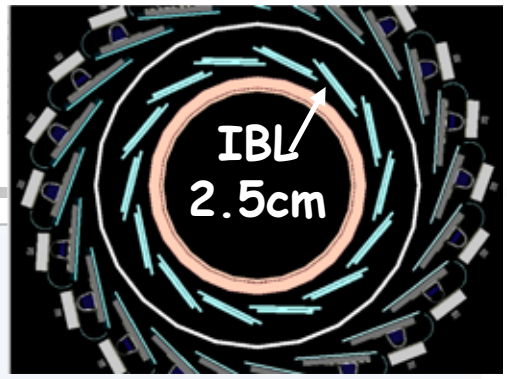


- ATLAS Pixel detector

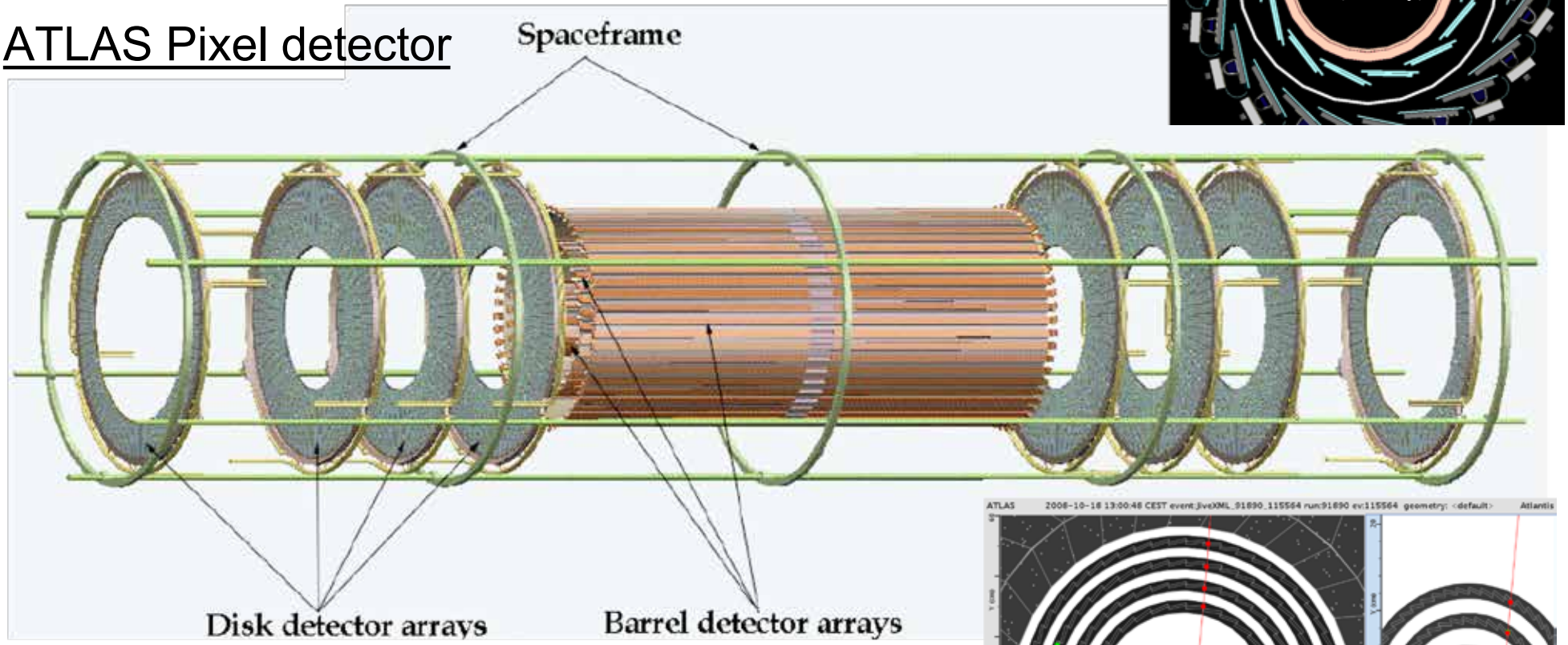


Barrel: r= 2.5 cm, 5.05 cm, 8.85 cm, 12.25 cm

Endcap: z=±49.5 cm, ±56 cm, ±65 cm

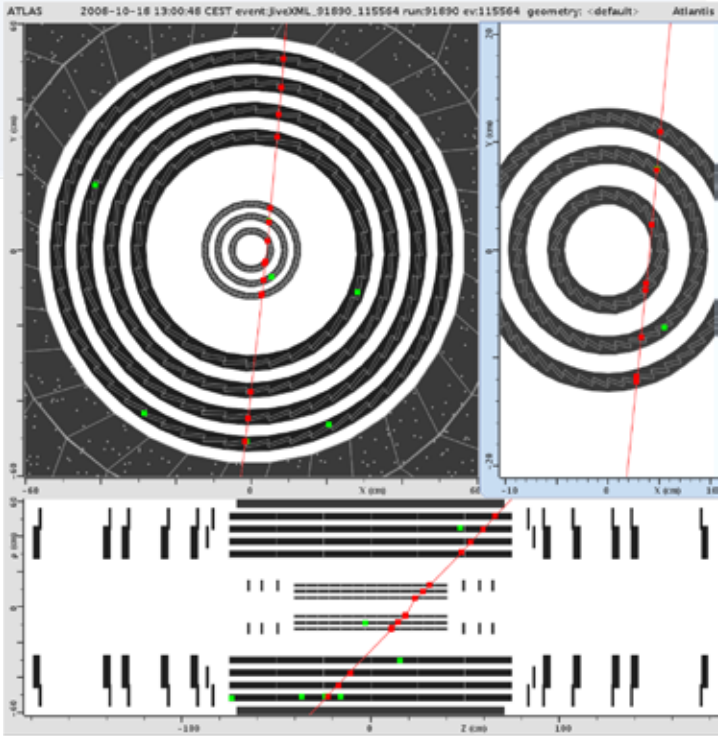

- Position resolution from $Z \rightarrow \mu^+\mu^-$:
  $\sigma_x$=9.0 μm, $\sigma_y$=87.0 μm

- Cosmic muon traversing through the pixel detector and SCT


ATLAS solonoid

# Deflections in Magnetic Fields

- Particles with transverse momenta $p_t$ placed in a magnetic field $\vec{B}$ =(0,0,B) are deflected along a circular orbit with radius $R = p_t/(e|\vec{B}|)$

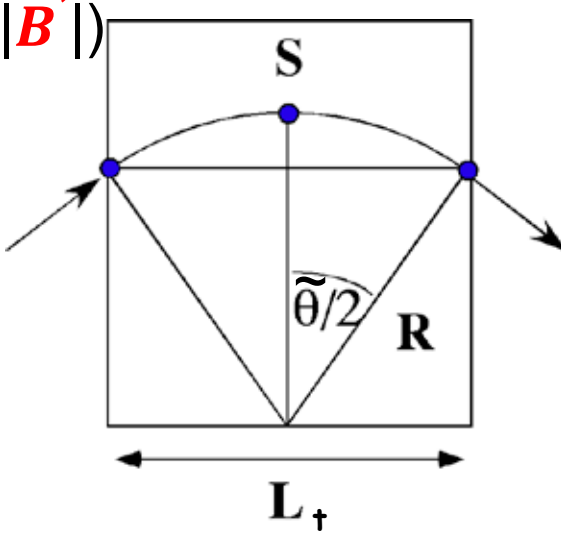


- If the magnetic field is active on length $L_t$, the change in transverse momentum for small deflection angles is $\Delta p_t = p_t \cdot \sin\tilde{\theta} \simeq -eBL_t$

- The error in position measurement $\sigma(x)$ leads to an error in the momentum measurement via

$$\frac{\sigma_{p_t}}{p_t} = \frac{2p_t}{\Delta p_t}\frac{\sigma_x}{h}$$

h: lever arm for angle measurement before & after magnet

- Example: $|\vec{B}|$=0.5 Tm, $\sigma$(x)=300 $\mu$m p= 100 GeV/c & $h$=3cm ➔ $\sigma_{pt}/p_t$~1.3%

- If the position is measured at 3 equidistant points along $L_t$, sagitta S of circular orbit is given by $S = 0.038 \cdot B_z L_t^2 / p_t$ with precision $\sigma_s = \sqrt{3/2}\sigma_x$

For $N$ measurements precision becomes $\sigma_s = \sqrt{\frac{720}{N+4}}\sigma_x$

# Momentum Resolution

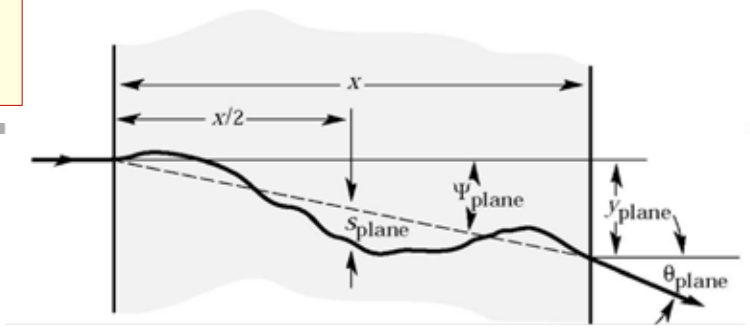


- The momentum resolution typically has a contribution from the position measurement and one from multiple scattering
- If $\sigma_{r\varphi}=\sigma_x$ is measurement error in (r-φ) plane, $p_t$ is measured with uncertainty:

$$\left(\frac{\sigma_{p_t}}{p_t}\right)^{M} = \frac{\sigma_{r\varphi} p_t}{0.3BL_t^2}\sqrt{\frac{720}{N+4}}$$

Typically is larger

- Multiple scattering yields mean $p_t$ change:

$$\Delta p_t^{MS} = 21\text{MeV}\sqrt{\left(\frac{L_t}{X_0}\right)}$$

- This leads to an multiple scattering error of:

$$\left(\frac{\sigma_{p_t}}{p_t}\right)^{MS} = \frac{0.05}{BL_t}\sqrt{\left(\frac{1.43L_t}{X_0}\right)}$$

Typically is smaller

- The two contributions have to be added in quadrature ➔ transverse momentum resolution has the form

$$\frac{\sigma_{p_t}}{p_t} = a \cdot p_t \oplus b$$

- Obtain total momentum from z-direction $p = \frac{p_t}{\sin\theta}$ where $\theta$ is the track angle wrt

# Electrons and Photons in Matter

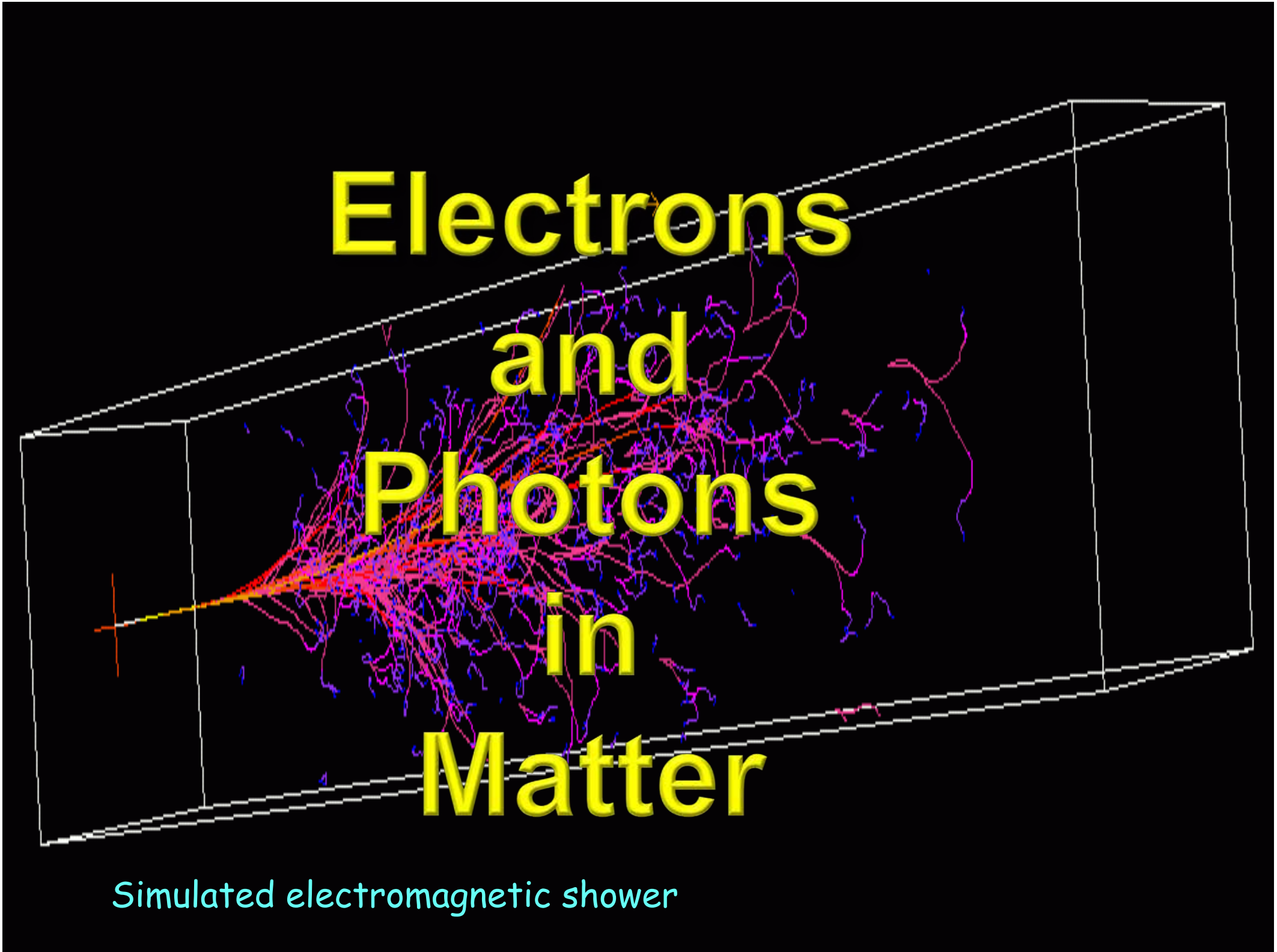

Simulated electromagnetic shower

# Energy Loss of Electrons & Positrons

- Electrons & positrons suffer energy losses via radiation in addition to the energy losses via collisions

- Thus $$\left(\frac{dE}{dx}\right)_{tot} = \left(\frac{dE}{dx}\right)_{rad} + \left(\frac{dE}{dx}\right)_{coll}$$

- The basic mechanism of energy loss via collisions is also valid for $e^{\pm}$, but Bethe-Bloch equation must be modified for 3 reasons:

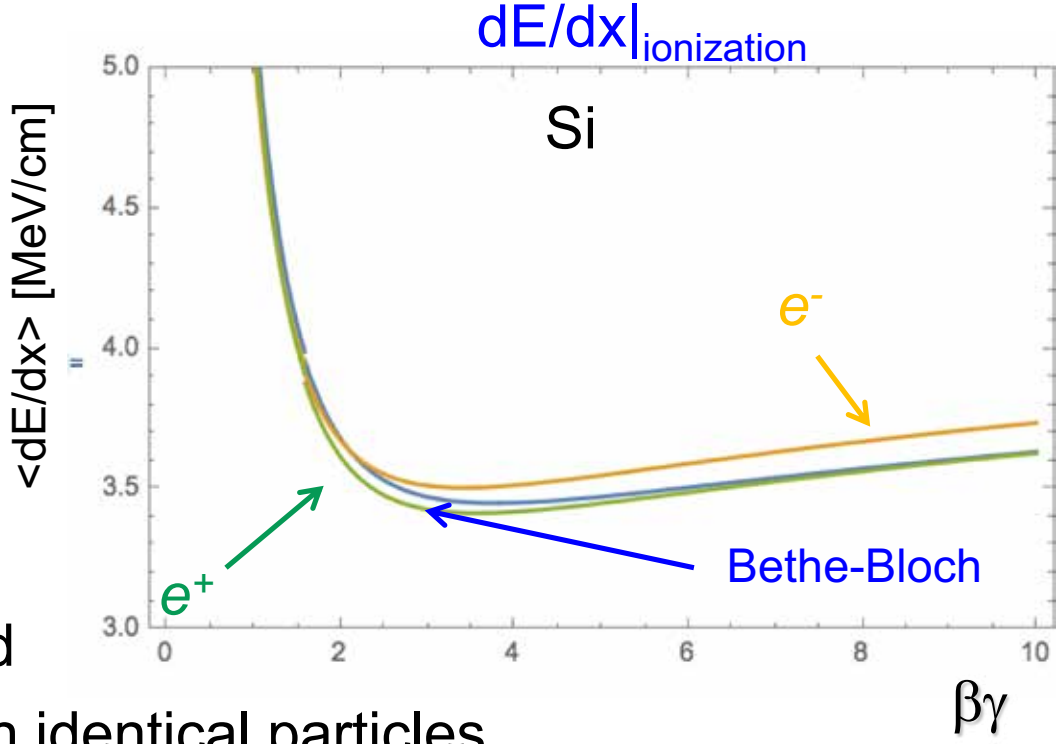


i) their small mass
➔ Incident particle may be deflected

ii) For $e^-$ we have collisions between identical particles
➔ Account for indistinguishable particles
➔ Obtain some modifications, e.g. $T_{max}=T_e/2$

iii) $e^+$ and $e^-$ are fermions while heavy particle are typically bosons

- The energy loss for $e^+$ ($e^-$) is obtained by replacing the photoabsorption ionization cross section (slide 6) with the Bhabha (Møller) cross sections

# Energy Loss of Photons

- A photon traversing a medium can experience different processes
  - i) **Photoelectric absorption**
  - ii) Rayleigh scattering
  - iii) **Compton scattering**
  - iv) **Pair creation in nucleon/electron field**
  - v) Photonuclear interaction

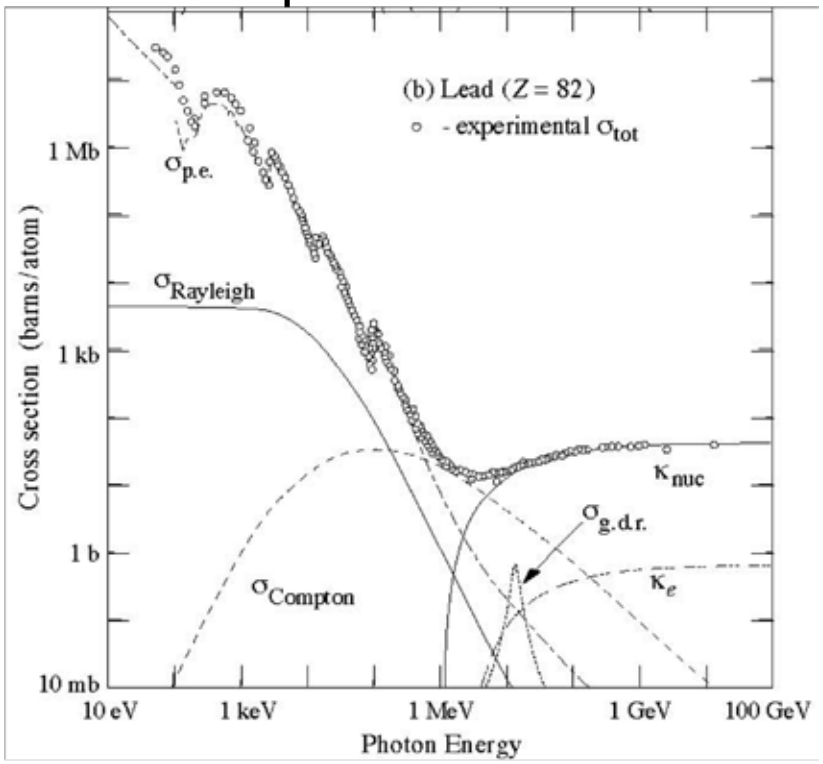


- All processes reduce initial intensity

$$I(z) = I_0 \cdot \exp(-\mu z)$$

where $\mu$ is linear absorption coefficient that is related to photon absorption cross section $\sigma$ by $\mu = \sigma N_0 \rho / A$

- **Photoelectric absorption** decreases as $\sim 1/E_\gamma^{3.5}$ & increases as $Z^5$ (e.g. for energies between K&L)

- **Compton scattering** decreases as $1/E_\gamma$ & increases as $Z$

- **Pair creation** requires minimum energy of $E_\gamma \geq 2m_e c^2$

# Critical Energy and Radiation Length

- The critical energy, $E_c$, is the energy where $(dE/dx)_{rad}=(dE/dx)_{ion}$
- Approximate formulae

$$E_c = \frac{610}{Z+1.24} \text{ for solids} \qquad E_c = \frac{710}{Z+0.92} \text{ for gases}$$

E.g. Pb: $E_c$=7.3 MeV
Air: $E_c$=102 MeV

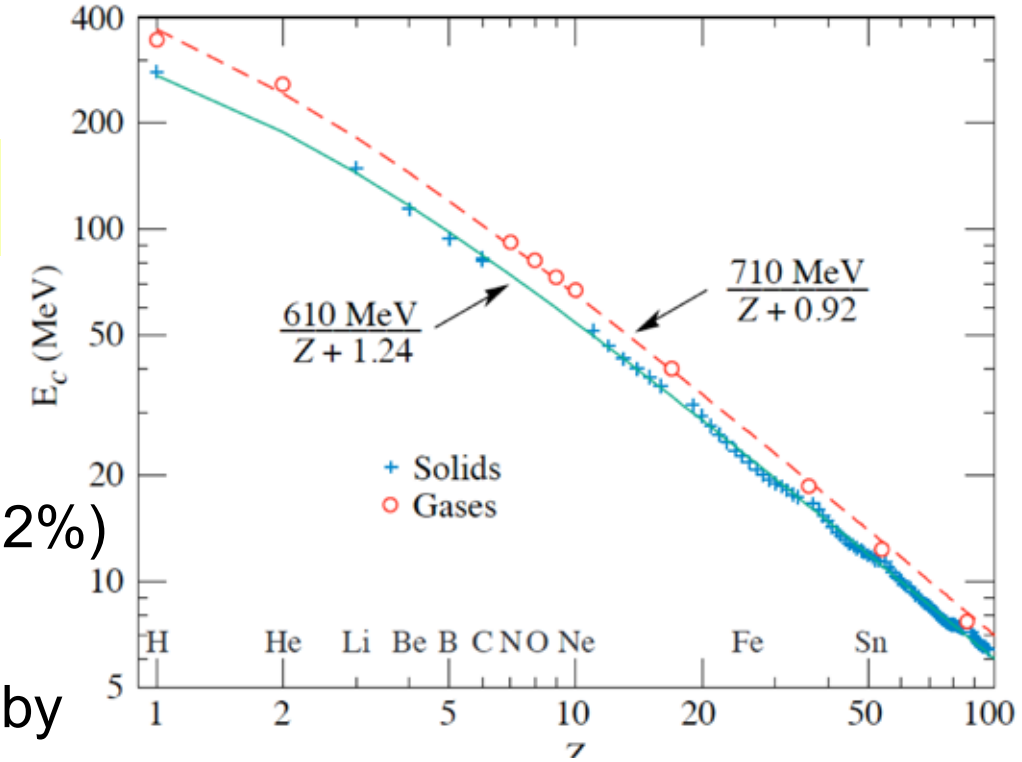


- Calculated $E_c$ values agree well with with approximate formulae (solids: <2%)
- The radiation length is the distance over which the $e^-$ energy is reduced by 1/e=37% due to radiation loss only
- The radiation length depends only on the parameters of the material

$$\frac{1}{X_0} \cong 4\alpha r_e^2 \rho \frac{N_0}{A}\left\{Z^2\left[\ln\left(184.15\cdot Z^{-\frac{1}{3}}\right)-f(Z)\right]+Z\cdot\ln\left(1194\cdot Z^{-\frac{2}{3}}\right)\right\}$$

$H_2$: $X_0$=63 [g/cm$^2$]
Al: 24 "
Pb: 6.3 "

$N_0$: Avogadro's # $6.022\times10^{23}$ mole$^{-1}$

protons

electrons

f(z): Coulomb correction

# Electron-Photon Showers

- At high energy a photon is likely to convert into $e^+e^-$
- $e^\pm$ particles loose energy via bremsstrahlung producing new $\gamma$'s that are likely to convert into $e^+e^-$
- Result is a cascade or shower of $e^+$, $e^-$, & $\gamma$'s
- Process stops once energies of $e^+$ $e^-$, & $\gamma$'s become so small that energy loss of $\gamma$'s occurs preferentially via photoelectric absorption & that energy loss of $e^+$ & $e^-$ occurs preferentially via ionization ($E_e \approx E_c$, $E_\gamma \approx E_c$)
- A similar shower is obtained if we start with a high-energy $e^-$ or $e^+$

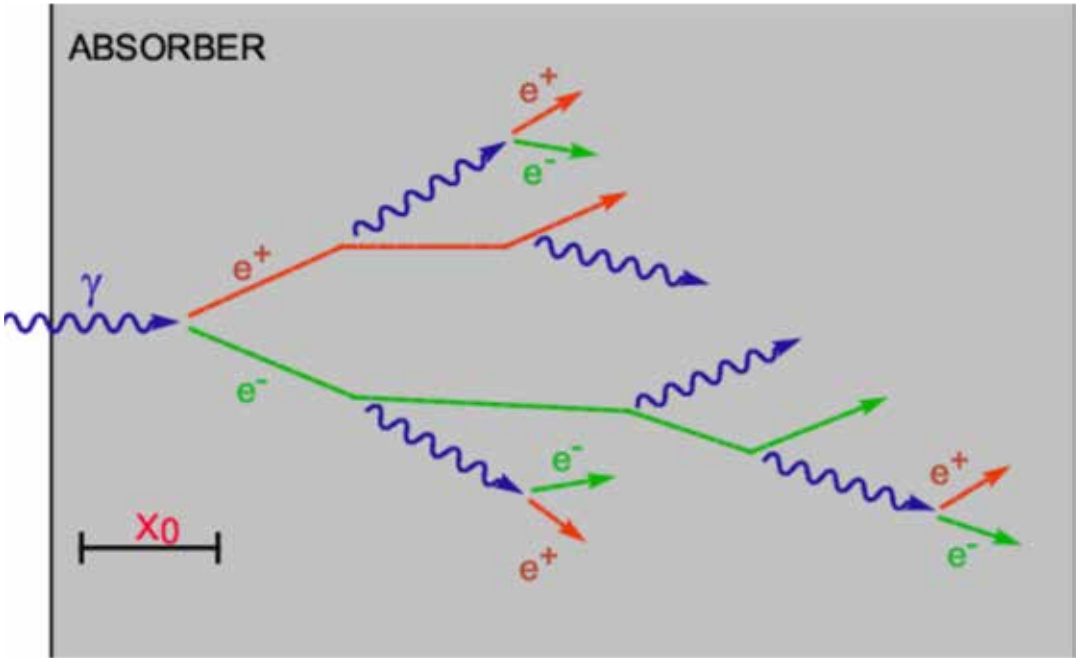

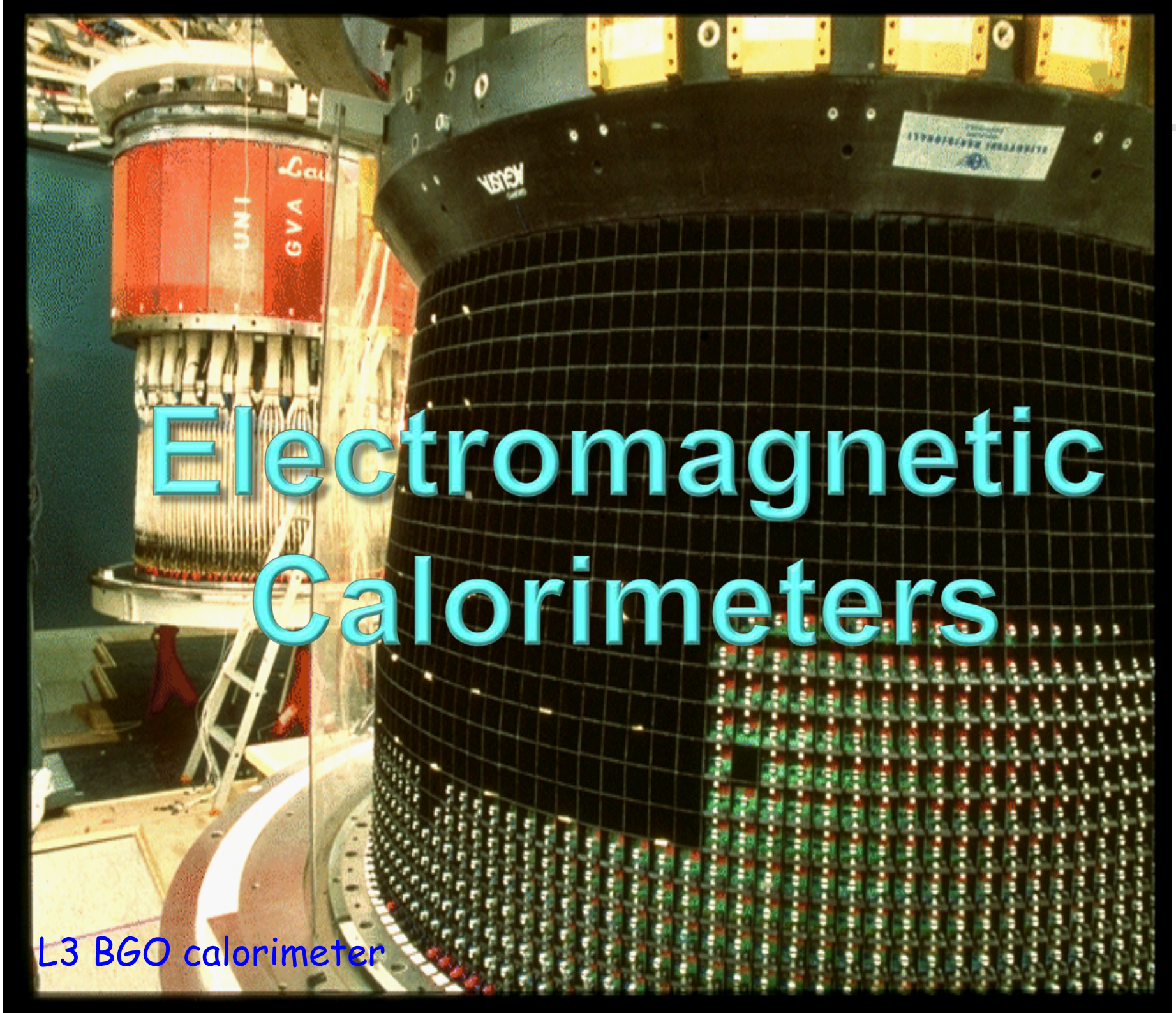
Electromagnetic
Calorimeters
L3 BGO calorimeter

# Characteristics of $e^-$-$\gamma$ Shower

- The most exact calculations of detailed shower development is obtained with MC simulations (based on program EGS IV)

- Properties of electron-photon shower started by $\gamma$ ($e^-$) with initial energy $E_0$
  - i) Number of particles at shower maximum, $N_p$, is proportional to $E_0$
  - ii) Total track length s of $e^-$ & $e^+$, is proportional to $E_0$
  - iii) Depth at which shower maximum occurs, $X_{max}$, increases as ln ($E_0$)

$$X_{max} = X_0 \left[ \ln\left(\frac{E_0}{E_c}\right) + t \right]$$

where t=-0.5 for $e^-$
& t= 0.5 for $\gamma$

- Example: photon in NaI crystal: $E_0$ =1 GeV, $X_0$=2.59 cm, $E_c$=12.5 MeV
  - ➔ $N_p$=80, n=6.3, & $X_{max}$=11.8 cm

- Basically 2 types of em calorimeters
  - 1) homogeneous shower counters:
    - inorganic crystals [NaI, CsI(Tl), BGO, $BaF_2$, $PbWO_4$, LSO, LYSO]
    - Pb glass
    - liquid noble gases [Ar, Kr, Xe]
  - 2) sampling shower calorimeters

# Energy Resolution of Homogeneous Calorimeter

- The energy resolution of a crystal calorimeter is given by:

$$\left(\frac{\sigma_E}{E}\right)^2 = a^2 + \left(\frac{b}{\sqrt{E}}\right)^2 + \frac{c^2}{E^2}$$

Constant term — stochastic term — noise term

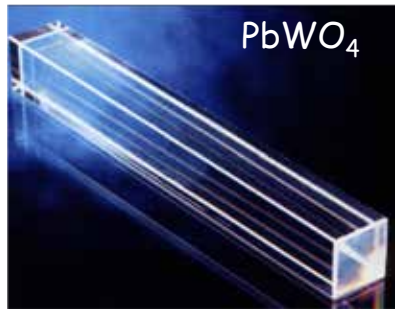


CMS ECAL: $PbWO_4$ calorimeter

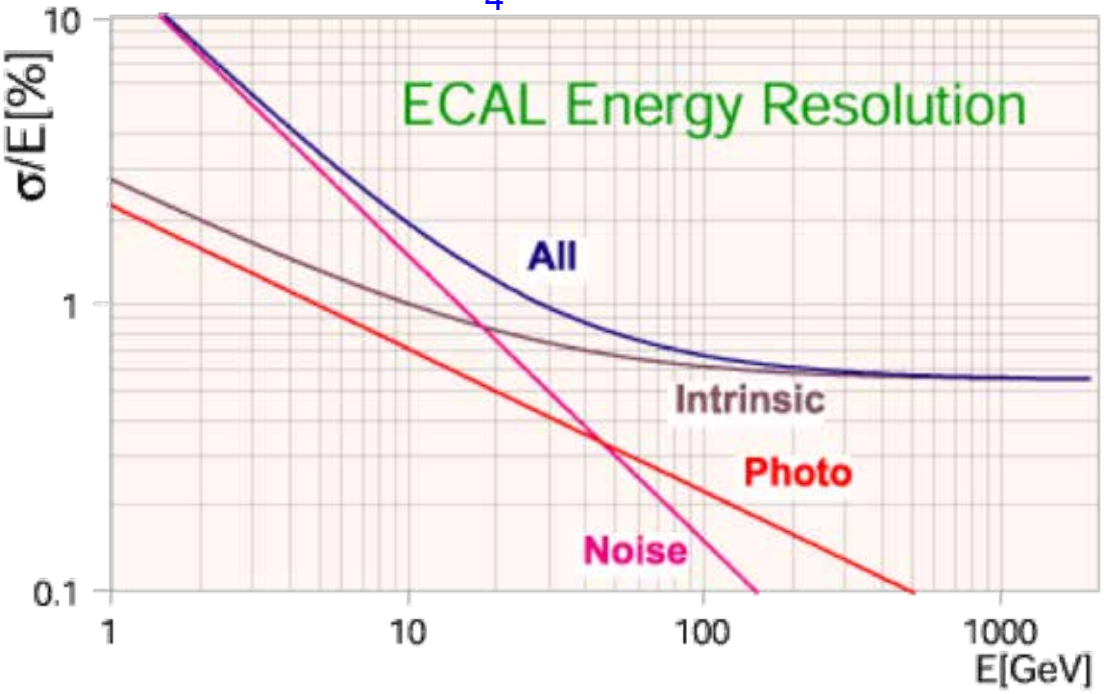


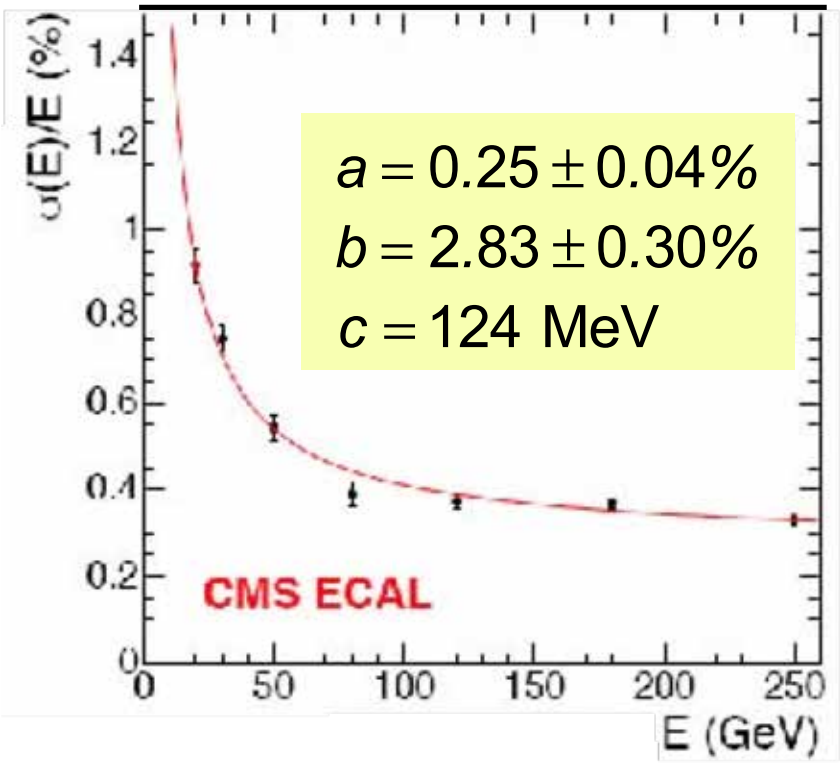


- For some crystals like NaI & CsI, stochastic term has $1/\sqrt[4]{E}$ dependence

# Sampling Shower Detectors

- In sampling calorimeters the fluctuations of energy degradation & energy measurement are separated in alternating layers of different substances
- The choices for passive absorber are plates of Fe, Cu, W, Pb, U
- For energy measurement a gas mixture, liquid noble gases, or plastic scintillators are used
- This allows to build rather compact devices & permits optimization for specific experimental requirements $\Rightarrow e^- - \pi$ discrimination
  - ➔ longitudinal shower profile
  - ➔ good angular measurements
  - ➔ good position measurements

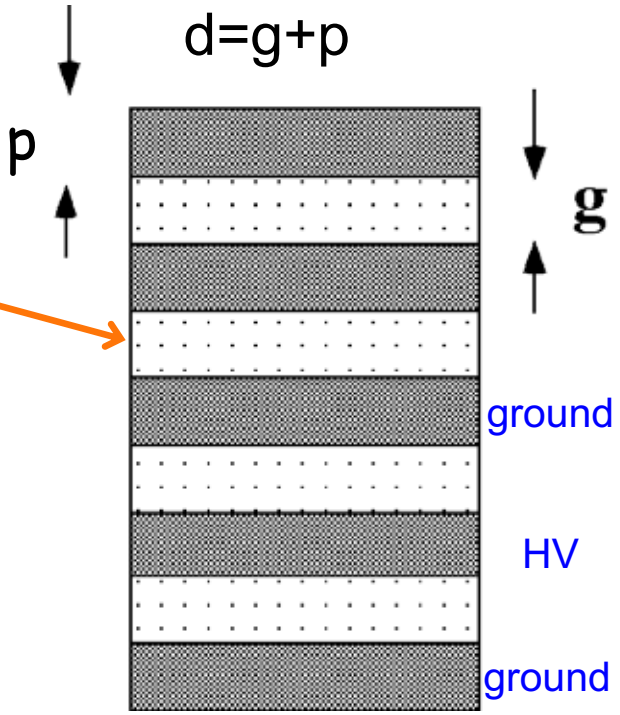


- Plate thickness p ranges from fraction of $X_0$ (EM) to few $X_0$(hadronic)
- Disadvantage: only a fraction of total energy of em shower is detected in active planes (sampling) ➔ additional sampling fluctuations
- Total energy resolution is quadratic sum of sampling fluctuations, Landau fluctuations and path length fluctuations (see backup)

# Longitudinal & Transverse Distributions

- Longitudinal energy distribution is parameterized by with $\beta=0.5$, $\alpha=\beta t_{max}$, $c=\beta^{\alpha+1}/\Gamma(\alpha+1)$,& $t=X/X_0$

$$\frac{dE}{dt} = E_0 C t^{\alpha} e^{-\beta t}$$

- Transverse shower dimensions results from MS of low-energy $e^+$ & $e^-$
- Useful unit for transverse shower is Molière radius $R_M = 21\,\text{MeV}\ X_0/E_c$
- Transverse energy distribution in units of $R_M$ independent of material
  ➔ inside $1R_M$ 90% of shower is contained ➔ inside $3R_M$, 99% of shower

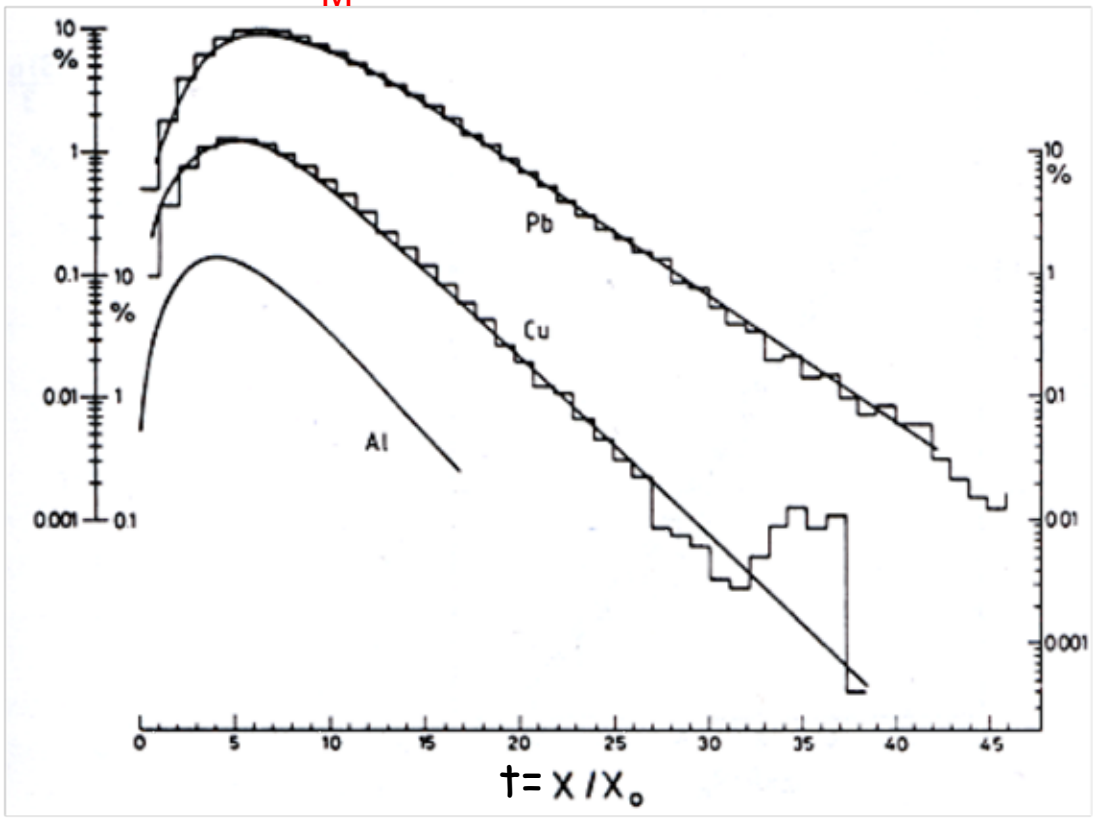


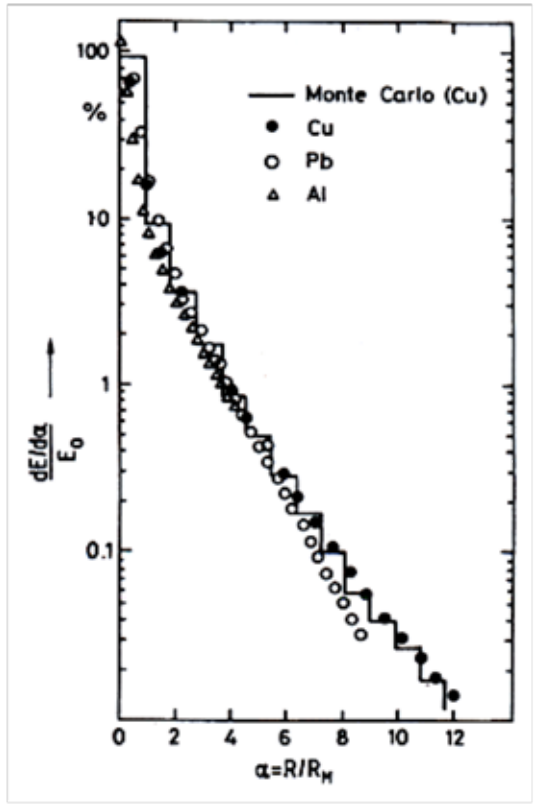

# A Simulated EM Shower

- Simulation of em shower using EGS IV

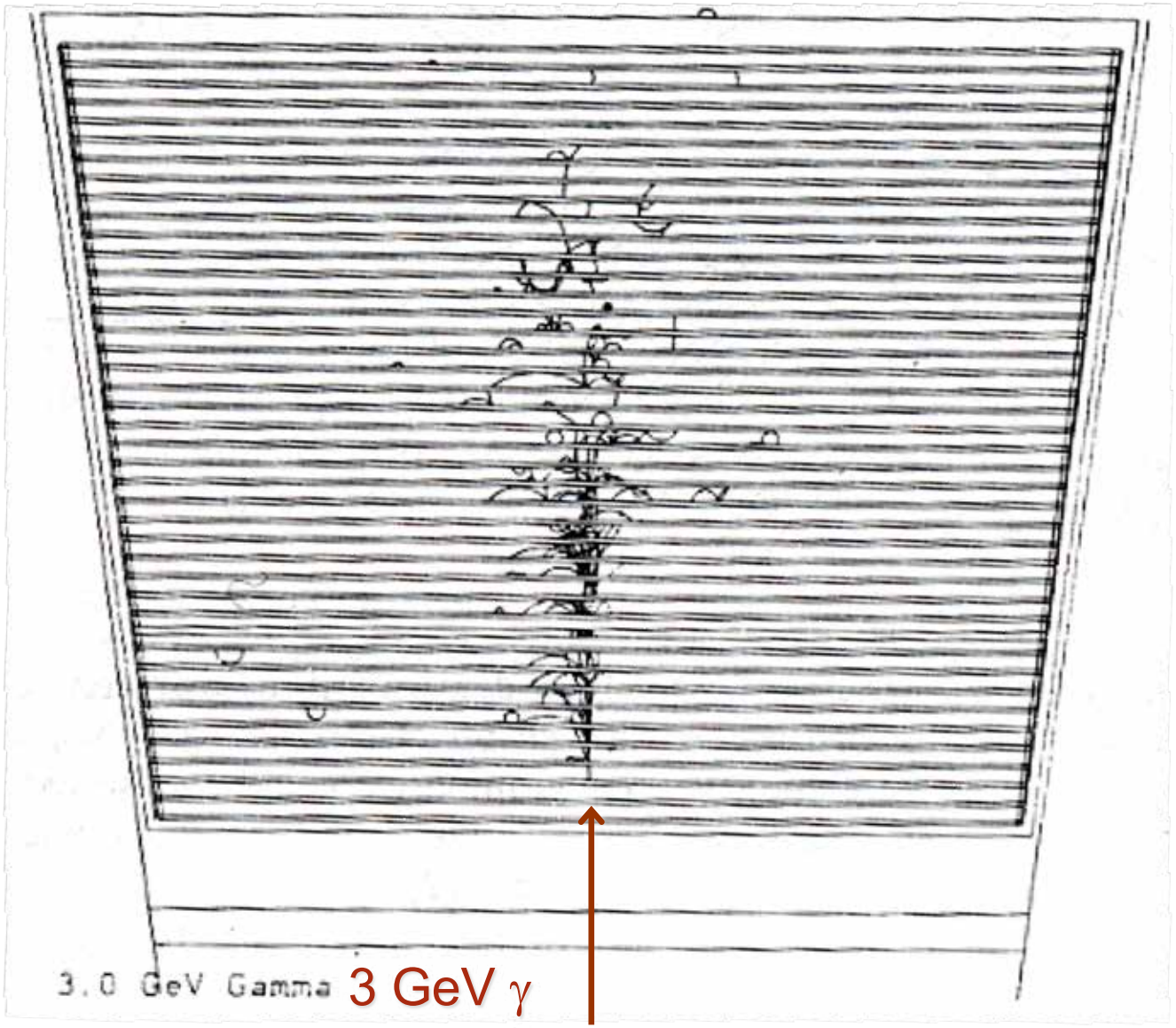

# ATLAS Liquid Argon ECAL

- ATLAS Pb-LiAr sampling calorimeter

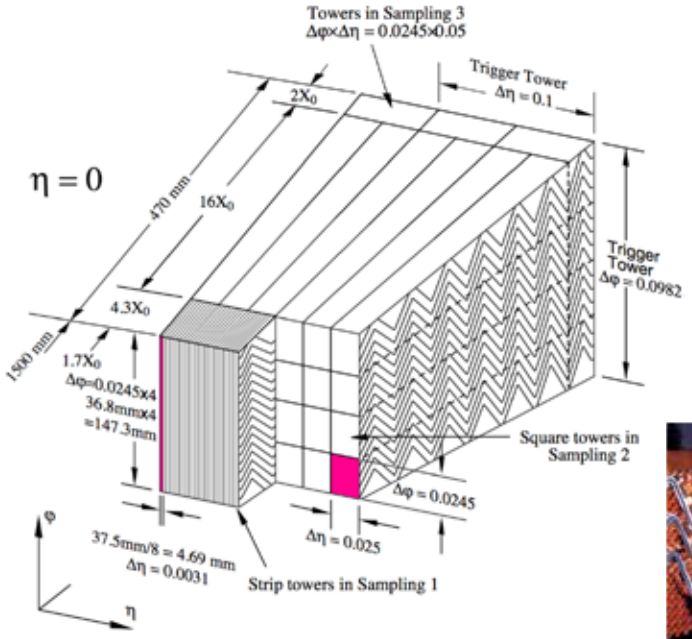


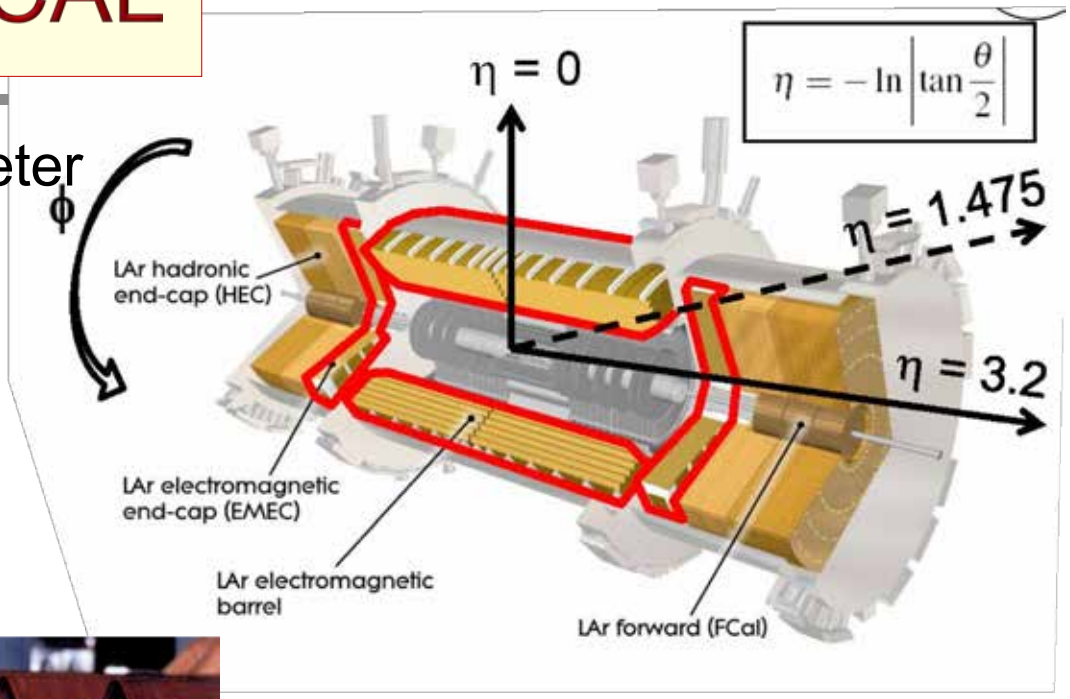


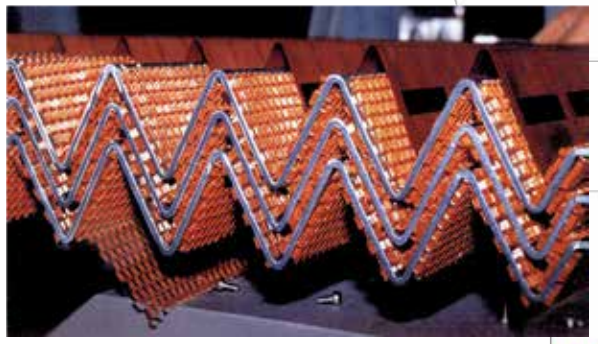

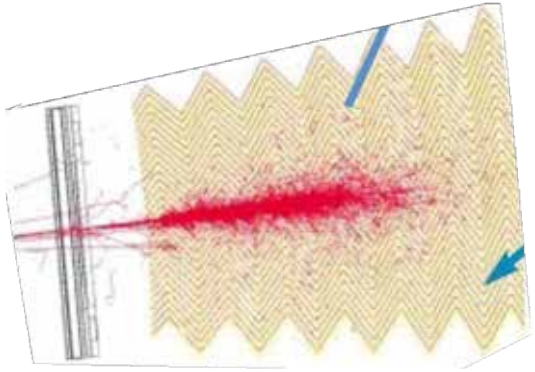

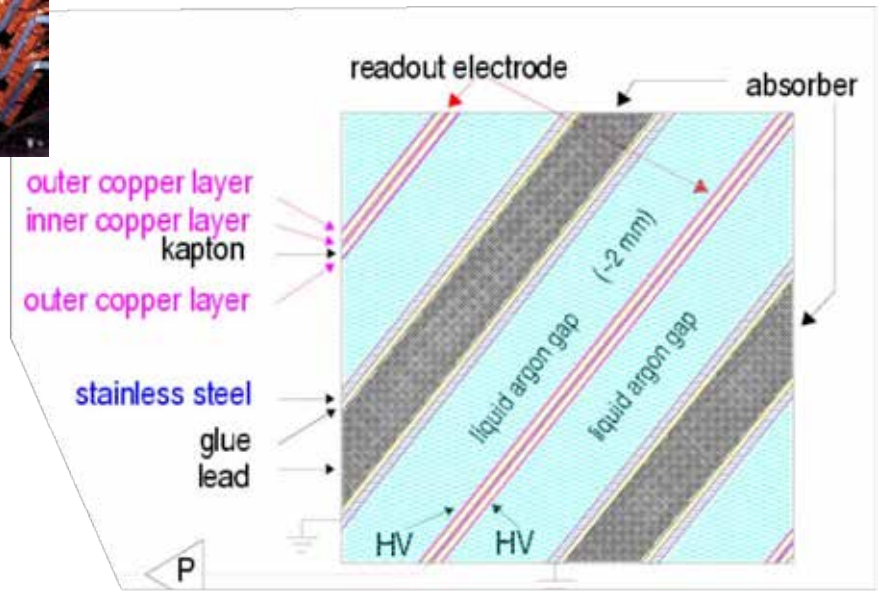


- Use accordion geometry
- Full $\phi$ coverage w/o cracks
- 3 layers with $|\eta|<3.2$
- 173312 readout channels (98.5% work)

# Performance of ATLAS LiAr ECAL

- The ATLAS LiAr calorimeter works well

Energy Linearity from test beam

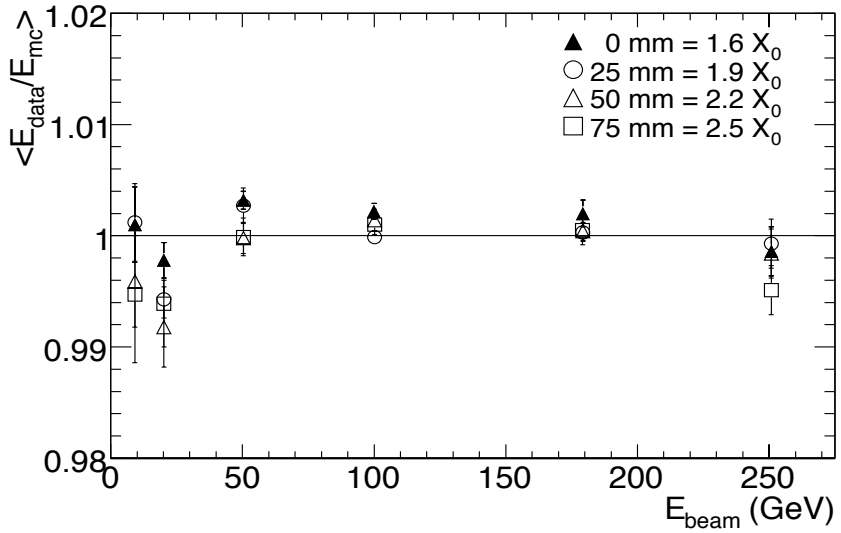


Energy Resolution from test beam

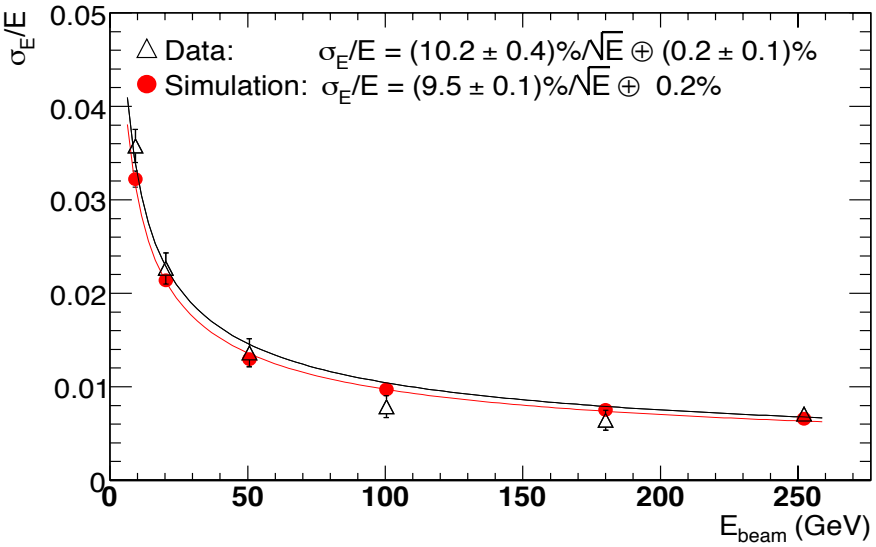


- Energy response is linear
- Energy resolution is

$$\frac{\sigma_E}{E} = \frac{0.1}{\sqrt{E}} \oplus 0.02$$

- $Z^0$ $\sigma_m$=1.73±.08 GeV is slightly worse than MC

$Z^0$ reconstruction

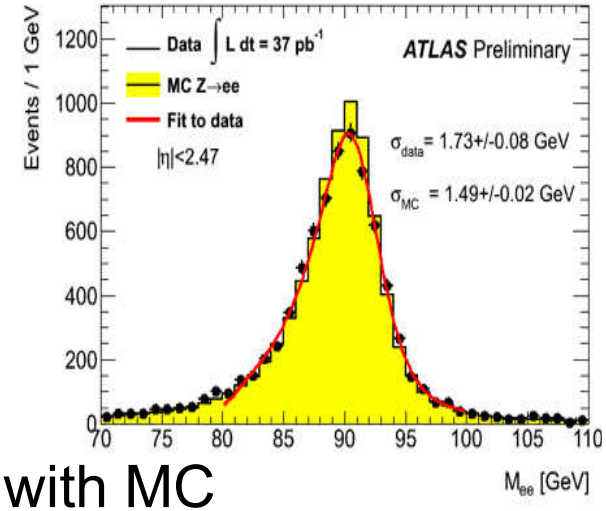


J/ψ reconstruction

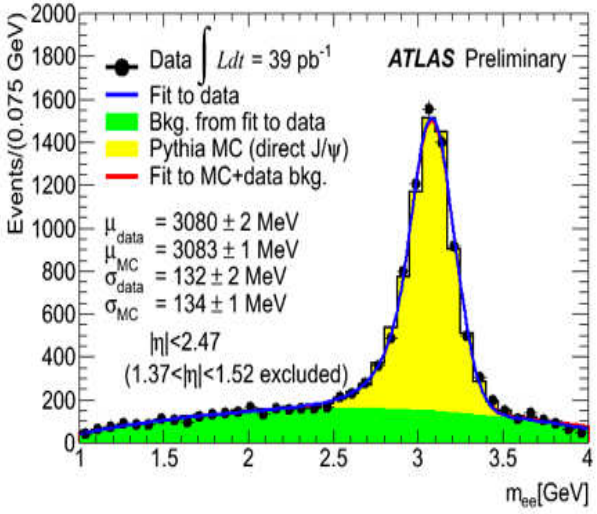


- J/ψ $\sigma_m$=132±2 MeV agrees with MC


Hadron
Calorimeters
ATLAS tile calorimeter

# Hadron Showers

- Conceptually, the energy measurement of hadronic showers is analogous to that of electromagnetic showers, but due to complexity & variety of hadronic processes, a detailed understanding is complicated
- Though elementary processes are well understood, no simple analytical description of hadronic showers exist
- Half the energy is used for multiple particle production ($\langle p_t \rangle \cong 0.35$ GeV), the remaining energy is carried off by fast, leading particles
- 2 specific effects limit the energy resolution of hadronic showers

i) A considerable part of secondary particles are $\pi^0$'s, which will propagate electromagnetically without further nuclear interactions
Average fraction of hadronic energy converted into $\pi^0$'s is

- $f_{\pi^0} \approx 0.1 \ln(E)$ [GeV] for few GeV $\leq E \leq$ several 100 GeV
- Size of $\pi^0$ component is largely determined by production in first interaction & by event-by-event fluctuations about the average value

ii) A sizable amount of available energy is converted into excitation or breakup of nuclei $\rightarrow$ only a fraction of this energy will be see

# Intrinsic Energy Resolution

- Unless event-by-event fluctuations are compensated, intrinsic hadron energy resolution is

$$\left(\frac{\sigma_E}{E}\right)_{intrinsic} = \frac{0.45}{\sqrt{E\,[\mathrm{GeV}]}}$$

holding for materials from Al to Pb (exception $^{238}$U)

- This applies likewise to homogeneous and to sampling calorimeters

- The level of nuclear effects and level of invisible energy is sensitively measured by comparing the calorimeter response to e and h at the same available energy
  - Ideally, we want e/h≅1
  - Typical values are e/h≅1.4
  - e/h drops to ~0.7 below 1 GeV

e/h ratio in different hadron calorimeters

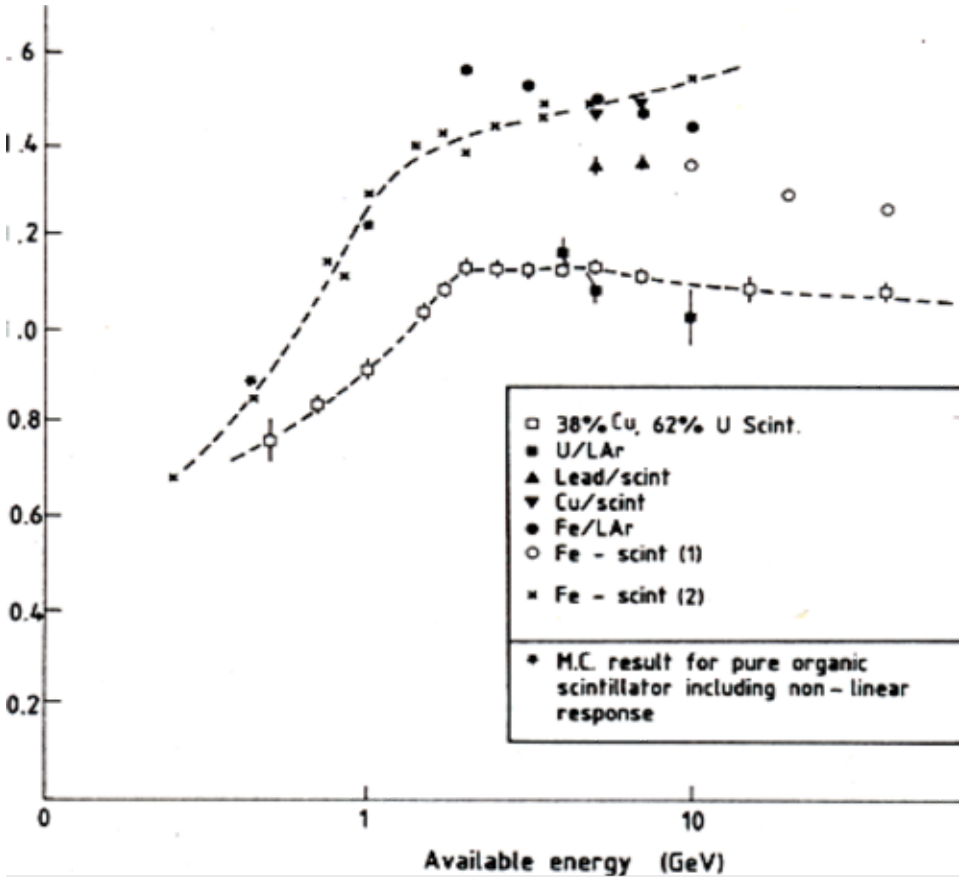


- Intrinsic resolution for $^{238}$U is

$$\left(\frac{\sigma_E}{E}(U)\right)_{intrinsic} = \frac{0.22}{\sqrt{E\,[\mathrm{GeV}]}}$$

as some of the fission energy produced in nuclear breakup is measured (see backup)

# Shower Containment

- In analogy to $X_0$ define a hadronic interaction length $\lambda$ as the length in which a hadron has interacted with probability of 63%

- Longitudinal shower distributions parametrized in $\lambda$ are similar for different materials

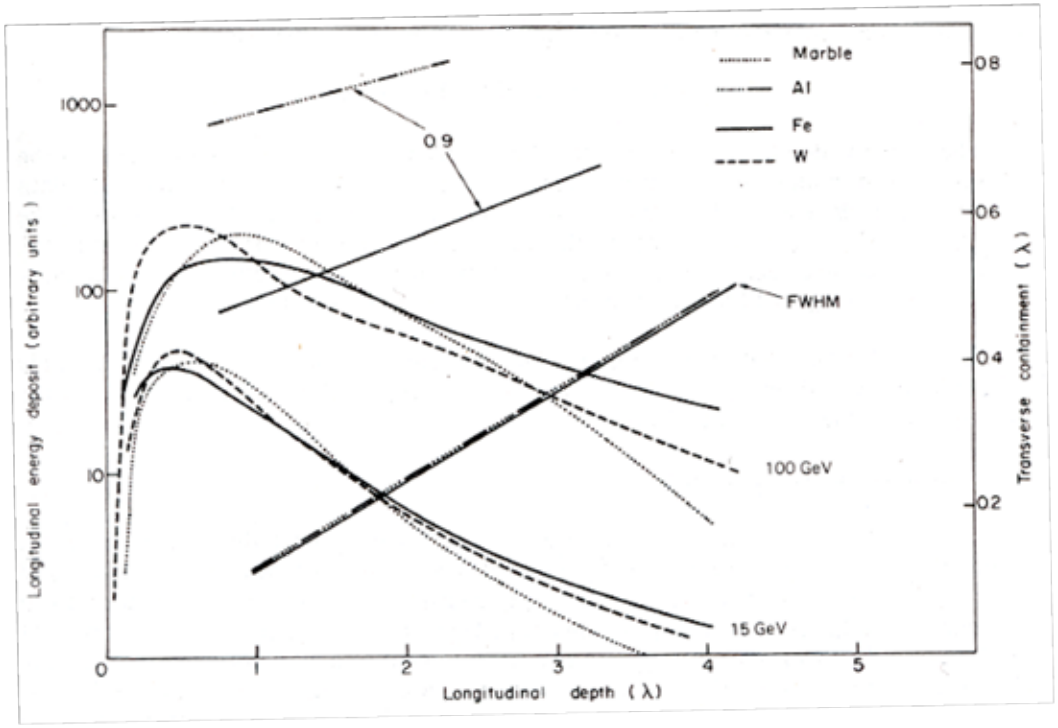


- Shower maximum

$$I_{max}(\lambda) \simeq 0.2 \ln E\left[\text{GeV}\right] + 0.7$$

- 95% longitudinal shower containment $L_{95}(\lambda) = I_{max} + 2.5\lambda_{att}$

where $\lambda_{att} \cong \lambda \cdot (E[\text{GeV}])^{0.13}$

➔ $L_{0.95}(\lambda)$ describes data in few GeV≤ E ≤few 100 GeV within 10%

- 95% radial shower containment is $R_{0.95} \leq 1\lambda$

- Useful parameterization of longitudinal shower development

$$dE/ds = K\left[w \cdot t^a e^{-bt} + (1-w) l^c e^{-dl}\right]$$

a,b,c,d: fit parameters
$t=s/X_0$, $l=s/\lambda$, f: fraction

# ATLAS Hadron Calorimeters

- Steel-scintillator sampling calorimeter (total thickness ~11$\lambda$)
  - 14 mm thick steel plates
  - 460 000 3 mm thick scintillator tiles
  - Calorimeter is built in 3 sections: barrel & 2 extended barrels

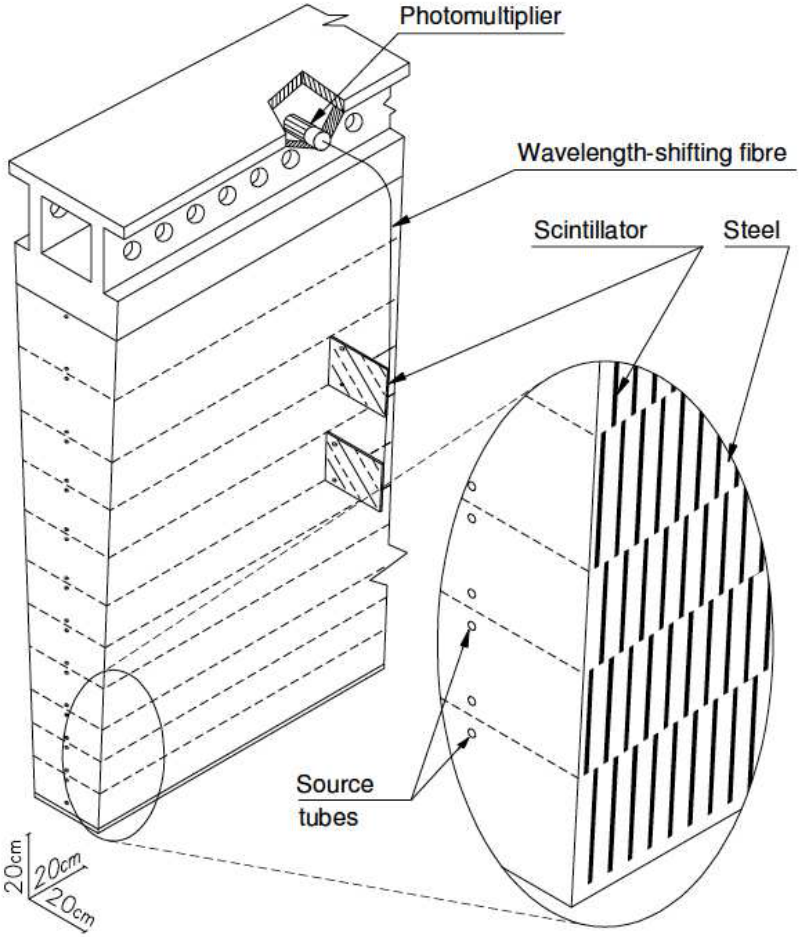


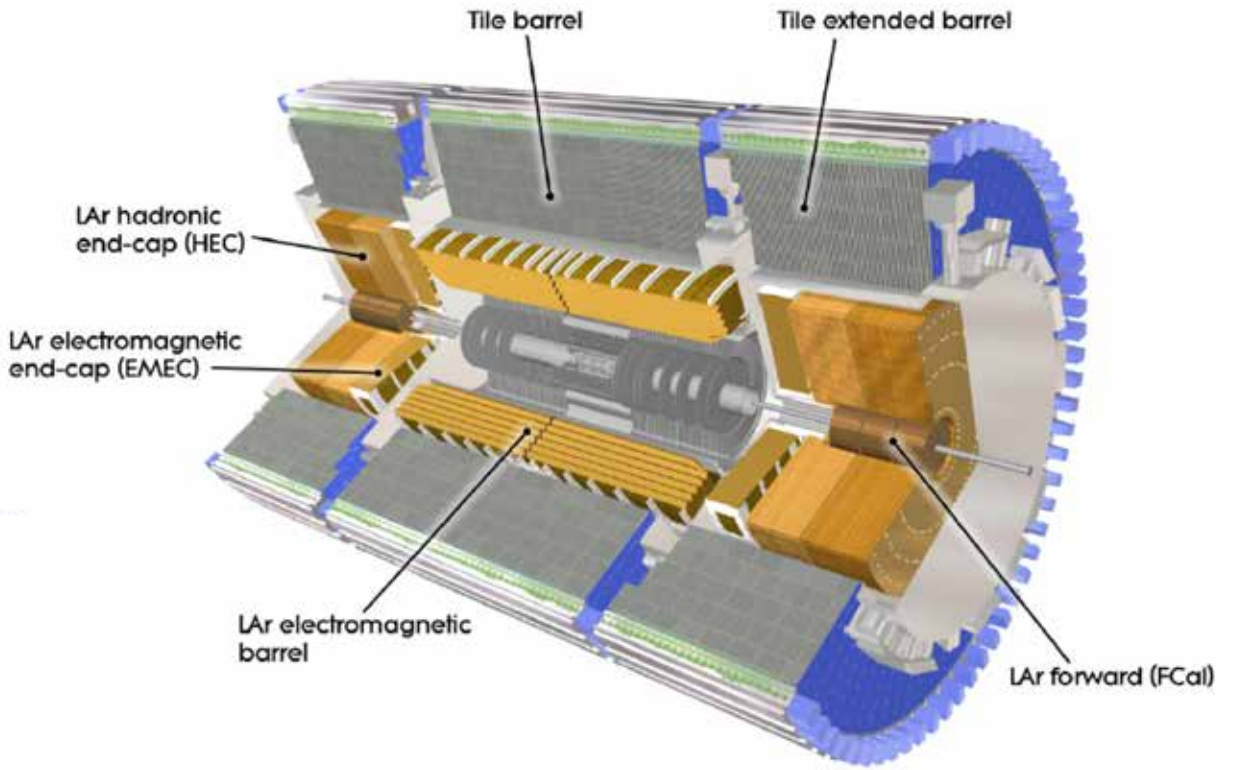

# Properties of ATLAS Tile Calorimeter

- Energy response in a cell of the ATLAS tile calorimeter showing noise plus showers
- Tile calorimeter energy resolution stochastic: a=52%; constant: b=3%
- e/h ratio is larger than 1

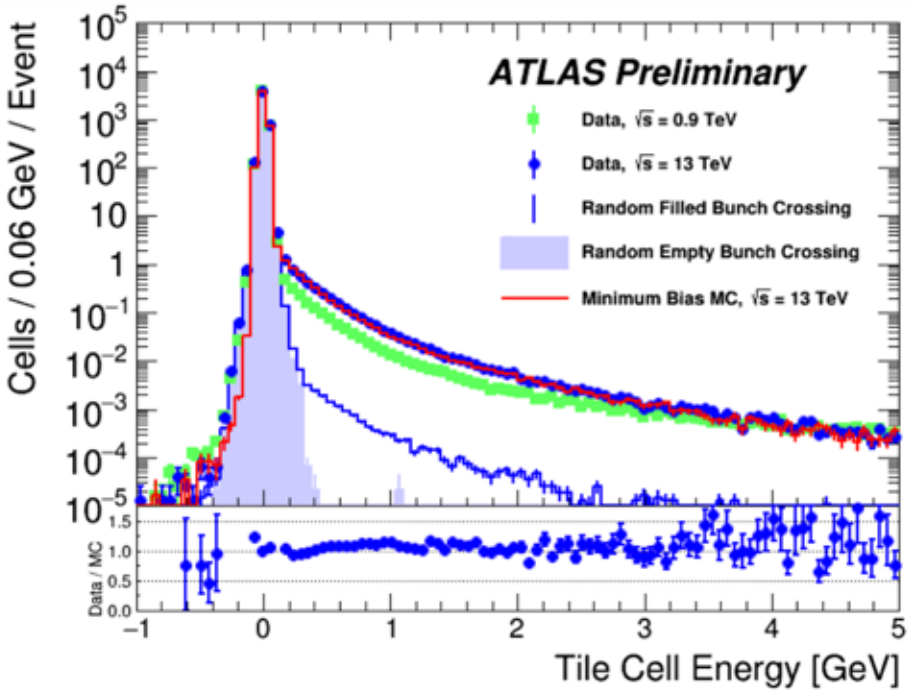


energy resolution

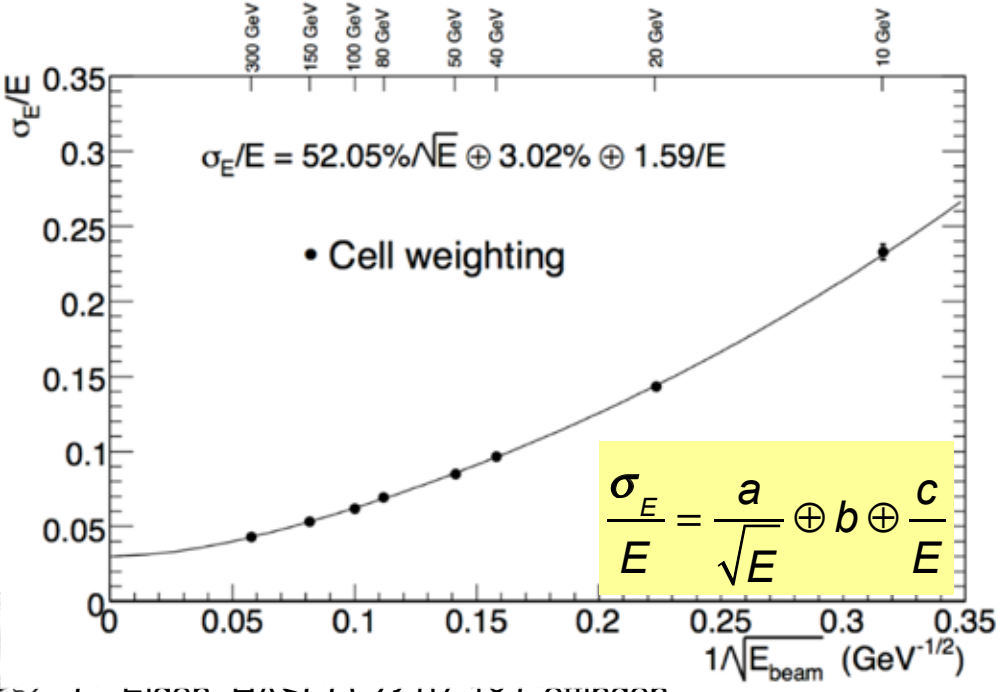


$$\frac{\sigma_E}{E} = \frac{a}{\sqrt{E}} \oplus b \oplus \frac{c}{E}$$

e/h ratio

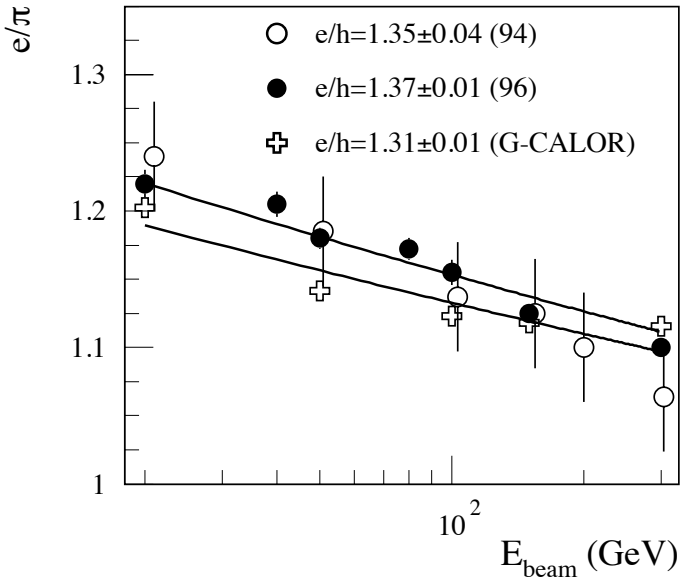

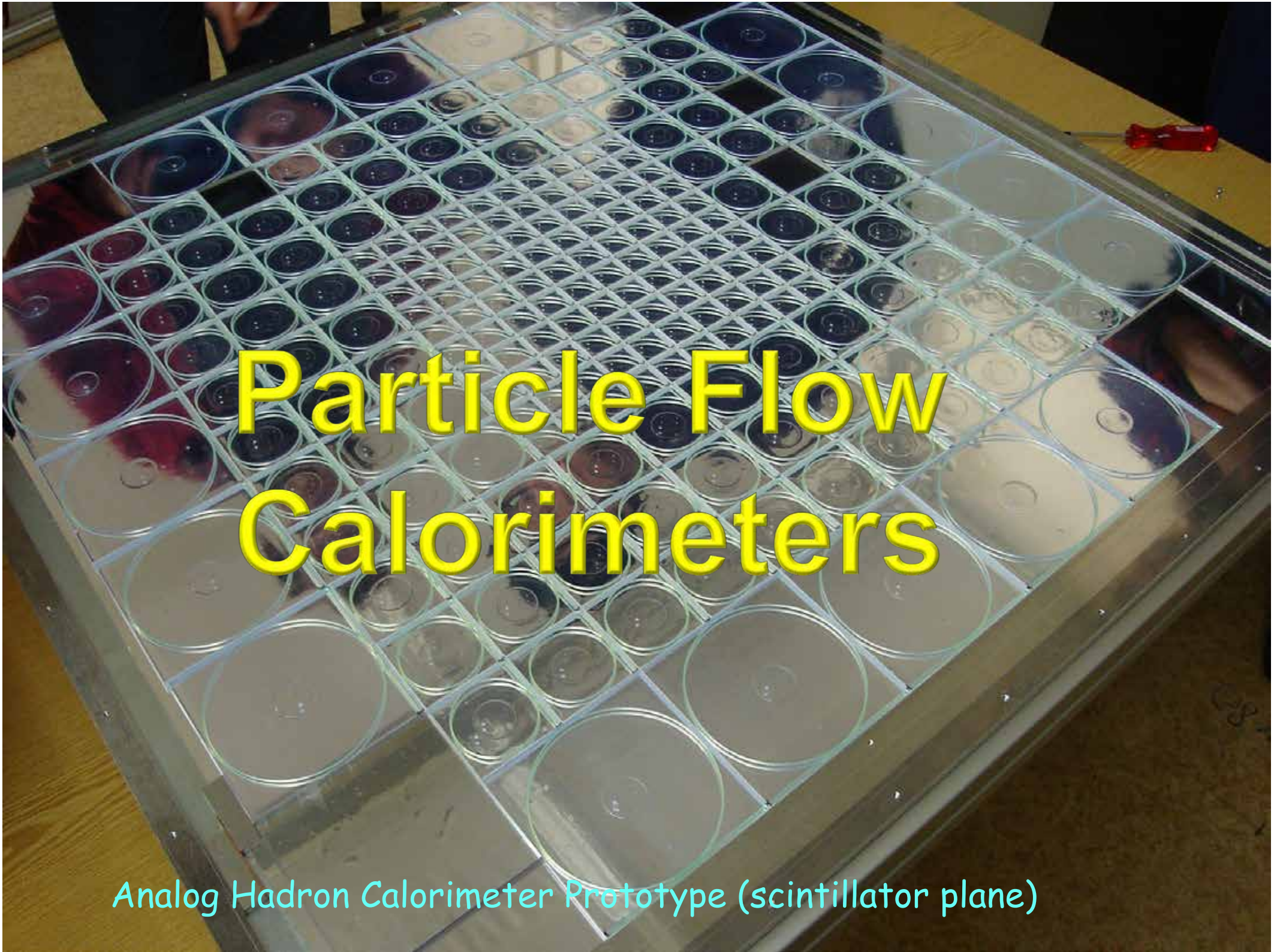
Particle Flow
Calorimeters
Analog Hadron Calorimeter Prototype (scintillator plane)

# Particle signatures

- New idea: Perform particle tracking inside a jet, since individual particle species have characteristic signatures

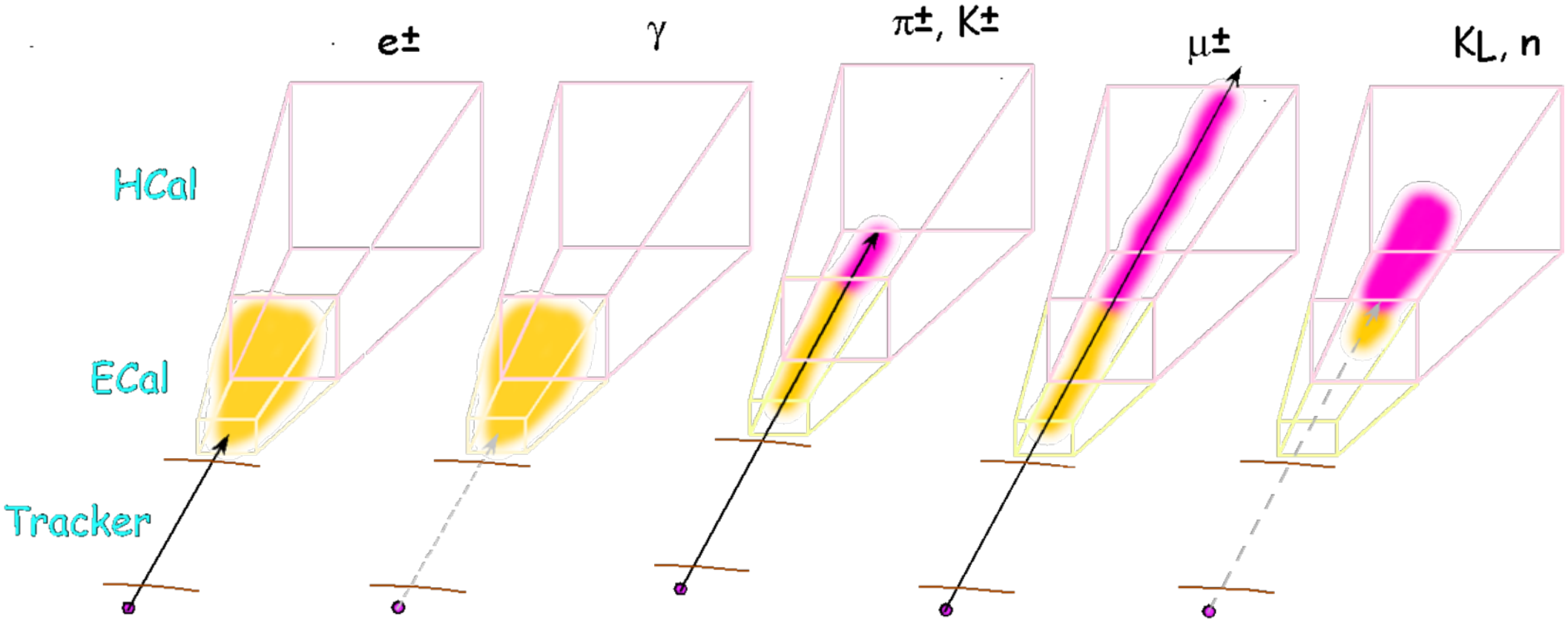


- Need high granularity in ECal & HCal to isolate single particles
- jet composition: 65% charged tracks, 25% photons, 10% neutral hadrons

# Jet Energy Resolution

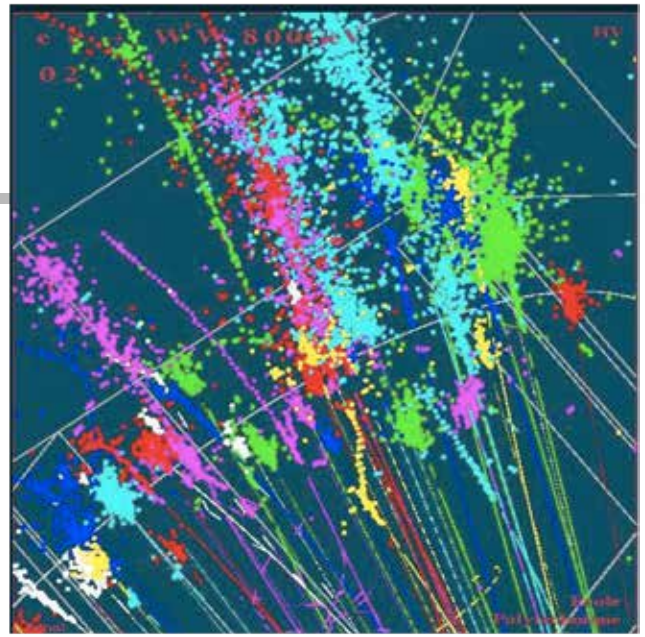

- Jet energy: $E_{\text{jet}} = E_{\text{charged}} + E_{\text{photons}} + E_{\text{neutral hadron}}$

65% 25% 10%

- Implementing particle flow we get jet energy resolution $\sigma^2_{E_{\text{jet}}} = \sigma^2_{E_{\text{charged}}} + \sigma^2_{E_{\text{photons}}} + \sigma^2_{E_{\text{neutral hadrons}}} + \sigma^2_{E_{\text{confusion}}}$
- With anticipated resolutions

$$\sigma^2_{E_{\text{charged}}} \approx \left(5\times10^{-5}\right)^2 \sum \frac{E^4_{\text{charged}}}{\text{GeV}^2} \approx \left(0.02\ \text{GeV}\right)^2 \sum \left(\frac{E_{\text{charged}}}{10\ \text{GeV}}\right)^4$$

$$\sigma^2_{E_{\text{photons}}} \approx \left(0.10\right)^2 \sum E_{\text{photons}} \cdot \text{GeV} \approx \left(0.52\ \text{GeV}\right)^2 \sum \left(\frac{E_{\text{jet}}}{100\ \text{GeV}}\right)$$

$$\sigma^2_{E_{\text{neutral hadrons}}} \approx \left(0.50\right)^2 \sum E_{\text{neutral hadrons}} \cdot \text{GeV} \approx \left(1.6\ \text{GeV}\right)^2 \sum \left(\frac{E_{\text{jet}}}{100\ \text{GeV}}\right)$$

- Ignoring the (typically) negligible tracking term:

$$\sigma^2_{E_{\text{jet}}} \approx \left(0.17\right)^2 \left(E_{\text{jet}} \bullet \text{GeV}\right) + \sigma^2_{\text{confusion}} \approx \left(0.3\right)^2 \left(E_{\text{jet}} \bullet \text{GeV}\right)$$

$\sigma^2_{\text{confusion}}$ is the largest term of all >25%

# VII.6.5 EM Calorimeter

- Si-W ECAL prototype, 3 W structures
- 15 active layers (Si)
- 1 cm × 1 cm Si pixels

$$\frac{\sigma_E}{E} = \frac{16.5 \pm 0.14\%}{\sqrt{E}} \oplus 1.1 \pm 0.1$$

- This technology is adapted for CMS endcap upgrade

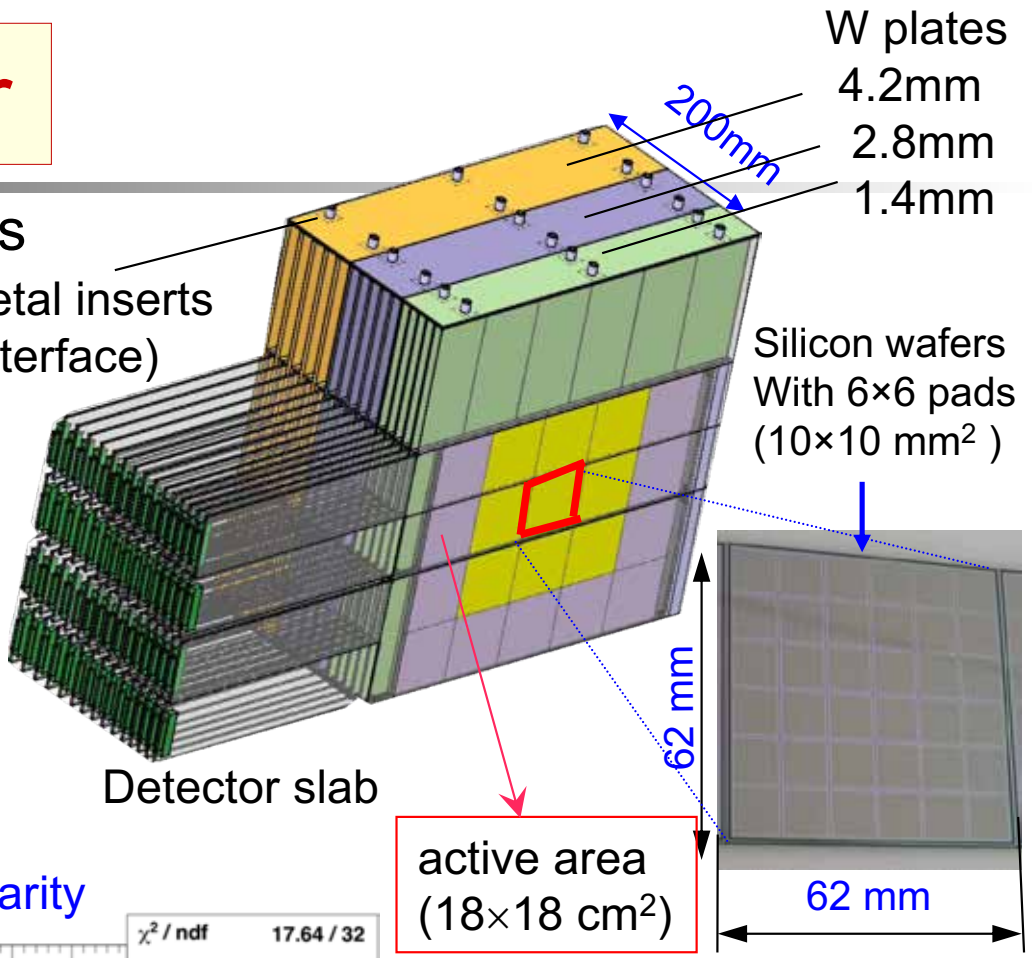


resolution

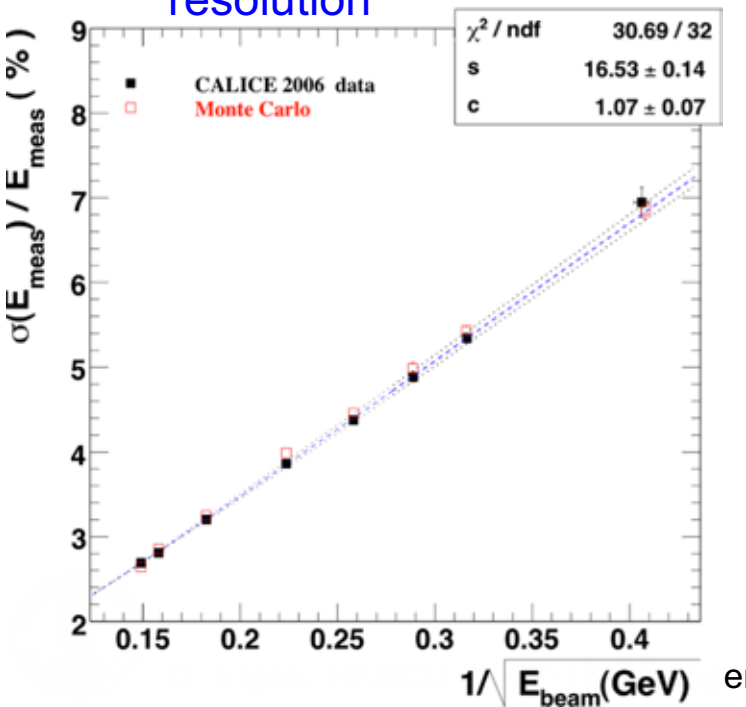


linearity

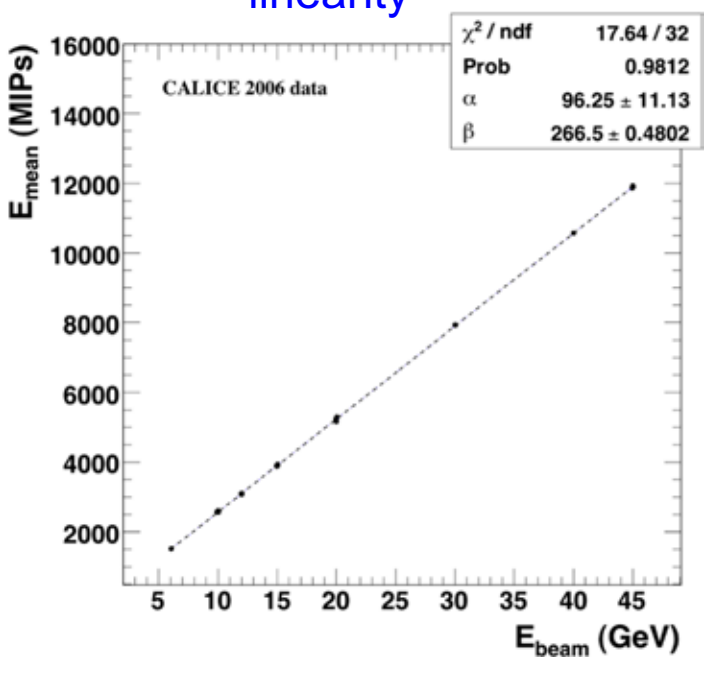


en

# Analog Hadron Calorimeter

- 38-layer Fe-scintillator sampling calorimeter (4.5 $\lambda$)
- Layer: 2 cm steel absorber plates + 1/2 cm scintillator tiles
  - core tiles: 3×3 cm$^2$ (10×10 matrix) increasing towards outside
- Total of 7608 tiles, each is read out with wavelength-shifting (WLS) fiber + SiPM (216 tiles/layer)

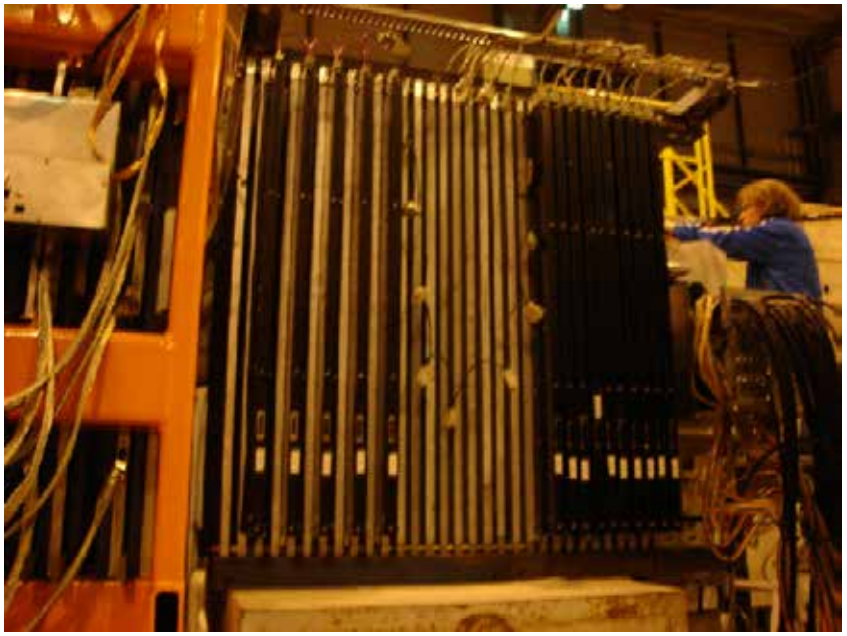

3M reflector

SiPM

SiPM

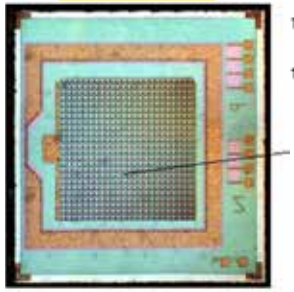

Photoelectrum spectrum

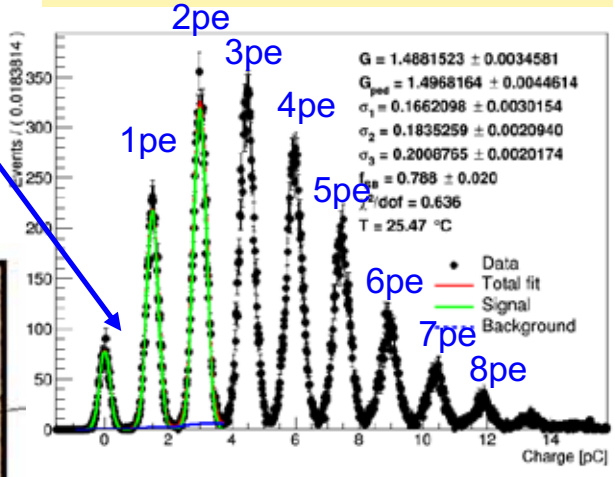


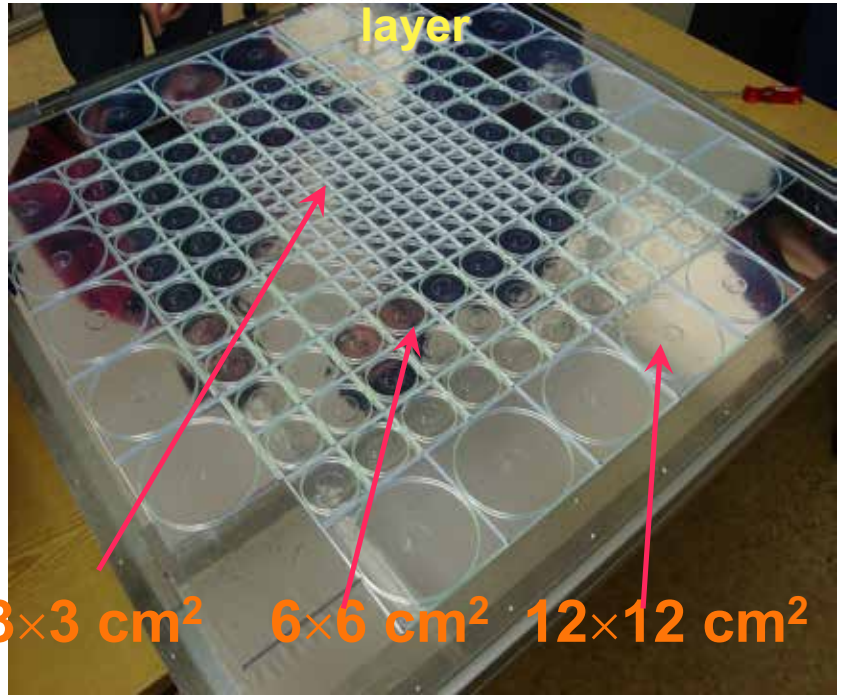

# Performance of Analog Hadron Calorimeter

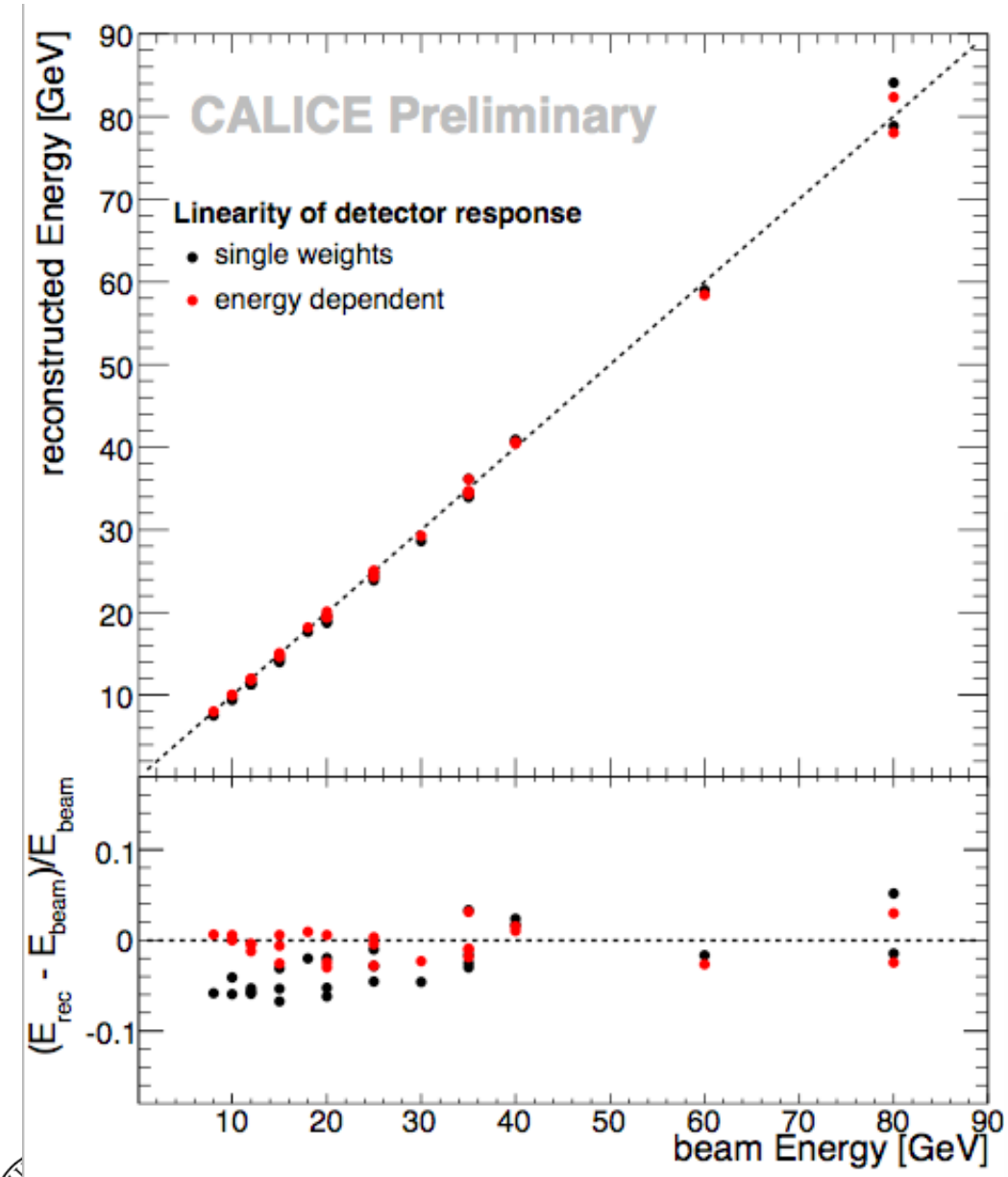


- Response of the hadron tile calorimeter is linear
- Resolution with appropriate energy weighting yields

$$\frac{\sigma_E}{E} = \left[\frac{48.8 \pm 0.2}{\sqrt{E[GeV]}} \oplus 0.0 \pm 0.23\right]\%$$

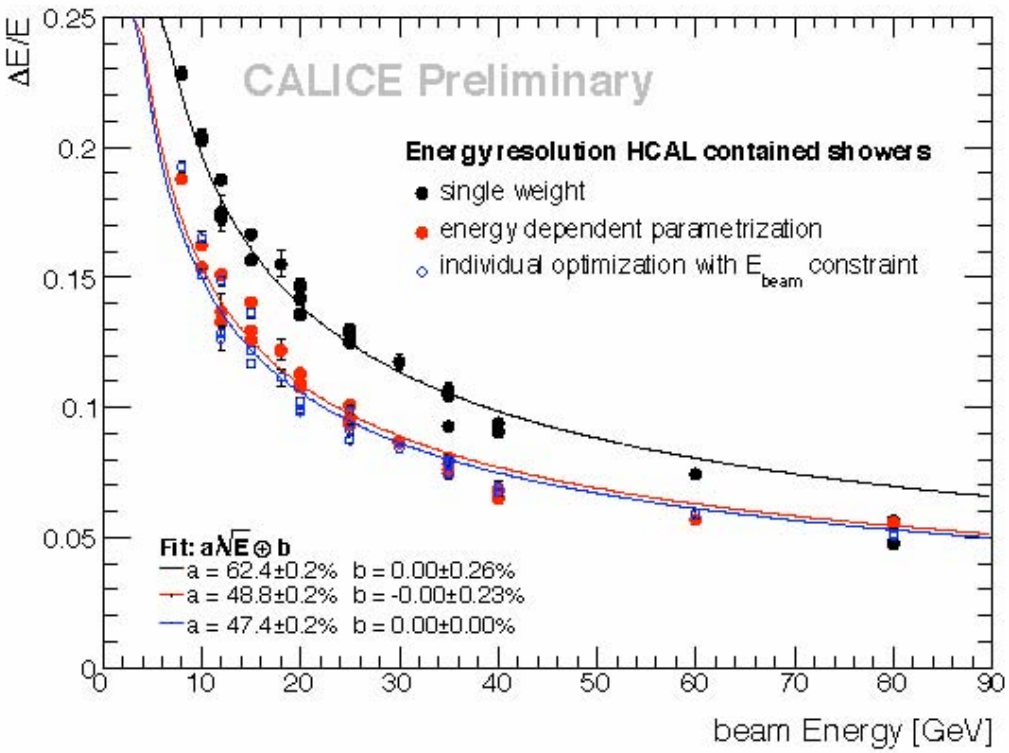

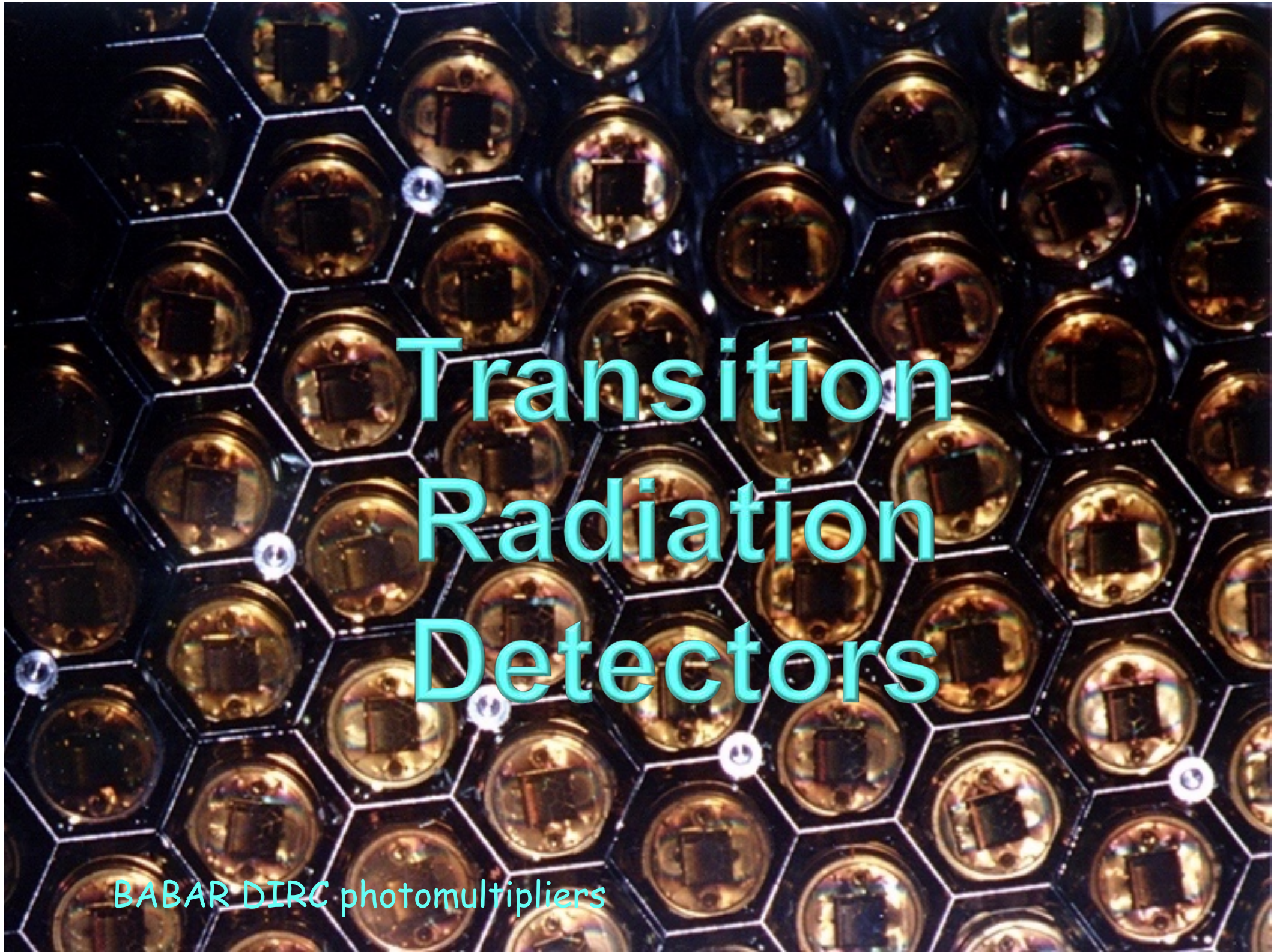
Transition
Radiation
Detectors
BABAR DIRC photomultipliers

# Transition Radiation

- Transition radiation arises from rapidly changing refractive indices: foil-gas
  - ➔ since phases at entrance and exit are different, we get interference
  - ➔ multiple layers increase yield

e: $(\vec{p}_e,\ E_e)$

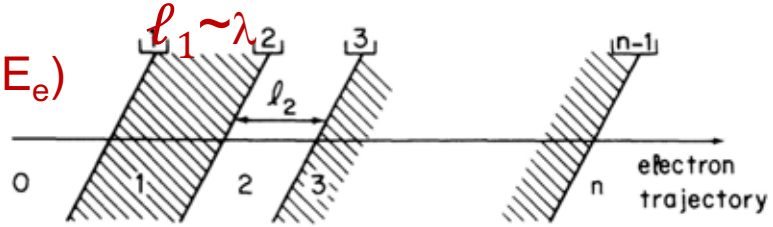


- The intensity $|A|^2$ is modulated by interference term $4 \sin^2(\delta/2)$ where phase $\delta = L/\zeta$ where $\zeta$ is the formation zone

$$\zeta = \frac{2c}{\omega}\left(\frac{1}{\gamma^2} + \frac{\omega_p^2}{\omega^2} + \theta^2\right)^{-1}$$

($\hbar\omega$: photon energy, $\omega_p$: plasma frequency $\theta$: emission angle ~$1/\gamma$, c: speed of light, $\gamma = E_e/m_e$)

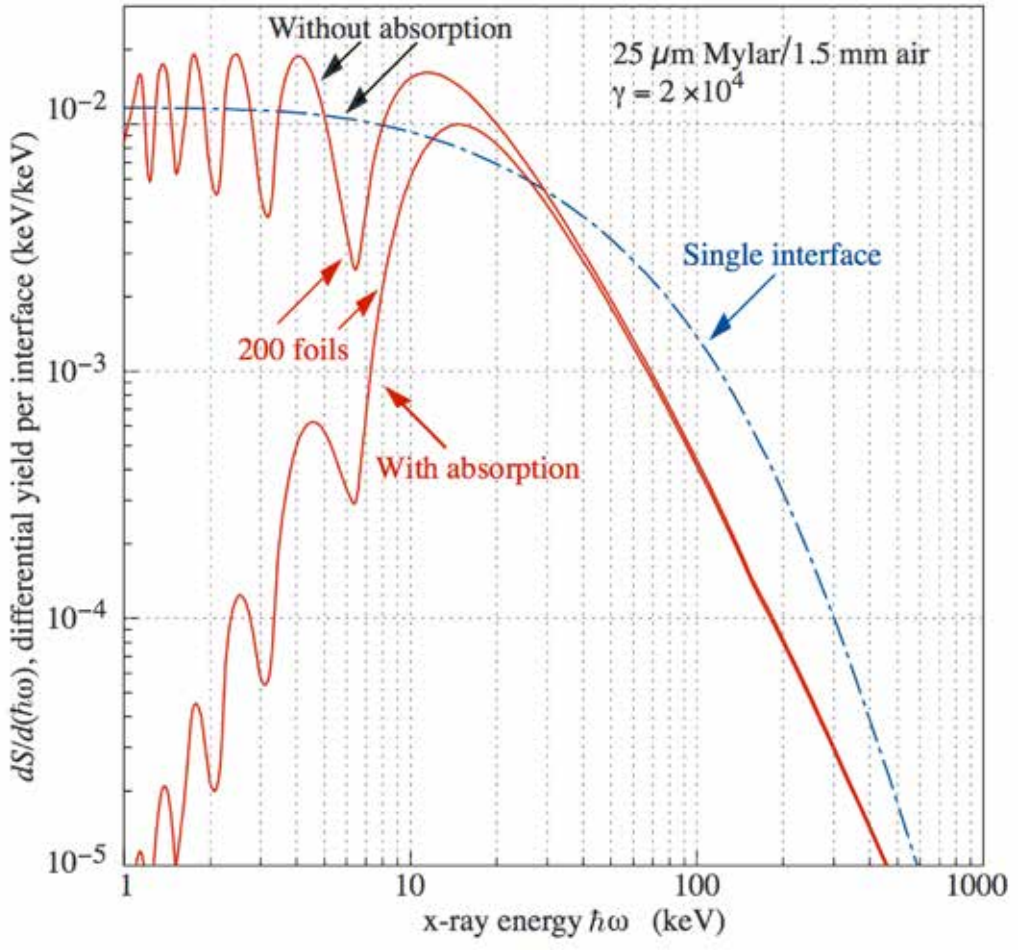


- Radiated photon energies are in the soft x-ray range 5-40 keV

- Above a fixed photon energy $\hbar\omega_0$ number of transition radiation photons increase as $(\ln \gamma)^2$

# Transition Radiation

Pulse height spectrum

- As an example, look at the pulse height spectrum in 1000 Li foils, L=51 μm & Xe chamber (1.04 cm)
- Measure response of 1.4 GeV $e^-$ and $\pi^-$ ($\gamma=2.7\times10^3$)
- To separate ionization from transition radiation, measure total energy deposited by TR quanta & ionization along track
- # clusters is Poisson distributed, while energy loss distribution has very long tail
- For threshold of 4 keV on energy and discriminator for recording clusters, $\pi$ contamination is < $10^{-3}$ for electron efficiency of 85%

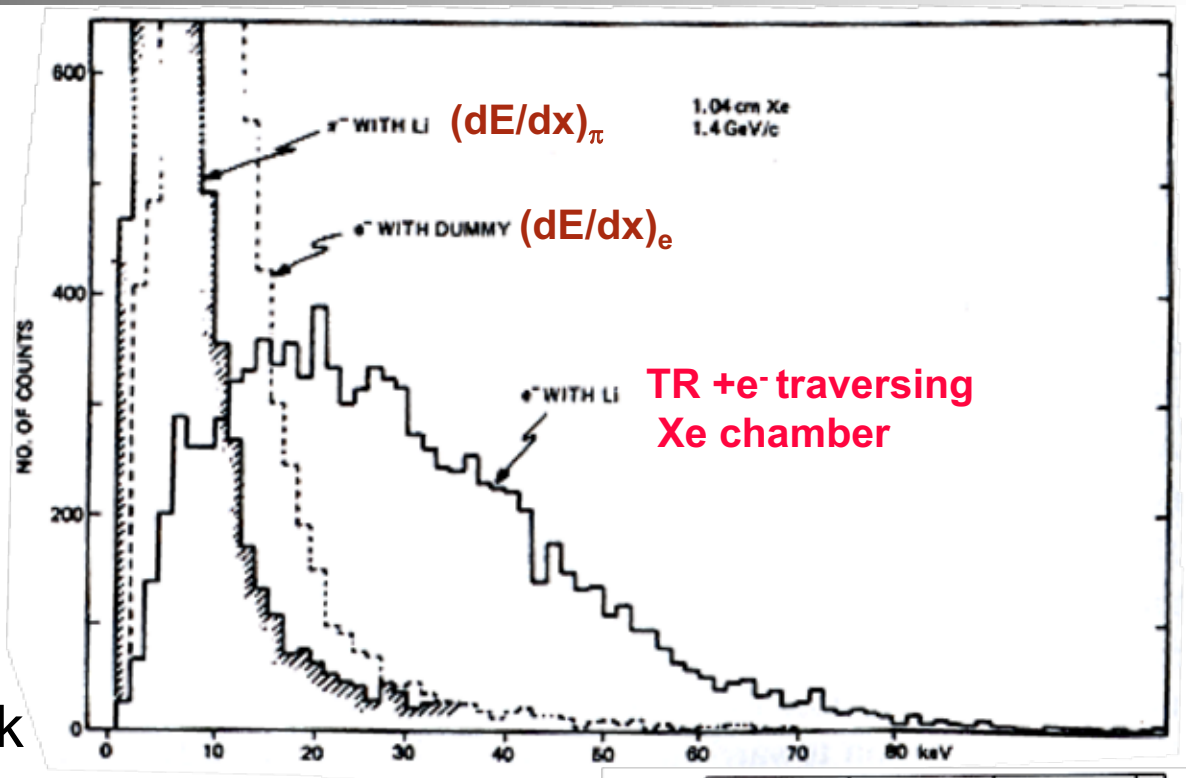


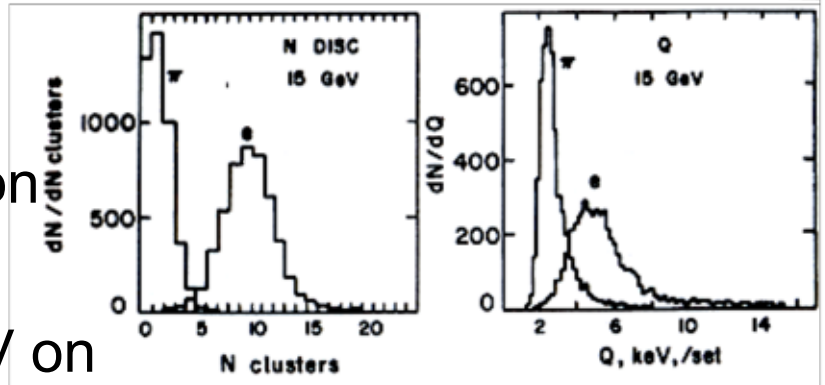


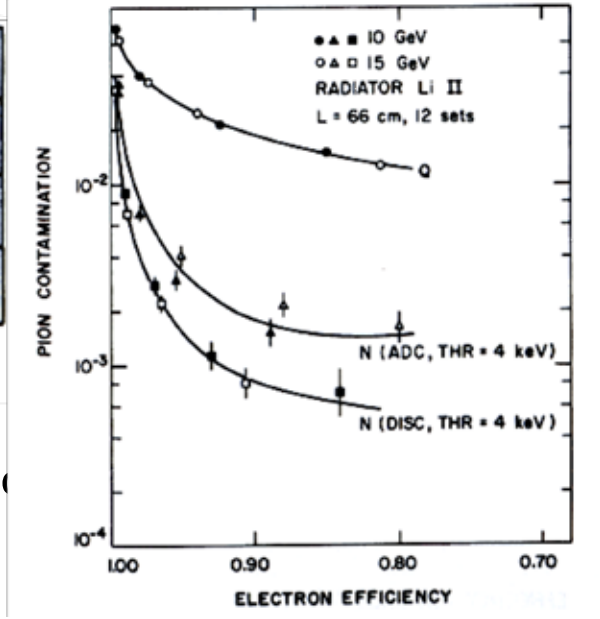

# ATLAS Transition Radiation Tracker

- The ATLAS TRT consists of 36 layers of straw tubes, 4 mm in diameter with position resolution of 200 mm interspersed with Xenon as radiator
- Separation between hadrons and electrons via transition radiation turns on when $\beta\gamma$>~1000

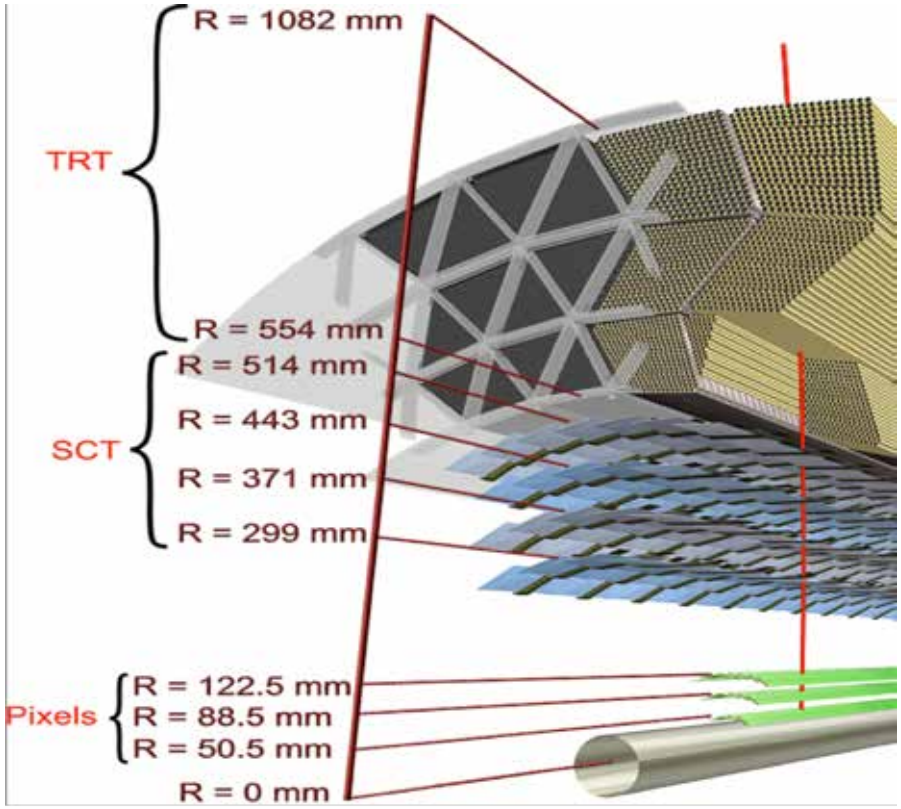


Endcaps

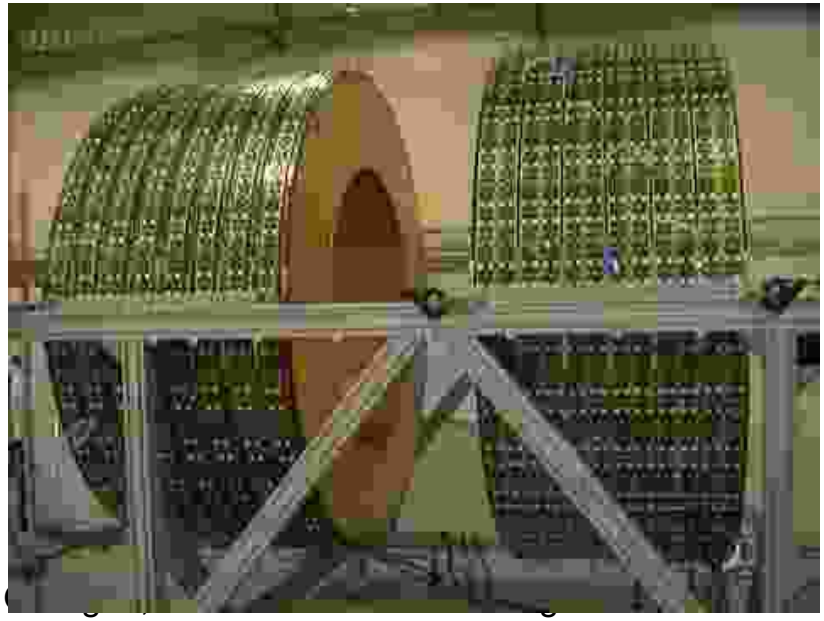

Barrel

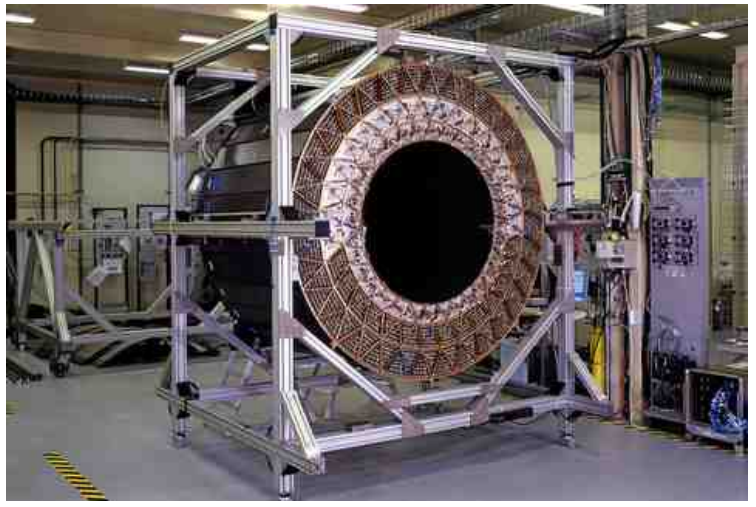

# Performance of ATLAS TRT

## Time over threshold distribution

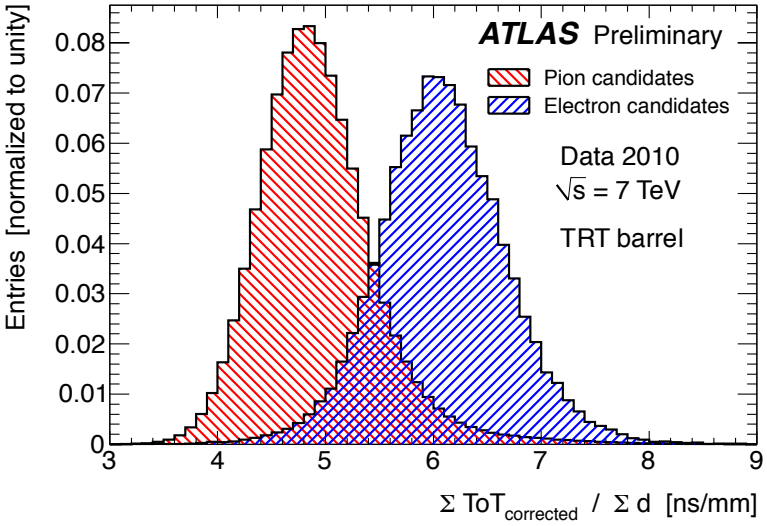


## High threshold probability vs γ

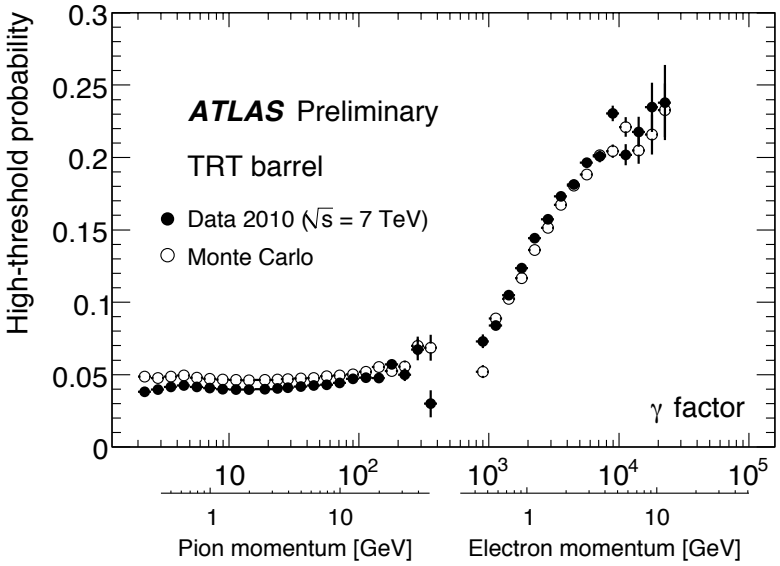


## Efficiency vs distance to straw center

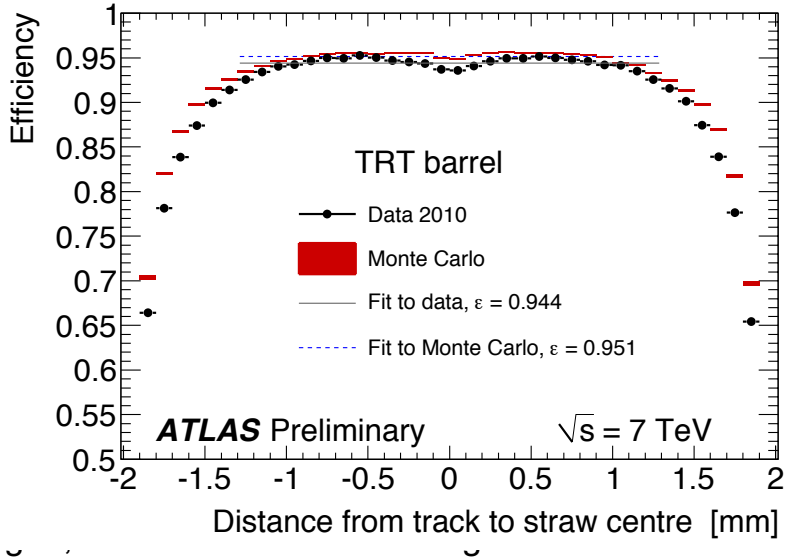


## Pion misidentification probability

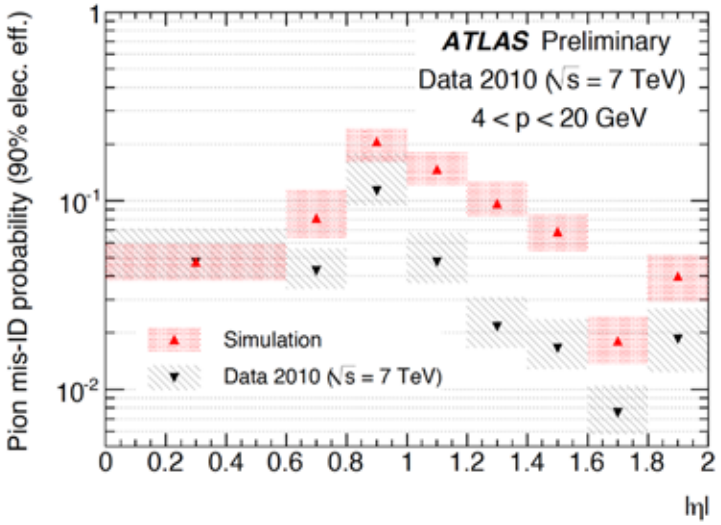

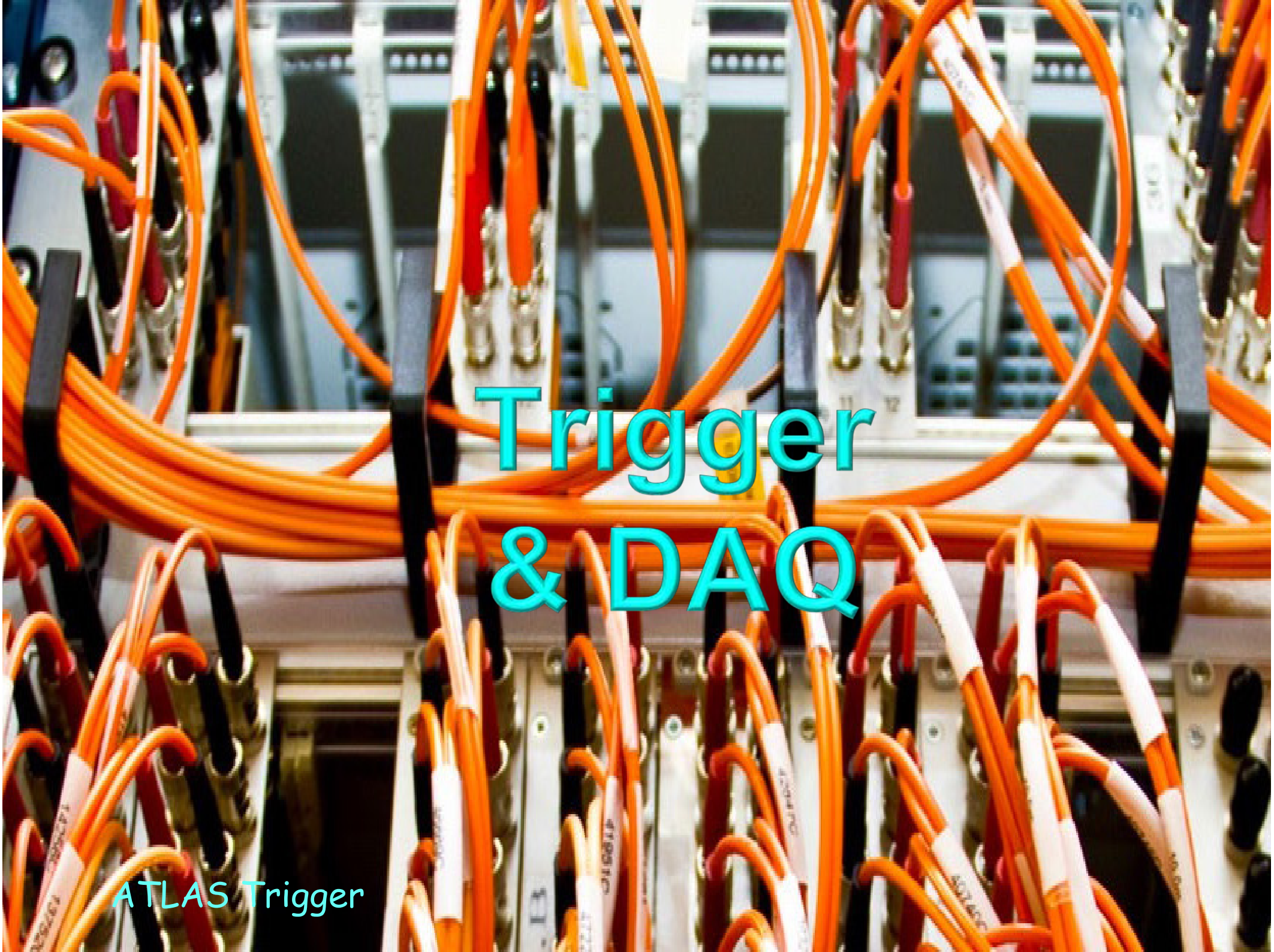
Trigger
& DAQ
ATLAS Trigger

# ATLAS Trigger

- L1: hardware-based trigger reduces beam crossing rate of 30 MHz to 100kHz within 2.5 μs
- HLT: software-based trigger reduces 100 kHz to 1 kHz within 200 ms
- L1 uses custom electronics to determine regions of interest taking coarse granularity calorimeter & muon detector information
- HLT uses ROIs from L1 and runs sophisticated algorithms on ROI or full event with full-granularity detector information
- If any of various trigger configurations is satisfied, event is kept

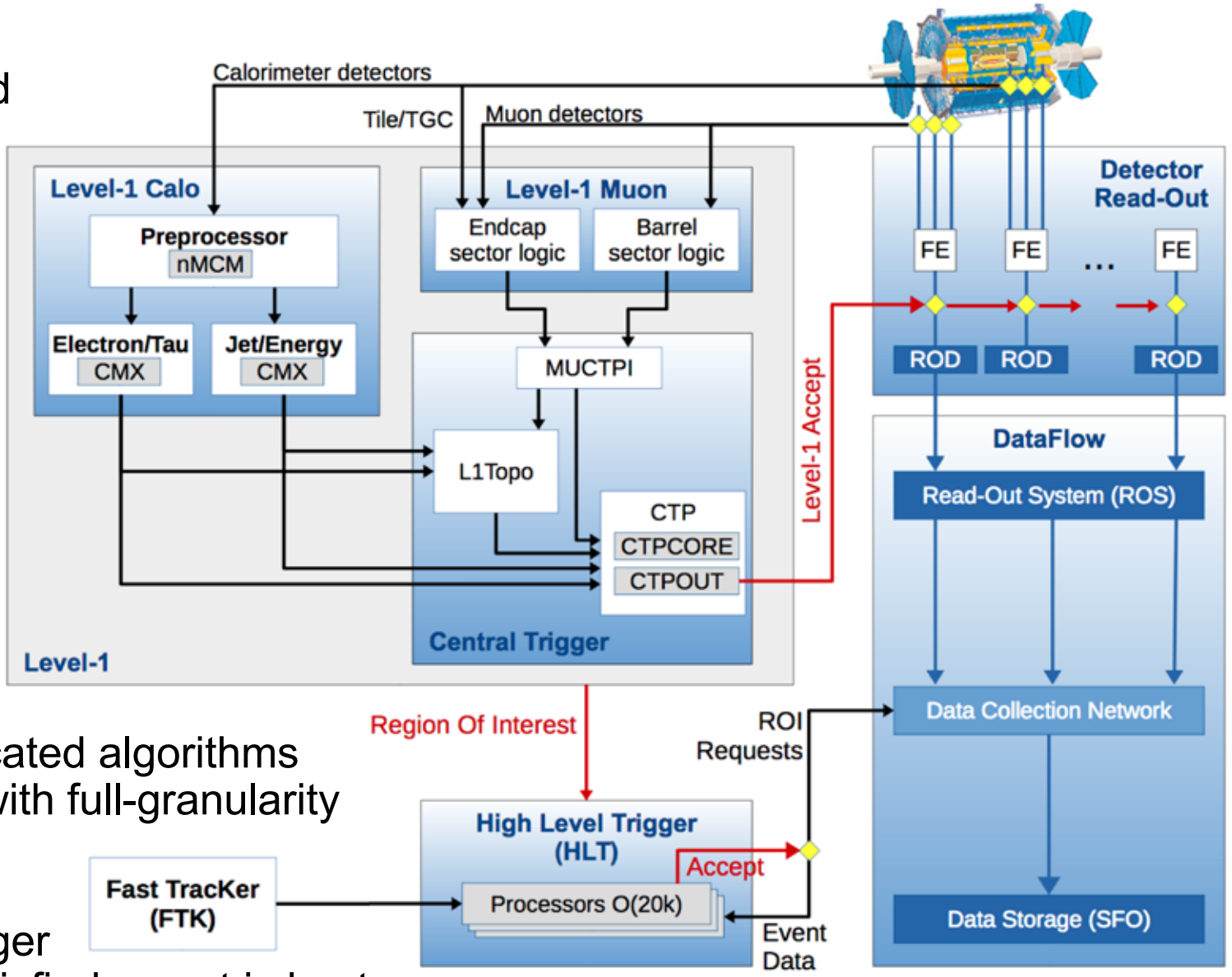

# ATLAS Trigger Efficiencies

- As an example, we show performance of a few specific triggers

Single photon trigger

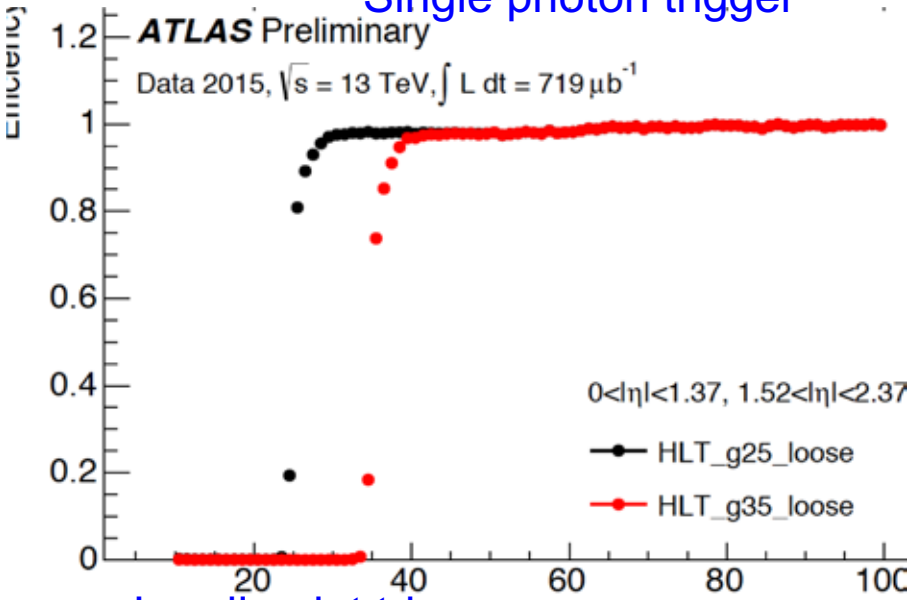


Single electron trigger

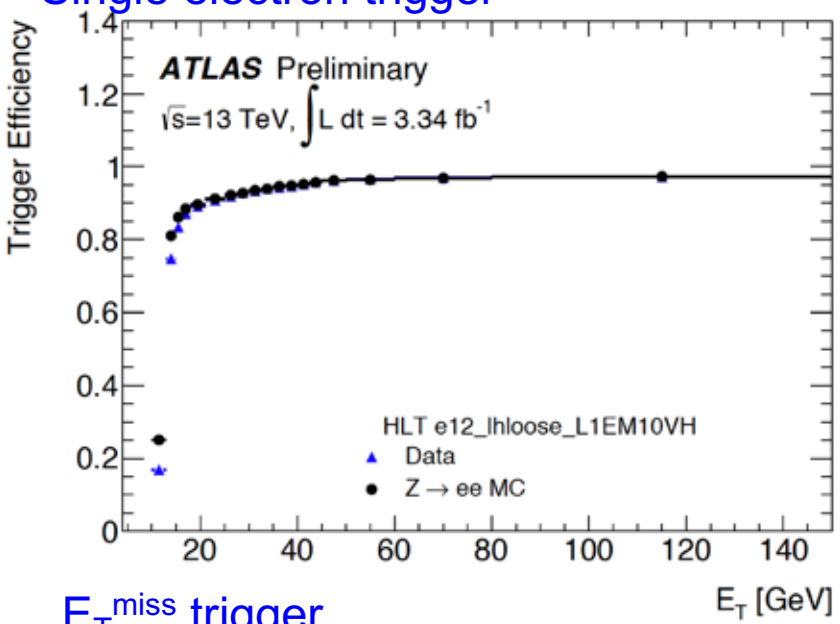


Leading jet trigger

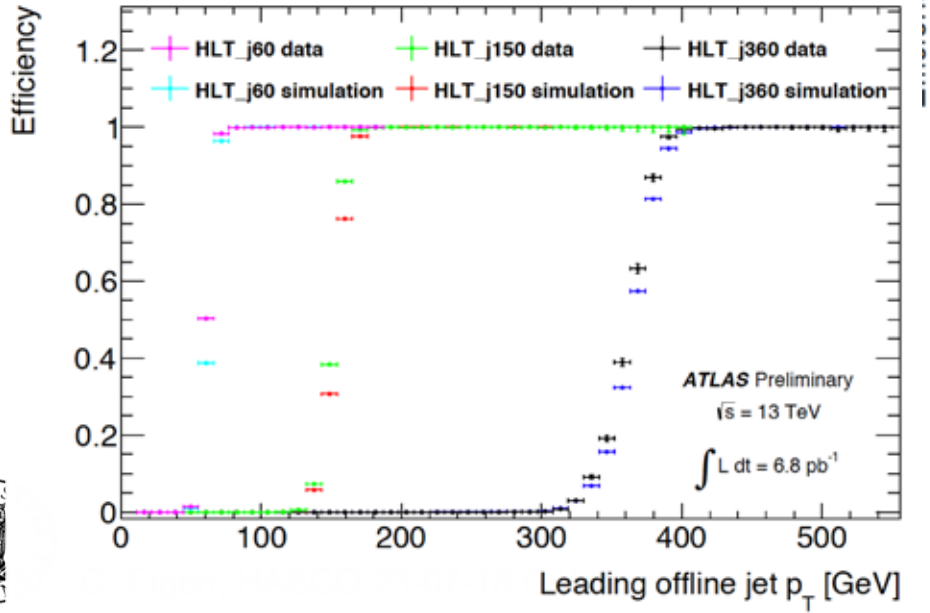


$E_T^{miss}$ trigger

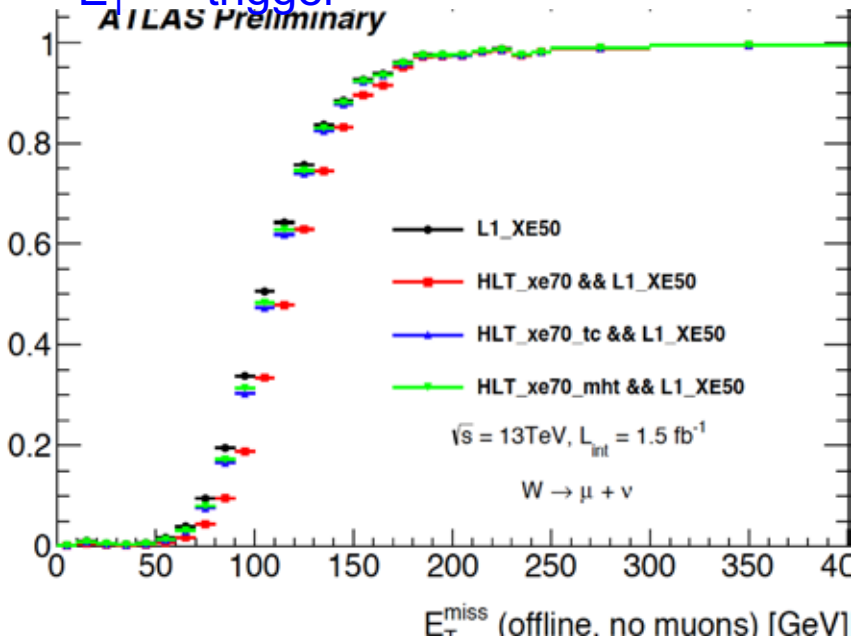

# Conclusion

- Within the given time limit I tried to cover all main detector components of multipurpose LHC detectors, ATLAS and CMS
- Both detectors use state-of-art technologies with respect to hardware, electronics software and computing
- This is necessary to achieve the physics goals (precision measurements of the Higgs particle and searche for physics beyond the Standard Model
- With the high-luminosity LHC upgrade all detectors need to be upgraded to cope with higher radiation levels, higher occupancies in detector cells, higher event rates and higher pile up of minimum bias interactions
- Both experiments conduct R&D to deal with the harsher environment

➔ For example, time measurements of various will play a central role

**Thank you for your attention**

# Backup

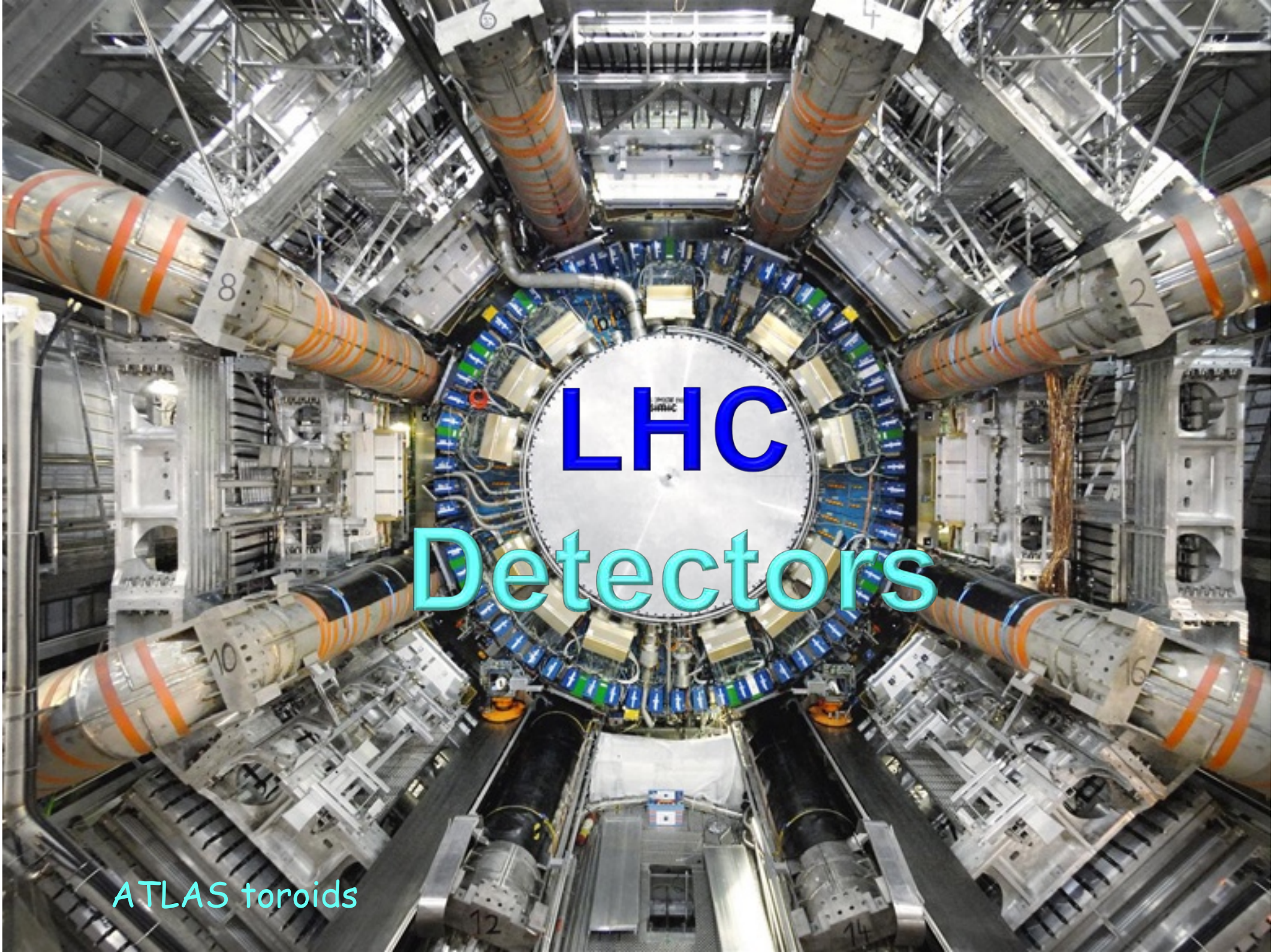
LHC
Detectors
ATLAS toroids

# The ATLAS Detector

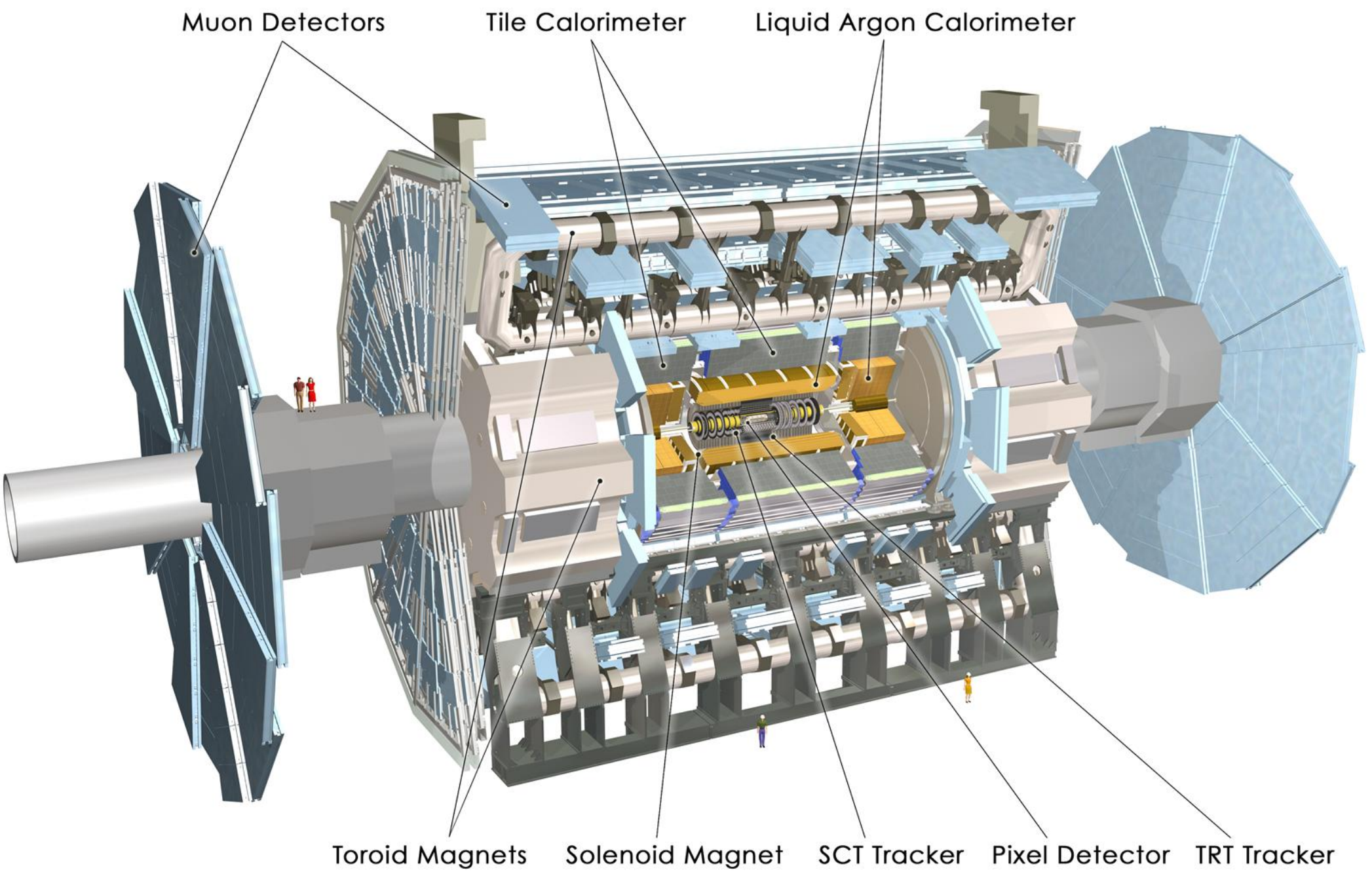

# The CMS Detector

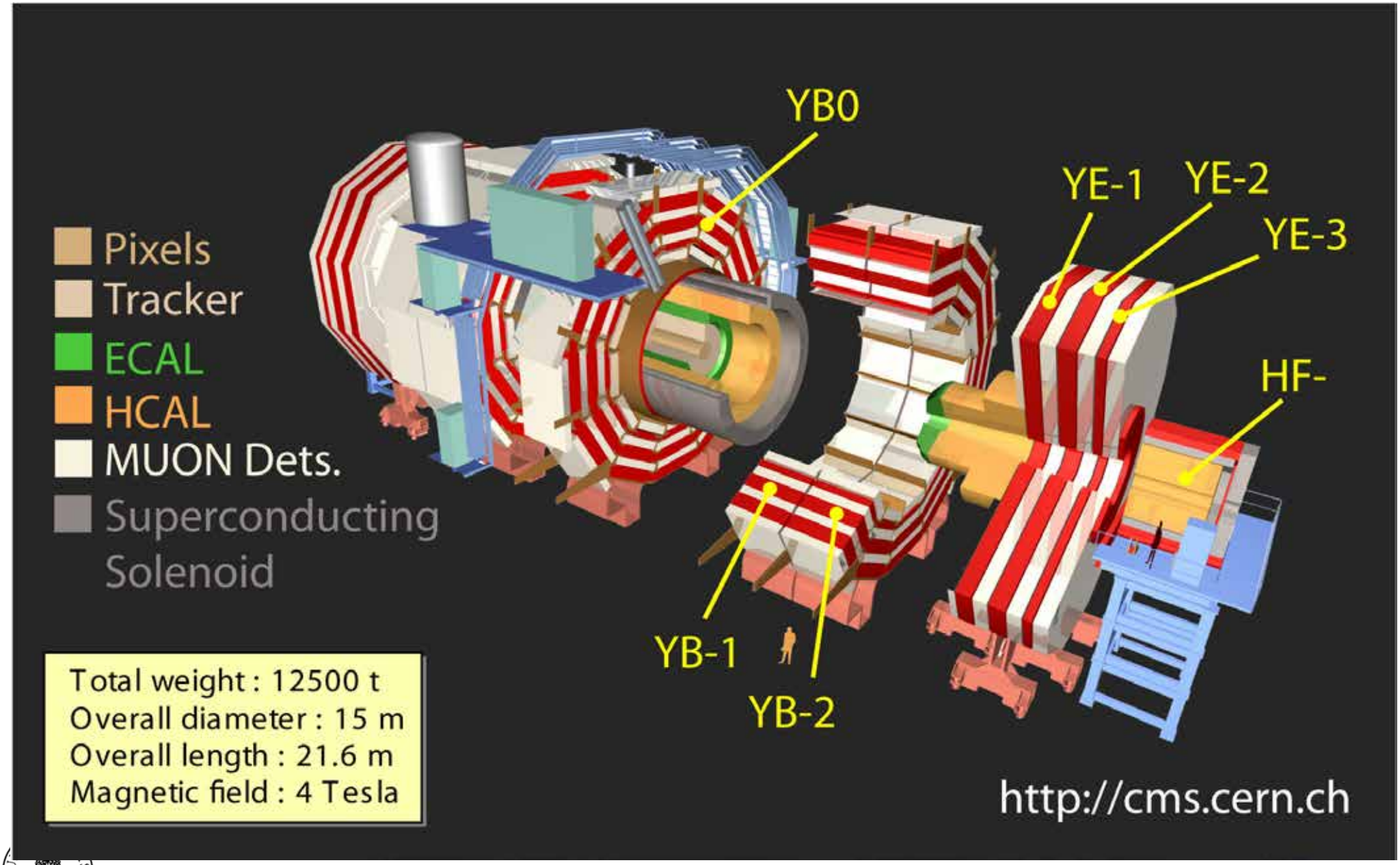

# Mobility of Ions

- A charged particle traversing a gas produces $e^-i^+$ pairs
- A cloud of positive ions, $i^+$, placed in an electric field of strength $\vec{E}$, is accelerated by the $\vec{E}$ field and decelerated by collisions in the gas
  ➔ the motion can be described by a constant drift velocity $\vec{v}_D$
- According to measurements, $\vec{v}_D$ is proportional to $\vec{E}/P$

$$\vec{v}_D^{+} = \mu^{+}\vec{E}\frac{P_0}{P}$$

pressure

where $\mu^+$ is the ion mobility, units [$cm^2/(Vs)$] $P_0$=760 Torr

- Examples:

| | | | For $\vec{E}$=1kV/cm |
|---|---|---|---|
| $He^+$ | in He: | $\mu^+$= 10.2 $cm^2/(Vs)$ | $\vec{v}_D$ = 0.01 cm/μs |
| $Ar^+$ | in Ar: | 1.7 " | 0.0017 " |
| $CH_4^+$ | in Ar: | 1.87 " | 0.00187 " |
| $(OCH_3)CH_2^+$ | in $(OCH_3)CH_2$ | 0.26 " | 0.00026 " |

- Mobility is high (low) for small (big) atoms/molecules

# Gas Amplification

- In addition to the secondary electrons, ionization processes due to UV photons contribute
- These UV photons originate from de-excitations of atoms excited in collisions & produce $e^-$ via photo-effect in gas atoms or cathode
  - ⇨ Assume that in avalanche formation $N_0 \cdot A$ electrons are produced from $N_0$ primary electrons
  - ⇨ From UV photons additional $N_0 \cdot A \cdot \gamma$ photoelectrons are formed ($\gamma \ll 1$)
  - ⇨ By gas amplification these photoelectrons produce $N_0 \cdot A^2 \cdot \gamma$ electrons
  - ⇨ From them another $N_0 \cdot A^2 \cdot \gamma^2$ photoelectrons are formed which in turn produce $N_0 \cdot A^3 \cdot \gamma^2$ electrons, and so on
- Summing up all terms we get the total gas amplification factor $A_\gamma$

$$N_0 A \sum_{n \geq 0} (A\gamma)^n = \frac{N_0 A}{1 - A \cdot \gamma} := N_0 A_\gamma$$

- For $A \cdot \gamma \rightarrow 1$, $A_\gamma$ diverges & signal no longer depends on primary ionization
  - ➔ This is called Geiger-Müller region ($A_\gamma \sim 10^8$-$10^{10}$)

# BABAR EMC Performance

- Energy & angular resolution of BABAR CsI(Tl) crystal calorimeter
  - Use photons & electrons from physics processes
  - Low-energy point is obtained from radioactive source

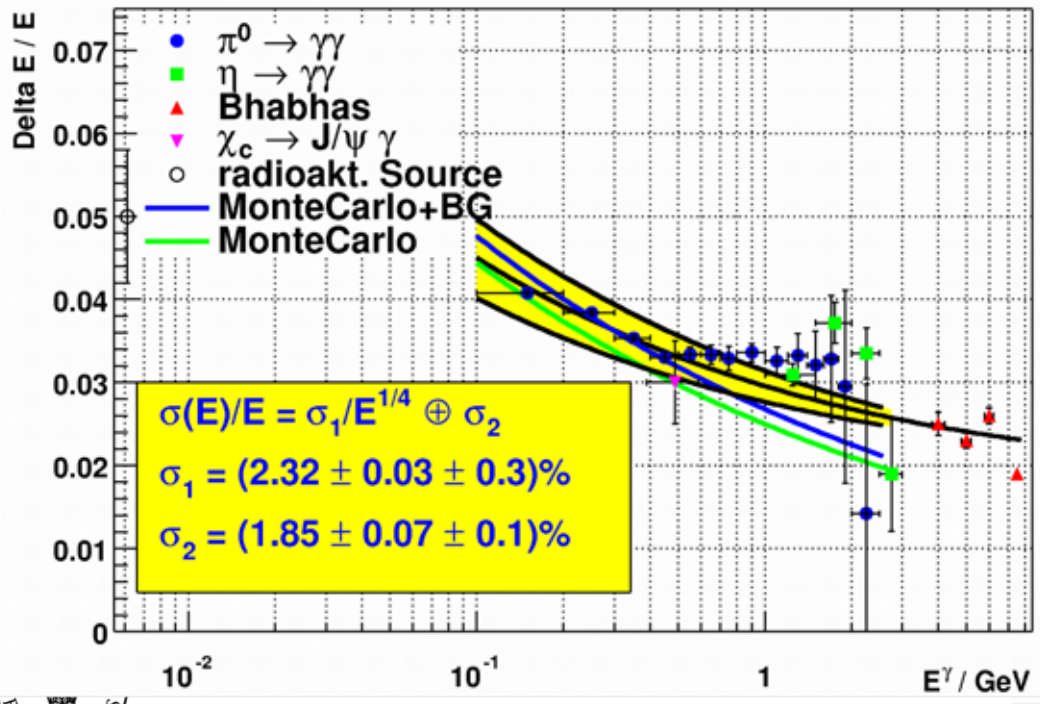


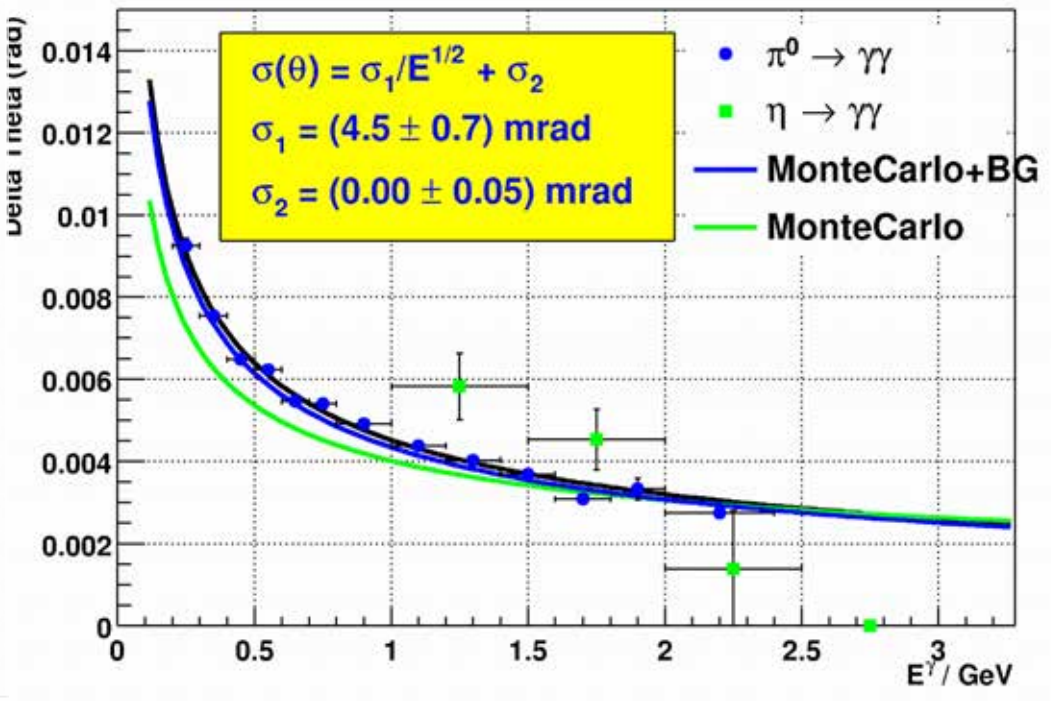

# Energy Resolution of Sampling Calorimeter

- The total energy resolution of a sampling calorimeter is

$$\left(\frac{\sigma_E}{E}\right)_{tot} = \left[\left(\frac{\sigma_E}{E}\right)^2_{sampling} + \left(\frac{\sigma_E}{E}\right)^2_{Landau} + \left(\frac{\sigma_E}{E}\right)^2_{path\ length}\right]^{1/2}$$

where

$$\left(\frac{\sigma_E}{E}\right)_{sampling} \geq 3.2\% \left[\frac{\Delta E\ [MeV]}{F(\xi)\cos\left(\frac{21\ MeV}{E_c^{\pi}}\right) E\ [GeV]}\right]^{1/2}$$

$$\left(\frac{\sigma_E}{E}\right)_{Landau} = \left[\frac{3}{\sqrt{N_x} \times \ln\left(1.3 \times 10^4 \delta\right)}\right]$$

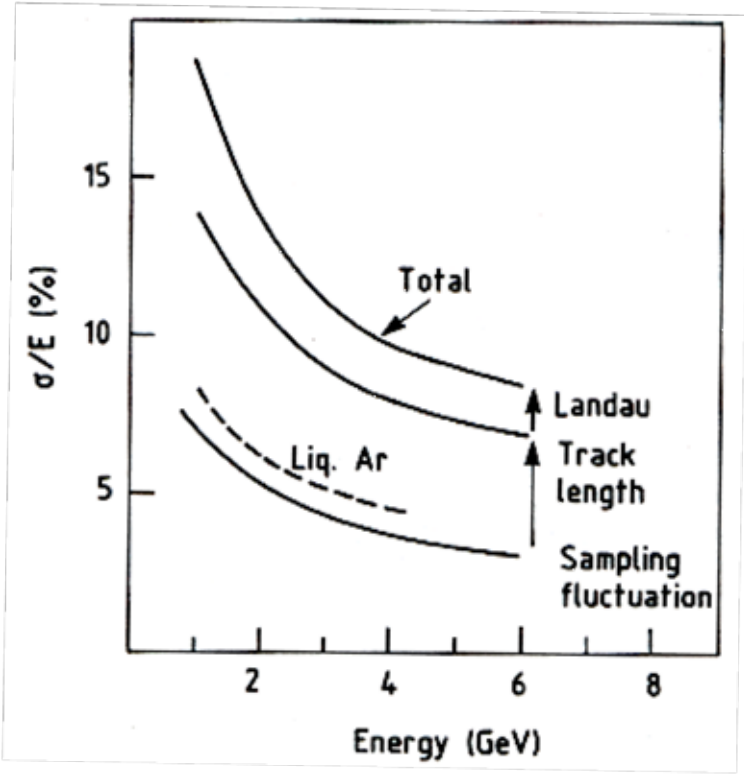


- The sampling fluctuations include multiple scattering and effects of an energy cut-off

- The path length fluctuations depend on the density of the medium

$N_x$: number of crossings in sampling calorimeter=total track length divided by distance between active plates

$$N_x = \frac{E_0 X_0}{E_c d} = \frac{E_0}{\Delta E}$$

# Compensation Fluctuations

- To cure these fluctuations we need to equalize response for $e^-$ & h
  $\Rightarrow$ either decrease $e^-$ response or boost h response
- The latter can be achieved in U-scintillator calorimeters
  - Due to nuclear break-up one gets neutron-induced fission liberating about 10 GeV of fission energy
  - Just need to detect 300-400 MeV to compensate for nuclear deficit measure either the few MeV $\gamma$ component or the fission neutrons
- Intrinsic resolution for $^{238}U$ is $\left(\frac{\sigma_E}{E}(U)\right)_{\text{int rinsic}} \cong \frac{0.22}{\sqrt{E\ [\text{GeV}]}}$
- This was achieved in the ZEUS calorimeter (U-scintillator)
- In addition sampling fluctuations contribute to the total energy resolution $\left(\frac{\sigma_E}{E}\right)_{hadronic\ \ sampling} \cong 0.09\sqrt{\frac{\Delta E[MeV]}{E[GeV]}}$
  where $\Delta E$ is energy loss per unit sampling for MIPs
- Hadronic sampling fluctuations are approximately twice as large as EM sampling fluctuations

# Test of Particle Flow

- In a test beam concept of particle flow cannot be studied directly since the beam typically consists of a single particle and not of jets ➔ do a trick to simulate this dependence: select hadron shower of a given energy and then overlay another hadron shower at a selected distance
- Consider 2 examples: 10 GeV neutral hadron separated from 10 GeV $\pi$ & 10 GeV neutral hadron separated from 30 GeV $\pi$ separated by $\Delta z$=5-30 cm
- For a 10 GeV $\pi$ with $\Delta z$=5cm, a fair amount of energy is assigned wrong
- Mean value of the difference between recovered and measured energy approaches zero with $\Delta z$ faster for 10 GeV $\pi$ than for 30 GeV $\pi$
- For sufficient separation particle flow works

10 GeV $\pi$, $\Delta z$=5 cm

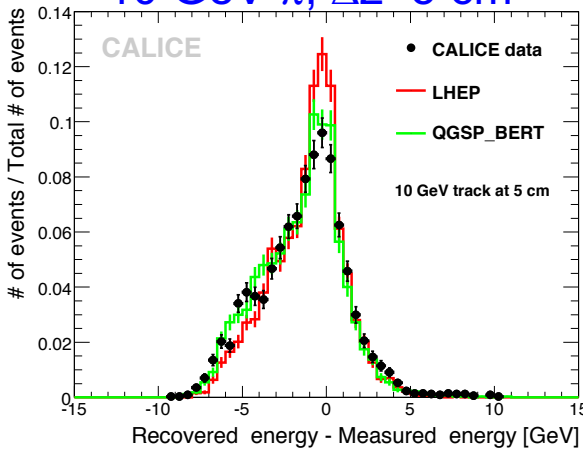


10 GeV $\pi$, $\Delta z$=30 cm

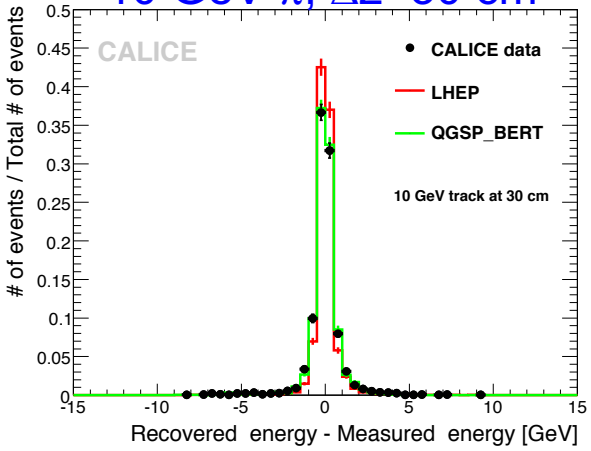


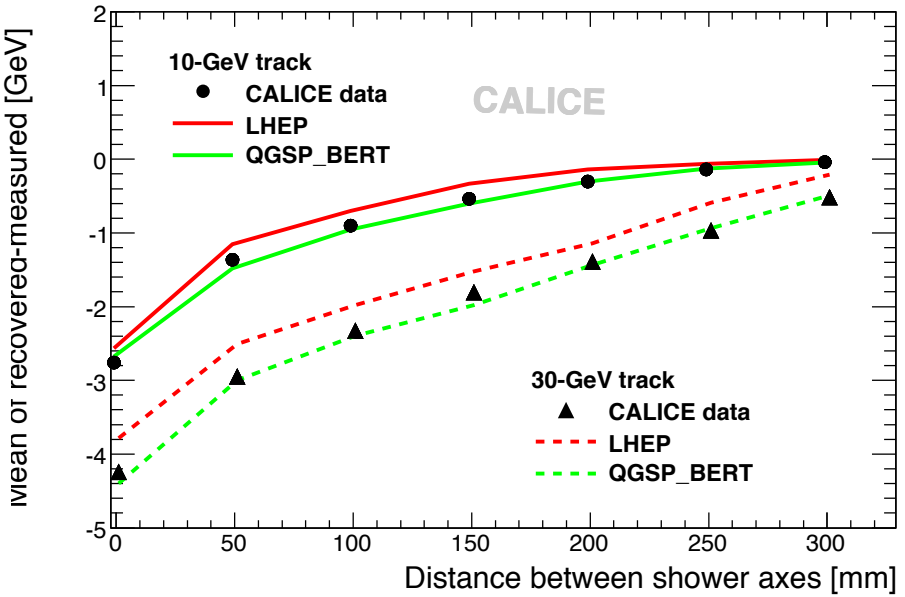

# Cherenkov Radiation and Detectors

- A charged particle traversing a medium emits Cherenkov radiation if $\beta \cdot \cos\theta_c = 1/n$
- Cherenkov photons are emitted preferentially in the UV region $\frac{dN}{d\lambda} = \frac{2\pi\alpha}{\lambda^2} L \sin^2\theta_c$
- Cherenkov counters have been used in fixed target experiments in which particles are parallel to the optical axis of detector
- To use this technology in a colliding-beam experiment, a new approach was suggested

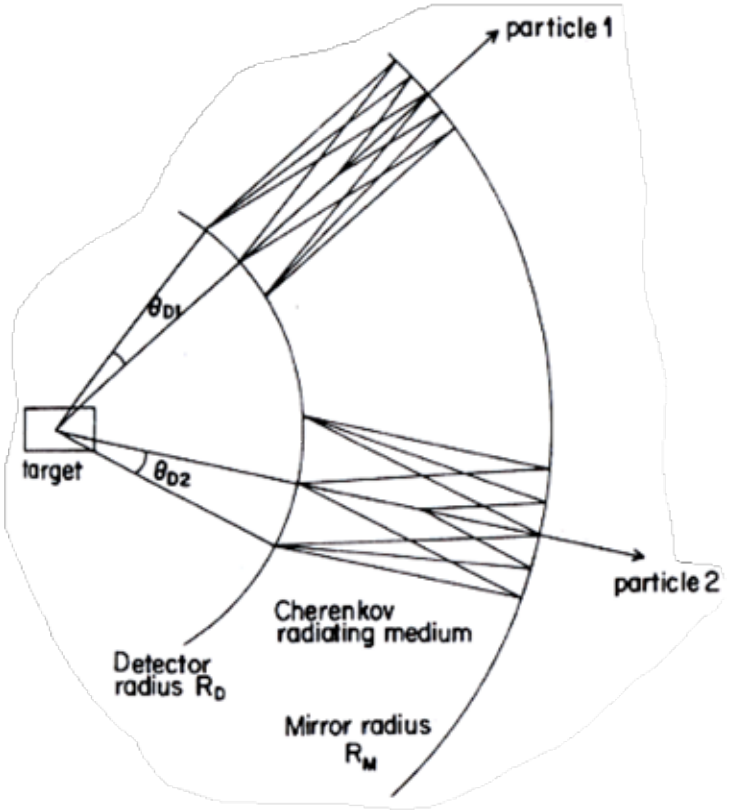


- A spherical mirror of radius $R_M$ centered at IR focuses the Cherenkov cone produced in the radiator between the sphere radius $R_D$ & the mirror into a ring-shaped image on the detector sphere ($R_D$=1/2$R_M$)
- Opening angle $\theta_D$ of the ring is ~$\theta_c$
- The radius of the ring image yields $\theta_c$ via $\tan\theta_c = \frac{2r}{R_M}$
- Both SLD and Delphi used this approach

# Particle Identification with DELPHI RICH

- Particle separation in DELPHI RICH
- Observation of a ring

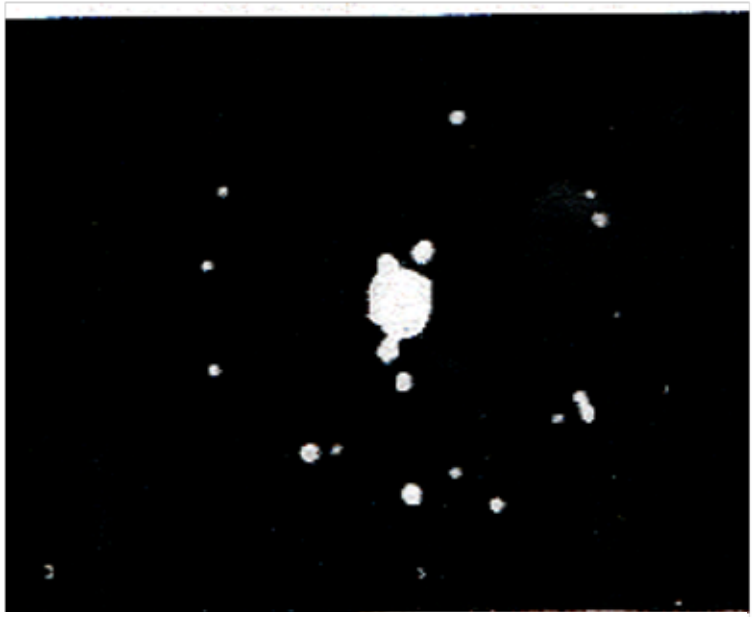

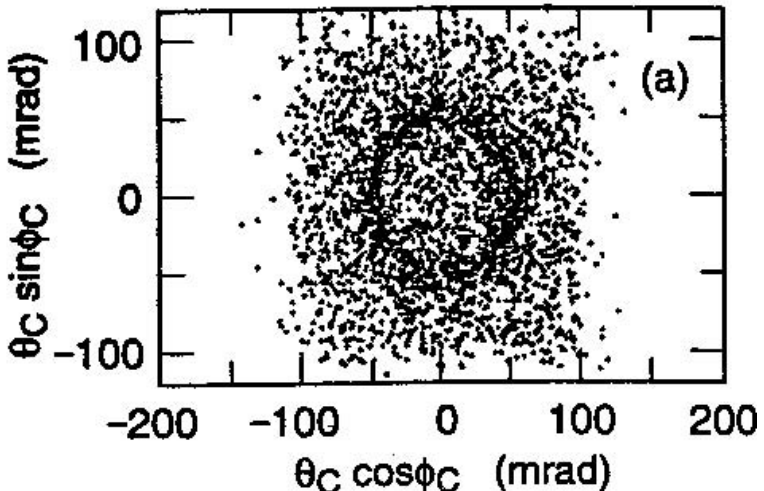


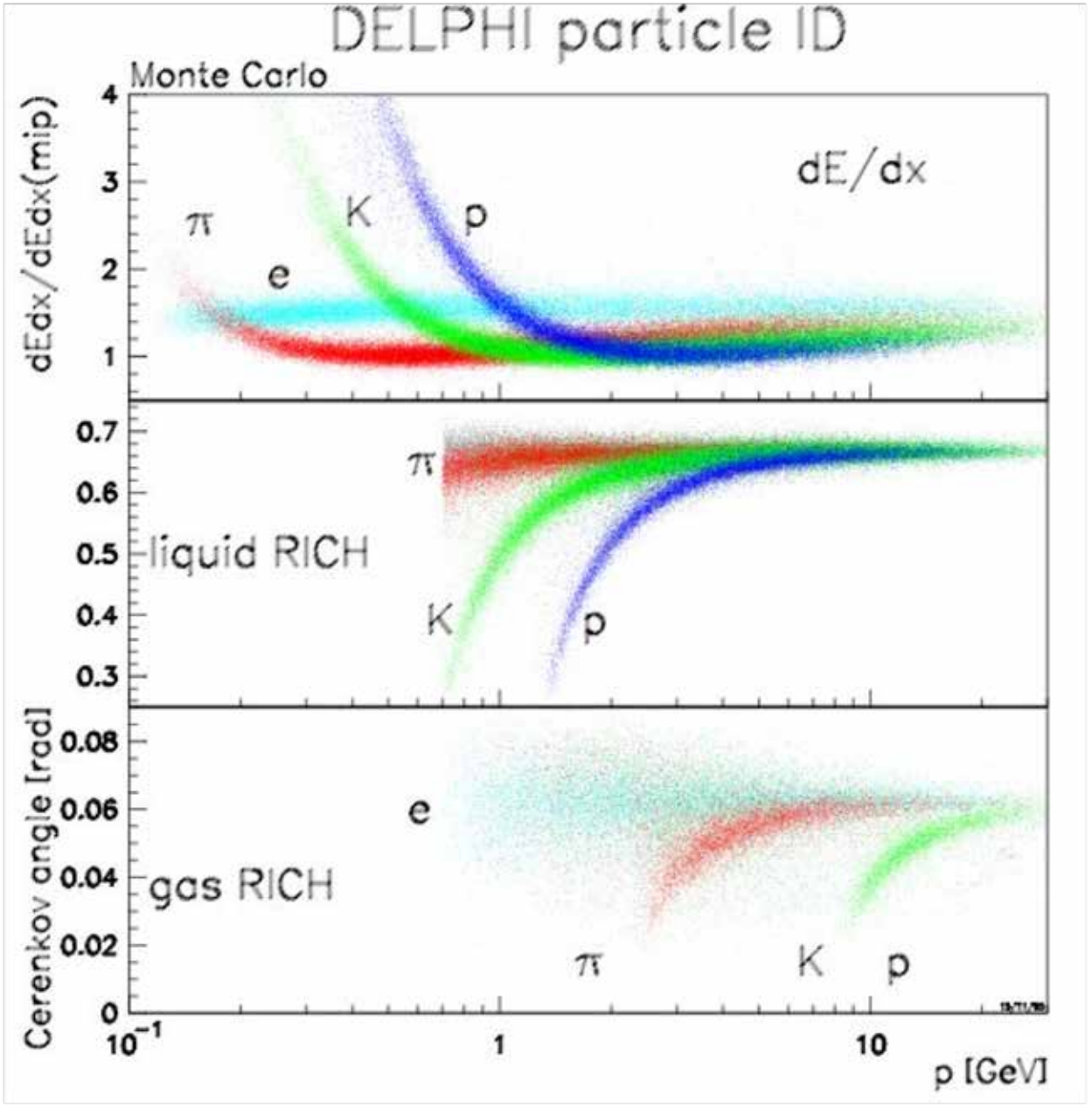

# Heavy Charged Particle in Medium

- A heavy charged particle traversing a medium looses average energy $\langle\Delta\rangle$ in a collision in thickness $\Delta x$
- The probability density function